VISIBLE LIGHT COMMUNICATIONS WITH ADVANCED PHYSICAL LAYER FEATURES AND INTEGRATION WITH EXISTING WIRELESS COMMUNICATION TECHNOLOGIES

A Dissertation

by

Ömer Narmanlıoğlu

Submitted to the
Graduate School of Sciences and Engineering
In Partial Fulfillment of the Requirements for
the Degree of

Doctor of Philosophy

in the
Department of Electrical and Electronics Engineering

Özyeğin University
June 2020

VISIBLE LIGHT COMMUNICATIONS WITH ADVANCED PHYSICAL LAYER FEATURES AND INTEGRATION WITH EXISTING WIRELESS COMMUNICATION TECHNOLOGIES

Approved by:

Prof. Dr. Murat Uysal, Advisor
Department of Electrical and Electronics Engineering
Özyeğin University

Prof. Dr. Sinem Çöleri
Department of Electrical and Electronics Engineering
Koç University

Assist. Prof. Dr. Cenk Demiroğlu
Department of Electrical and Electronics Engineering
Özyeğin University

Assoc. Prof. Dr. Serhat Erküçük
Department of Electrical and Electronics Engineering
Kadir Has University

Date Approved: 3 June 2020

Assist. Prof. Dr. Kübra Kalkan Çakmakci
Department of Computer Science
Özyeğin University

To My Father Prof. Dr. Ünal Narmanlıoğlu,

My Mother Nilgün Narmanlıoğlu,

and Tuğçe Taştan

ABSTRACT

Optical wireless communication systems that operate in the visible light frequency band (390-700 nm) are called as visible light communication (VLC). VLC systems are based on the principle of modulating light emitting diodes (LEDs) at very high speeds without any adverse effects on the human eye and illumination levels. LEDs, utilized as VLC access points (APs), are increasingly used both indoors (e.g., home and office lighting, etc.) and outdoors (e.g., street lights, traffic lights, vehicle front/rear lights, etc.). The dual use of LEDs for both lighting and communications purposes is a revolutionary solution and has the potential to open a new era in wireless communications. In this context, VLC has attracted industrial attention and related international standardization works have already begun.

In this dissertation, high-speed VLC systems with high link reliability are developed. Under the consideration of dual functionality to support both illumination and communication, advanced physical layer (PHY) techniques including adaptive transmission, orthogonal frequency division multiplexing (OFDM), multiple-input multiple-output (MIMO), and massive MIMO with beamforming are explored in order to meet the targeted high data speeds and link reliability. To utilize the multiple LEDs available within an indoor room environment for MIMO transmissions, a coordinated and joint signal processing mechanism has to be deployed. For this purpose, a centralized platform where baseband units (BBUs) are separated from the VLC APs and shifted to a centralized unit (CU) in which all signal processing units work is first proposed. Then, two different advanced PHY techniques are designed and run over the proposed platform. Firstly, adaptive bit and power loading for OFDM based VLC system with MIMO mode switching between repetition coding and spatial

multiplexing is designed. The adaptive algorithm design as an optimization problem where the aim is to maximize data rate through the proper selection of modulation order, power level, and MIMO mode, while satisfying a targeted bit error rate, is formulated and resolved. As a second advanced PHY technique, massive MIMO transmission is explored. In order to obtain the full benefits of massive MIMO, channel state information must be available in transmitter side. Estimation of downlink (DL) channel through DL pilot signals leads huge pilot overhead in both DL and uplink (UL) and makes the implementation of massive MIMO system infeasible if not properly designed. Therefore, the analysis is done under the consideration of limited number of DL pilot signals. Different pilot arrangements (PAs) in spatial, frequency, and time domains where interpolation is performed to obtain global channel matrix taking advantage of the indoor environment geometry and layout of luminaries are proposed. An adaptive selection of PAs to balance DL and UL data rates regarding to varying network conditions is further designed.

Centralized platform benefits to integrate VLC with existing wireless communication technologies (such as millimeter wave (MMW) transmission) in a heterogeneous network architecture as well. In the centralized platform, similar to VLC network, BBU is separated from MMW AP and located inside the same CU. Through the benefiting from global view of overall network architecture, an adaptive vertical (between MMW and VLC APs) and horizontal (between VLC APs) handover protocol is further designed to increase the overall network performance. The protocol includes technology specific offset parameters whose values are adjusted on-the fly based on already available network performance metrics (e.g., data rates, number of connected user equipment).

ÖZETÇE

Görünür ışık frekans bandında (390-700 nm) çalışan optik kablosuz iletişim sistemleri, görünür ışıkla haberleşme (visible light communication, VLC) olarak adlandırılır. VLC sistemleri, insan gözü ve aydınlatma seviyeleri üzerinde herhangi bir olumsuz etki yaratmadan, ışık yayan diyotların (light emitting diode, LED) çok yüksek hızlarda modüle edilmesi prensibine dayanmaktadır. VLC erişim noktası (access point, AP) olarak kullanılan LEDlerin hem iç mekanlarda (örn. ev ve ofis aydınlatması vb.) hem de dış mekanlarda (örn. sokak lambaları, trafik ışıkları, aracın ön/arka ışıkları vb.) kullanımı giderek artmaktadır. LEDlerin hem aydınlatma hem de haberleşme amaçları için ikili kullanımı, devrim niteliğinde bir çözümdür ve kablosuz iletişimde yeni bir dönem açma potansiyeline sahiptir. Bu bağlamda, VLC endüstriyel ilgiyi çekmiş ve ilgili uluslararası standardizasyon çalışmaları çoktan başlamıştır.

Bu tezde, yüksek bağlantı güvenilirliğine sahip, yüksek veri hızlı VLC sistemleri geliştirilmiştir. Hem aydınlatmayı hem de iletişimi destekleyen ikili işlevsellik göz önünde bulundurularak, hedeflenen yüksek veri hızlarını ve bağlantı güvenilirliğini karşılamak için; adaptif iletim, dikey frekans bölmeli çoklama (orthogonal frequency division multiplexing, OFDM), çok girişli çok çıkışlı (multiple-input multiple-output, MIMO) ve hüzmeleme (beamforming) ile yoğun (massive) MIMO iletim dahil olmak üzere gelişmiş fiziksel katman teknikleri araştırılmıştır. MIMO iletim amacıyla birden fazla sayıda LEDleri kullanmak için, koordineli ve ortak bir sinyal işleme mekanizması kurulmalıdır. Bu amaçla ilk olarak, merkezi (centralized) bir platform önerilmiştir. Bu platformda, temel bant birimleri (baseband unit, BBU) LEDlerden ayrılıp; tüm sinyal işleme birimlerinin birlikte çalıştığı, merkezi birime (centralized unit, CU) kaydırılmıştır. Ardından, iki farklı gelişmiş PHY tekniği tasarlanmış ve önerilen

platform üzerinde çalıştırılmıştır. İlk olarak, bit ve güç yükleme (bit and power loading) özelliğine sahip, tekrarlı kodlama (repetition coding) ve uzamsal çoklama (spatial multiplexing) arasında MIMO mod geçişi yapabilen OFDM tabanlı VLC sistemi tasarlanmıştır. Hedeflenen bit hata oranını karşılarken, veri hızını en üst düzeye çıkarmayı amaçlayan adaptif algoritma; modülasyon tipine, güç seviyesine ve MIMO moduna bağlı olan bir optimizasyon problemi olarak formüle edilmiş ve çözülmüştür. İkinci ileri PHY tekniği olarak, yoğun MIMO iletimi araştırılmıştır. Yoğun MIMOnun tüm avantajlardan yararlanmak için; kanal durumu bilgisi, verici tarafında mevcut olmalıdır. Aşağı (downlink, DL) kanal referans sinyalleri yoluyla DL kanalın tahmini, hem DL hem de yukarı (uplink, UL) kanalda büyük bir sinyalleşme yüküne neden olur ve düzgün tasarlanmadığı takdirde yoğun MIMO sisteminin uygulanmasını mümkün kılmaz. Bundan dolayı analiz, sınırlı sayıda referans sinyalini dikkate alarak yapılmıştır. Küresel kanal matrisini elde etmek için, iç ortam geometrisinden ve LEDlerin düzeninden yararlanarak enterpolasyonun yapıldığı, uzamsal, frekans ve zaman alanlarında farklı referans sinyal düzenlemeleri önerilmiştir. Bunların değişen ağ koşullarına göre adaptif bir seçimi, DL ve UL veri hızları arasında denge sağlamak amacıyla, ayrıca tasarlanmıştır.

Merkezi platform, heterojen ağlarda VLCyi var olan kablosuz haberleşme teknolojilerle (örn. milimetre dalga (milimeter wave, MMW) iletimi) entegre etme sürecine de birçok fayda sağlar. Merkezi platform yapısında, VLC ağında olduğu gibi; BBU, MMW APden ayırılıp ve aynı CU içine yerleştirilir. Bu sayede, tüm network farkında ağ mimarisinden yararlanarak, adaptif dikey (MMW ve VLC APler arasında) ve yatay (VLC APler arasında) geçiş (handover) mekanizması, ağ performansını artırmak için tasarlanmıştır. Geçiş mekanizmaları teknolojiye özgü ofset parametreleri içerir ve bu parametreler, CUda halihazırda bulunan ölçülere göre (örn. veri hızları, bağlı kullanıcı ekipmanı sayısı) anında ayarlanmıştır.

ACKNOWLEDGEMENTS

I would like to thank my supervisor, Prof. Dr. Murat Uysal, for the patient guidance, encouragement and the invaluable insights and suggestions. I will never forget his support and for providing me numerous opportunities to learn and develop as a researcher.

I am truly grateful to the members of my dissertation committee, Assist. Prof. Dr. Cenk Demiroğlu, Assist. Prof. Dr. Kübra Kalkan Çakmakci, Prof. Dr. Sinem Çöleri, and Assoc. Prof. Dr. Serhat Erküçük for their time serving on my committee and carefully reviewing my dissertation.

I would like to thank my family for always supporting me as I have pursued my education.

TABLE OF CONTENTS

LIST OF TABLES

LIST OF FIGURES

GLOSSARY

3GPP	3rd Generation Partnership Project
ADC	Analog-to-digital converter
AP	Access point
ATC	Adaptive Transmission Controller
AWGN	Additive white Gaussian noise
BBU	Baseband unit
BER	Bit-error-rate
CDF	Cumulative distribution function
CIR	Channel impulse response
CP	Cyclic prefix
C-RAN	Cloud (or Centralized) Radio Access Networks
CSI	Channel state information
CSK	Color-shift keying
CU	Centralized unit
DAC	Digital-to-analog converter
DCO-OFDM	Direct current biased optical OFDM
DCO-OFDMA	Direct current biased optical OFDMA
DFT	Discrete Fourier transform
DL	Downlink
DPC	Downlink Pilot Controller
DSP	Digital signal processing

FDD	Frequency division duplexing
FoV	Field-of-view
HetNet	Heterogenous network
HG	Home gateway
IDFT	Inverse discrete Fourier transform
IES	Illuminating Engineering Society
IM/DD	Intensity modulation direct detection
IP	Internet-protocol
IR	Infrared
ISI	Intersymbol interference
LB	Load Balancer
LED	Light emitting diode
LoS	Line-of-sight
LPF	Low-pass filter
LTE	Long Term Evolution
MAC	Medium access control
MIMO	Multiple-input multiple-output
ML	Maximum-Likelihood
MMSE	Minimum mean square error
MMW	Millimeter wave
MNO	Mobile Network Operator
MRT	Maximum ratio transmission
MSE	Mean squared error
MU	Multi-user
NOMA	Non-orthogonal multiple access
NR	New Radio
NRT	Neighbor relation table

OFDM	Orthogonal frequency-division multiplexing
OFDMA	Orthogonal frequency-division multiple access
OFE	Optical front-end
O-OFDM	Optical OFDM
OOK	On-off keying
PA	Pilot arrangement
PAM	Pulse amplitude modulation
PAPR	Peak-to-the-average-power-ratio
PD	Photodetector
PF	Proportional Fair
PHY	Physical layer
PLC	Power line communication
PoE	Power-over-ethernet
POR	Pilot overhead ratio
PPM	Pulse-position modulation
PSD	Power spectral density
PSK	Phase-shift keying
QAM	Quadrature amplitude modulation
QoS	Quality-of-service
RB	Resource block
RC	Repetition Coding
RF	Radio frequency
RRU	Remote radio unit
SE	Spectral efficiency
SINR	Signal-to-interference plus noise ratio
SISO	Single-input single-output
SM	Spatial Multiplexing

SMOD	Spatial Modulation
SNR	Signal-to-noise ratio
SU	Single-user
SVD	Singular value decomposition
TDD	Time division duplexing
UE	User equipment
UL	Uplink
VLC	Visible light communication
ZF	Zero-forcing

CHAPTER I

INTRODUCTION

As a result of the significant growth in the number of internet-enabled electronics equipments and bandwidth-hungry multimedia applications, currently deployed wireless network technologies will not be able to handle with increasing data traffic in coming years. The IP traffic forecasted by Cisco Visual Networking Index [1] is depicted Fig. 1 and 396 exabytes per month is foreseen to be carried in 2022. In order to handle with the requirements of reliable transmission to carry this amount of traffic, several solutions have been discussed and proposed [2].

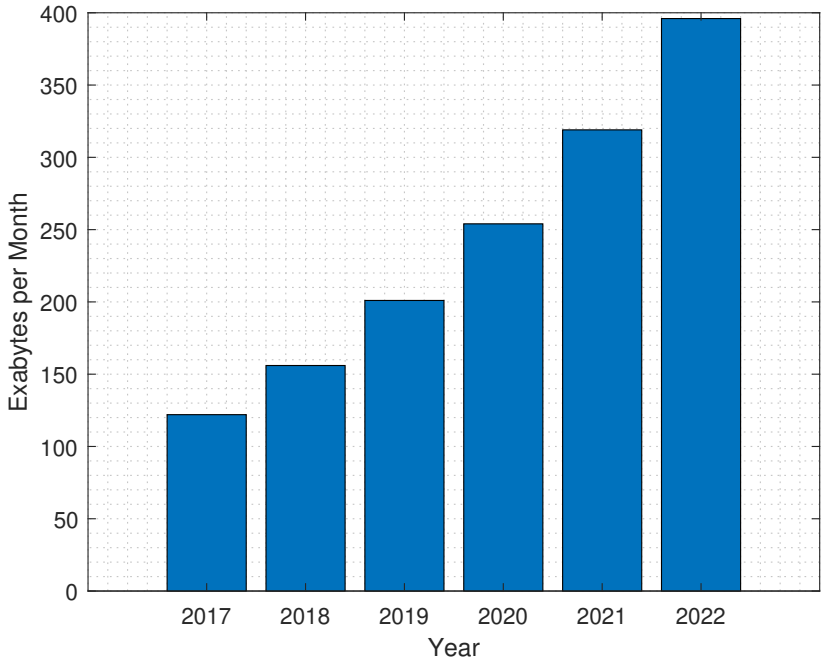

Figure 1: IP traffic forecasted by Cisco Visual Networking Index

The currently used wireless network access technologies operating at radio frequency (RF), such as Long Term Evolution (LTE), WiFi etc., work below 6 GHz. On the other hand, this part of the spectrum is almost fully-utilized and heavily regulated.

Moreover, the spectral efficiency (SE) for LTE approaches to the Shannon Limit [3]. For these reasons, network densification, also called as heterogenous network (HetNet) [4], and integration of different wireless access technologies such as LTE and WiFi [5, 6] become two of the most prominent ways that have been preferred by Mobile Network Operator (MNO) and utilized in their network infrastructures. Network densification allows spatially reuse of the same spectrum and results in significant capacity improvements through the deployment of greater number of access points (APs) with different power levels (e.g., small-cells, femto-cells, macro base stations etc.). On the other hand, HetNets bring about several challenges as well, such as, non-negligible interference between the APs operating at same frequencies, which imposes a fundamental limit on the network capacity. Additionally, an effective coordination between different access technology APs is required to enhance the network capacity. These issues provide additional opportunities to the vendors in wireless communication industry [7, 8, 9, 10].

Usage of wider transmission bandwidth is a common solution to handle with the forecasted traffic growth. It is, however, possible in the upper segments of the electromagnetic spectrum, particularly in millimeter waves (MMWs). In upcoming communication and networking technologies, this part of the spectrum is planned to be utilized. For example, 5G New Radio (NR) is planned to operate at the frequencies up to 52.6 GHz [11], IEEE 802.15 Task Group 3c [12] considers 57-64 GHz band, and 60 GHz is selected as an operation band for IEEE802.11ad [13].

Another recent advance in the wireless communication industry that has been provided to MNOs is massive multiple-input multiple-output (MIMO) transmission [14] in which the source node is equipped with very large transmitter in collected or distributed manner. It was firstly introduced by [15] and becomes an emerging transmission technique to meet the future requirements of wireless communication systems

through serving several user equipment (UE) at the same time and frequency slot using beamforming. Increment on the number of transmitters leads the propagation channels between UEs and source nodes favorable which means pair-wisely orthogonal that makes low-costed linear processing optimal.

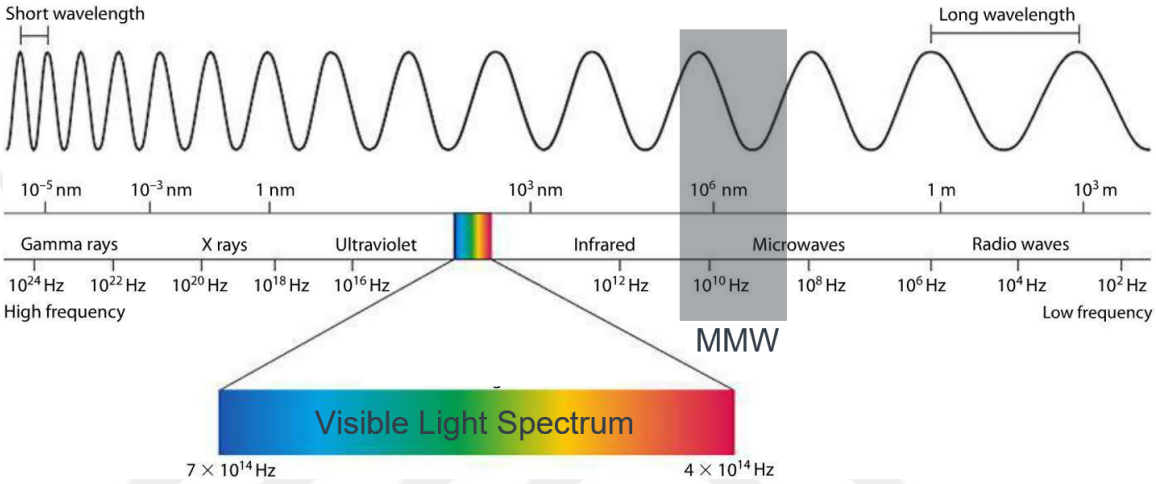

Figure 2: Electromagnetic spectrum

Operating at unlicensed optical bands (see Fig. 2) is another radical approach to handle with the spectrum congestion. Visible light communication (VLC), also referred as LiFi [16, 17], is an emerging wireless transmission technology that is based on the principle of modulating light emitting diodes (LEDs) without any adverse effects on the human eye and illumination levels [18]. It uses the visible wavelength range between $390-700$ nm. In VLC, LEDs, whose number has been significantly increased in both indoors (e.g., home and office lighting) and outdoor environments (e.g., street lights, traffic lights, vehicle front/rear lights) as a result of their energy efficient characteristics, are utilized as transmitter, whereas, photodetector (PD) is used in receiver side to capture optical signal and convert it to electrical signal. The utilization of existing lighting infrastructure including LEDs with the aim of data transmission is a revolutionary solution that opens a new era in wireless communication industry.

Therefore, it can be taken into account as an alternative and/or complementary technology for existing RF/MMW networks, particularly in user-dense environments, to improve the network performance.

VLC transmission relies on intensity modulation direct detection (IM/DD) in which the signal is transmitted using the intensity of the light and detected with the use of PD. As a difference from the conventional RF communications, the propagated waveform, which drives the LED, should be non-negative and real-valued. For this purpose, the initial works on VLC utilized simple modulation techniques (e.g., on-off keying (OOK) or pulse-position modulation (PPM) [19]). The first standard of VLC, IEEE 802.15.7, was issued in 2011 and included these two techniques at physical layer (PHY) [20][1]. On the other hand, with the aim of improving data rates over frequency-selective VLC channels as a result of wider bandwidth utilization, multi-carrier transmission, particularly orthogonal frequency-division multiplexing (OFDM), has been adapted for optical transmission [21, 22, 23, 24, 25]. While accomplishing this target, there are also several important challenges that need to be addressed in system design [26]. The main challenges with their proposed solutions are described in Table 1.

Table 1: VLC challenges and proposed solutions

Challenge	Description	Solution
Inter-AP Interference	The dense deployment of LEDs within an indoor room environment causes severe interference to each other and performance degradation becomes inevitable due to high interference levels.	Utilizing LEDs as a MIMO elements provides a coordination of interference and enhances the system performance.

[1] A more advanced modulation scheme, which is color-shift keying (CSK) that requires multiple optical sources with different operating wavelengths, is used in the third PHY option of the standard.

Challenge	Description	Solution
Uplink Transmission	Almost all of the existing studies have been utilizing VLC in downlink (DL) side without taking uplink (UL) part into account. Even though most of smartphones (as UE) have a flashlight, they cannot be considered as VLC transmitter for UL transmission as a result of their huge energy consumption and their visual disturbance to humans when they are active.	Different part of the spectrum (e.g., infra-red or MMW bands etc.) can be considered for UL transmission.
Receiver Orientation	The optical received power shows a significant variation in the case of UEs' mobility and PDs' rotation. In the presence of misalignment between PD and LED or a shadowing event as a result of object or human blockage, reliable transmission becomes impossible due to insufficient received power levels.	In order to provide a reliable transmission in these misalignment or shadowing conditions, hybrid architectures in which VLC supported by RF-based transmissions can be taken into account.
Coverage and Mobility	In the case of using LEDs within an indoor room environment as a single VLC AP (instead of MIMO element), each has a limited coverage as result of huge interference levels and required proper LED-PD alignment to avoid from huge channel attenuation.	In order to provide a reliable transmission and seamless mobility in VLC context, efficient horizontal (between VLC APs) and vertical (between inter-technology) handover mechanisms should be designed.

The commercial VLC products are already available from various vendors [27, 28]. Following growing industrial interest, the international standardization processes have been also continued. IEEE has established the 802.11bb Light Communications Task Group [29] in January of 2018. The standard, which supports a minimum throughput of 10 Mbps while achieving 5 Gbps using at least one mode, is planned to be released until the end of 2021. In order to achieve these ambitious data rates, advanced PHY features such as adaptive transmission, MIMO, or even beamforming in conjunction with optical OFDM (O-OFDM) [30, 31] should be taken into account. It should be also noted that MIMO is a natural solution as a consequence of the fact that multiple light sources (e.g., ceiling lights) are already available in most of indoor environments (e.g., conference halls, classrooms, and similar public places etc.) and massive number of LED installation provides a base for beamforming.

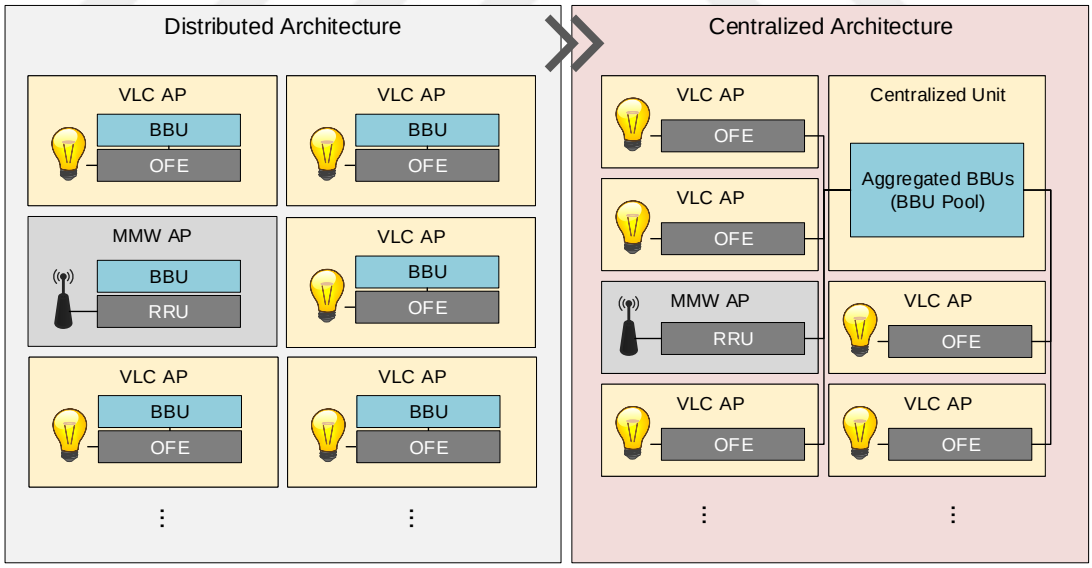

Figure 3: BBU/RRU/OFE locations in distributed and centralized architectures

In order to utilize the multiple LEDs as VLC AP for MIMO transmission or beamforming, a coordination and joint processing for transmitted and received signals across multiple VLC APs is required. For this purpose, inspiring from the Cloud (or

Centralized) Radio Access Networks (C-RAN) architectures [3, 32] in which base stations' digital functional units are separated from radio units and located in a centralized place, a centralized wireless indoor network architecture is first proposed and then utilized in this dissertation. In conventional distributed architectures, VLC APs consist of baseband unit (BBU) followed by an optical front-end (OFE), whereas, BBUs are decoupled from VLC APs and shifted to a centralized unit (CU) in which all computational resources are aggregated in the new architecture (see Fig. 3). It provides significant benefits to the deployment, management, and optimization phases [33] in addition to joint processing for (massive) MIMO applications. Following the practical use cases (e.g., see [27, 28]), an MMW AP is located within the same indoor room environment to support UL transmission. It also benefits DL side through hybrid access transmission. Similar to VLC APs, MMW AP also includes two functional units which are BBU and remote radio unit (RRU). In the proposed HetNet architecture, BBU of MMW AP available in the same indoor environment is also decoupled from its RRU and located in the same CU. Then, CU has a capability to provide an effective coordination between MMW and VLC APs in DL side as a result of awareness of global network view.

1.1 Literature Review

In the following, the studies related to adaptive MIMO OFDM-based VLC, massive MIMO VLC, and hybrid network architectures including VLC technology are reviewed.

1.1.1 Adaptive MIMO OFDM-Based VLC

Various types of single-user (SU) and multi-user (MU) MIMO systems with Repetition Coding (RC), Spatial Multiplexing (SM), Spatial Modulation (SMOD) modes have been proposed and their performances have been investigated in the literature. Adaptive modulation in terms of bit and power loading is also evaluated with either

single-input single-output (SISO) or MIMO systems to increase data rate. Their analyses in conjunction with OFDM are summarized in Table 2 where A, O, M, and D denote the "adaptive transmission", "OFDM", "MIMO", and "domain", respectively.

Table 2: Overview of adaptive MIMO OFDM-based studies

	A	O	M	D	Overview
[34]	NO	NO	YES	VLC	The performance of RC, SM and SMOD MIMO modes are evaluated and compared with each other in frequency-flat VLC channels.
[35]	NO	YES	YES	VLC	The performance of RC, SM and SMOD MIMO modes are evaluated and compared with each other in frequency-selective VLC channels.
[36]	NO	YES	YES	VLC	The performance of RC, SM and SMOD MIMO modes are evaluated and compared with each other in frequency-selective VLC channels including the effect of wiring and cabling technologies.
[37]	NO	YES	YES	VLC	Index modulation in which the sign information and in-phase and quadrature components of the conventional OFDM signals are transmitted through different LEDs is investigated.
[38]	NO	YES	YES	VLC	OFDM system in which in-phase and quadrature components are encoded to the different LEDs instead of using Hermitian symmetry is investigated and compared with conventional Hermitian symmetry imposed MIMO O-OFDM transmission.

	A	O	M	D	Overview
[39]	NO	YES	YES	VLC	The effect of channel correlation with the use of PDs with different field-of-views (FoVs) for SM MIMO is analyzed.
[40]	NO	YES	YES	VLC	Circulant matrix transform as pre-coding scheme is investigated for MIMO systems.
[41]	NO	YES	YES	VLC	A non-orthogonal multiple access (NOMA) method is analyzed to improve data rate performance of MIMO VLC network.
[42]	NO	YES	YES	VLC	MU transmission over MIMO VLC systems is analyzed with spatial dimming schemes based on the zero-forcing (ZF) and minimum mean square error (MMSE) pre-coding schemes.
[43]	NO	YES	YES	VLC	An experimental study for MIMO system including cubic receiver structure to solve ill-conditioned channel problem is conducted.
[44, 45]	NO	YES	YES	VLC	Experimental demonstration for MIMO VLC is conducted to achieve high data rates.
[46, 47, 48]	YES	YES	NO	VLC	A bit and power loading scheme is investigated for VLC systems.
[49]	YES	YES	NO	VLC	The rate of channel code and modulation size are adaptively selected to boost the network performance.
[50]	YES	YES	NO	VLC	A pairwise coding scheme is proposed for VLC systems.
[51]	YES	YES	YES	VLC	A bit and power loading scheme is presented for MIMO OFDM-based VLC systems with fixed SM mode.
[52]	YES	NO	YES	VLC	A bit and power loading scheme is presented for MIMO VLC systems with fixed SM mode.

	A	O	M	D	Overview
[53]	YES	NO	YES	VLC	An adaptive MIMO VLC system that uses SM and selects the modulation order in an adaptive way is proposed.
[54]	YES	NO	YES	VLC	Transmitters and receivers are adaptively selected in a novel SMOD based MIMO and compared with conventional RC, SMOD, and SM modes.
[55]	YES	YES	YES	VLC	An adaptive bit loading and MIMO mode selection mechanism is proposed with equal power allocation.
[56]	NO	NO	YES	RF	The usage of multiple transmitting and/or receiving antennas for SU transmission over various RF channel types is investigated in terms of ergodic capacity and error exponents.
[57]	YES	YES	NO	RF	Iterative water-willing as power allocation algorithm is investigated for ADSL modems.
[58]	YES	YES	YES	RF	Statistical water-filling algorithm and sub-channel grouping are analyzed for MIMO OFDM based RF systems.
[59]	YES	YES	YES	RF	A new link adaptation method employing eigenmode based signalling with imperfect channel state information (CSI) at the transmitter side is proposed for MIMO OFDM based RF system. The method includes bit and power loading schemes as well.
[60]	YES	YES	NO	RF	An optimal, computationally efficient, integer-bit power allocation algorithm for multi-carrier RF systems is proposed.

	A	O	M	D	Overview
[61]	YES	YES	NO	RF	A joint bit and power loading scheme is proposed for OFDM-based RF systems.
[62]	YES	NO	YES	RF	A MIMO communication system including a switching between SM and transmit diversity based on CSI is proposed.
[63]	YES	YES	YES	RF	Link adaptation techniques in terms of modulation order, coding rate, and multiplexing/diversity are investigated according to the varying RF channel conditions.

From Table 2, it can be observed that there are several studies on adaptive MIMO OFDM transmission including bit and power loading in RF domain such as [58, 59]. The adaptation of the MIMO modes are further investigated in [62, 63]. On the other hand, even though there are several VLC studies including adaptive MIMO OFDM-based transmission system with bit and power loading scheme, none of the studies in VLC, however, investigate such an adaptivity in conjunction with switching of MIMO modes.

1.1.2 Massive MIMO OFDM-Based VLC Networks

Beamforming techniques in the case of massive number of LED deployment have been proposed and their performances have been investigated in the literature (see Table 3). In the context of massive MIMO, acquisition of the CSI in DL transmission side is very crucial to get the full benefits. The channel estimation schemes, however, vary depending on system duplexing mode (e.g., either time division duplexing (TDD) or frequency division duplexing (FDD)). The propagation channels in both DL and UL sides are reciprocal when TDD mode is used [64]. It benefits massive MIMO system to use estimated UL channel responses during pre-coding phase in DL transmission.

In the context of VLC, on the other hand, since the UL transmission is operating in different part of spectrum such as infrared (IR) or RF bands (see product offerings from [27, 28]), TDD becomes impossible and FDD is the only possible solution for duplexing mode. However, in FDD systems, the amount of UL resource elements that are used to feedback estimated DL channel responses increases in proportion to the total number of active UEs. The feedback overhead is then resulted by low UL data rate values in the case of high number of active UEs. Therefore, an efficient DL pilot arrangement (PA) that determines the number of pilot signals and relatively their places within a transmission frame becomes critical to keep both DL and UL data rate at an acceptable level. The studies in massive MIMO VLC context are then separated into the following categories: (*i*) the studies that consider perfect CSI in transmitter side; (*ii*) the studies that estimate CSI, however, do not consider feedback overhead, and (*iii*) the studies that estimate CSI and consider overhead issue.

Table 3: Overview of massive MIMO-based VLC studies

	Perfect CSI	Overhead	Overview
[65]	Available	NO	A pre-coder using exponent singular value decomposition (SVD) approach is proposed for massive MIMO.
[66]	Available	NO	A certain combination of LED set is selected in massive MIMO system to decrease error rate for same SE.
[67]	Available	NO	A pre-coder for ill-conditioned massive MIMO channel is designed.
[68]	NO	NO	An iterative channel estimation technique is proposed for massive MIMO systems.

	Perfect CSI	Overhead	Overview
[69]	NO	NO	A channel estimation problem using convolutional neural networks as identifying channel matrix of massive MIMO VLC as two-dimensional natural image is proposed.

Even though the authors in [68, 69] estimate CSI, any of them does neither discuss the effect of training overhead nor the CSI feedback which have significant implications on UL data rate.

1.1.3 Hybrid MMW/VLC Access Networks

To exploit the complementary features of VLC and RF/MMW technologies, hybrid access networks have recently received much attention in the literature. Cooperation of VLC and different radio-access technologies including WiFi, LTE, MMW have been also investigated in several studies and reviewed in Table 4.

Table 4: Overview of hybrid access network studies including VLC

	>6 GHz	Other Technology	Overview
[70]	NO	Femto-Cell	A vertical handover mechanism for an indoor room environment including VLC APs and one RF femtocell is proposed.
[71]	NO	WiFi	A dynamic load balancing scheme taking user mobility and handover signalling overheads into account is proposed.
[72]	NO	Small-Cell	Power and bandwidth allocation is investigated for a system consisting of VLC and RF APs.
[73]	NO	WiFi	A load balancing scheme to achieve higher system throughput in hybrid VLC/WiFi networks is proposed.

	>6 GHz	Other Technology	Overview
[74]	NO	Small-Cell	An optimal load-aware algorithm in hybrid VLC/LTE network is proposed with the Lagrange dual decomposition to solve the load-aware optimization problem by relaxing the association variables.
[75]	NO	LTE	A mobility-aware load balancing scheme is proposed in hybrid VLC/LTE access networks.
[76]	NO	2.4 GHz RF	Power allocation across RF and VLC links to improve the hybrid network performance is investigated.
[77]	NO	WiFi	A novel AP selection mechanism for hybrid VLC/WiFi is proposed.
[78]	NO	2.4 GHz RF	A load balancing scheme based on evolutionary game theory is proposed for hybrid VLC/RF networks.
[79]	NO	2.4 GHz RF	A link selection mechanism over RF and VLC networks is proposed.
[80]	NO	Small-Cell	Coverage and rate analyses on hybrid VLC/RF networks are done.
[81]	YES	60 GHz RF	The advantages of combining the RF and VLC are depicted and a load-transfer from VLC to RF network is proposed to improve the network performance.
[82, 83]	YES	60 GHz RF	A joint load balancing and power allocation for a hybrid VLC/RF network is investigated.
[84]	YES	60 GHz RF	A hybrid VLC/RF communication which outperforms the stand-alone VLC system is proposed.

It can be observed that most of the above works assume operating RF band below 6 GHz. When > 6 GHz band, particularly MMW, is considered, there are relatively few works in the literature [81, 82, 83, 84]. When the algorithms proposed in these works are investigated, it is seen that periodical reporting of the received signal level (or signal-to-interference plus noise ratio (SINR)) from each AP for each UE is required.

On the other hand, this-type of reporting results in a significant increment on UL signalling overhead and huge battery consumption in UE. For these reasons, an event-based reporting process has been defined in addition to the periodical reporting for currently used wireless mobile networks [85].

1.2 Contributions

With the aim of addressing the problems and research gaps given in the previous section, contributions of the dissertation are summarized as following:

- In Chapter 2, a centralized indoor network architecture including multiple VLC APs and a single MMW AP is proposed. In the new architecture, BBUs are decoupled from APs and shifted to a CU that has a capability of joint processing for the signals that are transmitted and received through APs. It allows to perform distributed MIMO applications, beamforming in the case of massive LEDs deployment, and load balancing between intra- and inter-access technology APs in an effective way as a result of awareness of global network view.

- In Chapter 3, an adaptive SU DL distributed MIMO OFDM-based VLC system is analyzed. The data rate performance of DL system is first formulated as an optimization problem in terms of MIMO mode and subcarrier-level modulation order and power level. Then, an Adaptive Transmission Controller (ATC) that is implemented in CU and performs bit and power loading algorithm in conjunction with MIMO mode switching is designed to boost DL data rate regarding to the channel conditions. The results reveal that bit loading is a crucial process to improve the system performance and it is further enhanced with the use of power loading. Furthermore, in low signal-to-noise ratio (SNR) region, RC outperforms SM as a result of diversity gains, whereas, SM provides significant multiplexing gain and enhances the system data rate performance in high SNR region. Our designed algorithm benefits from both two MIMO mode and selects

one of them regarding to the obtained channel conditions.

- In Chapter 4, an FDD based MU massive MIMO OFDM-based VLC system is proposed. In order to keep the data rates in both DL and UL links at an acceptable level, various types of DL PAs are designed and investigated under the consideration of DL channel estimation and interpolation errors in conjunction with UL pilot and feedback overheads. From the Monte-Carlo simulations, it is obtained that channel estimation and interpolation are the main processes to determine the DL data rate. Lower error values in these processes provides higher data rates despite of higher DL pilot overhead ratios. On the other hand, the overhead ratios are the crucial factor to determine the UL data rate. As the number of UEs becomes larger, DL data rates increase as a result of UE diversity, however, UL data rates dramatically decrease due to higher feedback overhead. It is also observed that there is not even any resource element to feedback the estimated DL channel coefficients to CU within a single UL frame and an adaptation among PAs to provide relatively sufficient data rates in both DL and UL sides becomes mandatory. Accordingly, a Downlink Pilot Controller (DPC) that is implemented in CU is further proposed to select the proper PA to keep the data rates at an acceptable level regarding to the number of active UEs within an indoor room environment.

- In Chapter 5, VLC is considered as a complementary network technology to boost existing DL MMW network performance within an indoor room environment. MMW transmission is selected as primary technology, whereas, VLC is secondary technology for UE connection. In order to increase DL overall system performance, an adaptive vertical and horizontal handover mechanism with the introduction of technology-specific offset variables is proposed. The offset variables are then adjusted on-the-fly by a Load Balancer (LB) that is implemented

in CU. The LB uses an event-triggered reporting process that minimizes the signalling overhead as inspired from event-based reporting used in LTE [85]. Our results obtained through Monte-Carlo simulations demonstrate that significant improvements in average data rates can be obtained especially when the number of UEs increases. The system adapts itself in varying network conditions and signalling overhead is significantly reduced as comparing with conventional periodical reporting cases.

CHAPTER II

CENTRALIZED INDOOR NETWORK ARCHITECTURE

In this chapter, a centralized indoor network architecture including VLC and MMW transmission technologies is proposed as emphasizing the differences from currently used conventional distributed architectures.

2.1 Distributed Architecture

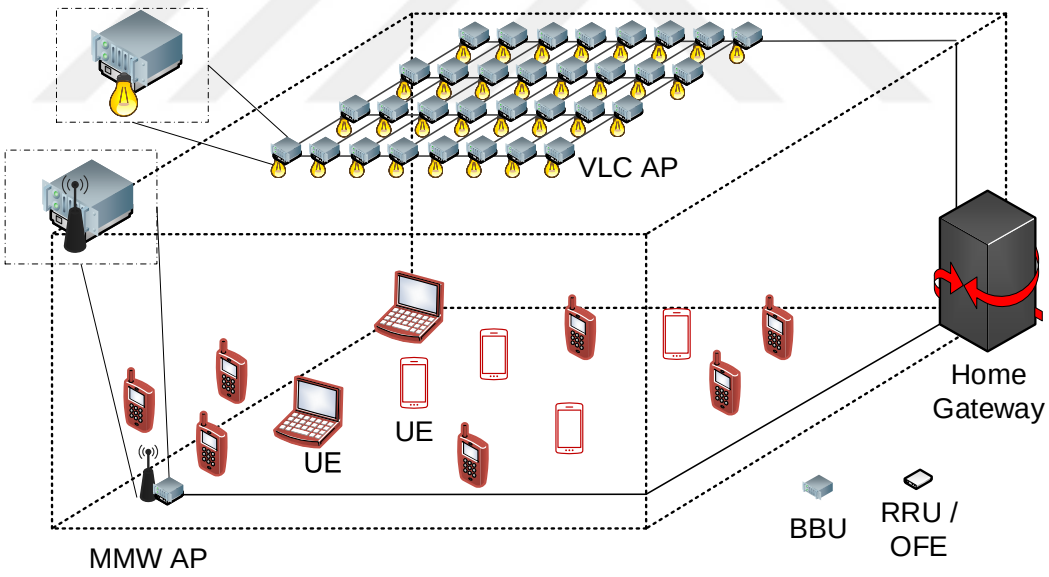

Figure 4: Conventional distributed indoor network architecture

Conventional distributed indoor network architecture including both VLC and

The content and results have been partially published in [33].

MMW transmission technologies is visualized in Fig. 4. In the distributed architecture, each light unit, enabled for VLC capabilities (see e.g., [27, 28]), is utilized as a VLC AP to serve the UEs locating in its coverage. The VLC-capable lights consist of two main functional sub-units which are BBU and OFE. The structure of lights is depicted in Fig. 5. The main responsibilities of BBU are sampling/desampling, signal transforms, modulation/demodulation, coding/decoding, error correction, re-transmission decision, handover, interference cancellation, performance indicators/counters pegging, resource management, medium access control (MAC) etc., whereas, OFE prepares the signal to be transmitted through optical wireless channel and the received analog signal for further digital signal processing (DSP) in BBU side.

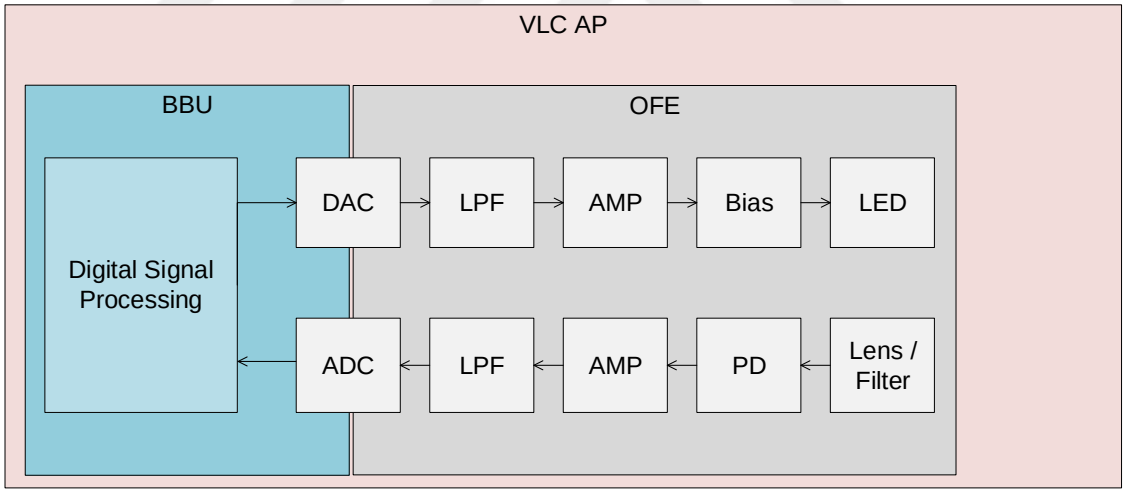

Figure 5: VLC-capable light unit

In DL side of VLC network, the signal produced by BBU is directly fed to the input of OFE through digital-to-analog converter (DAC). In OFE, the analog signal is passed from low-pass filter (LPF) and amplified. Then, a DC-bias is appended with the use of bias-tee. The resulting signal drives LED. In UL side, OFE consists of lens/filter, PD, filter, and amplifier. The PD converts the collected and filtered optical signal to electrical signal. After the signal is amplified and filtered, respectively,

it is fed into BBU through analog-to-digital converter (ADC). BBU is also connected to home gateway (HG) through a backhaul link which can be in the form of coaxial, fiber-optic, power line communication (PLC) (which uses the existing electrical infrastructure), or power-over-ethernet (PoE) (which carries both power and data), which can be decided based on infrastructure conditions.

MMW network has a similar architecture with VLC network. MMW AP serves the UEs locating in its coverage and consists of two main functional sub-units: BBU and RRU. The structure of MMW AP is depicted in Fig. 6. The functionality of BBU is the same with VLC network, however, the structures of RRU and OFE are different from each other. The aim of RRU is to prepare the digital signal to be transmitted through MMW wireless channel and prepare the received analog signal for further DSP.

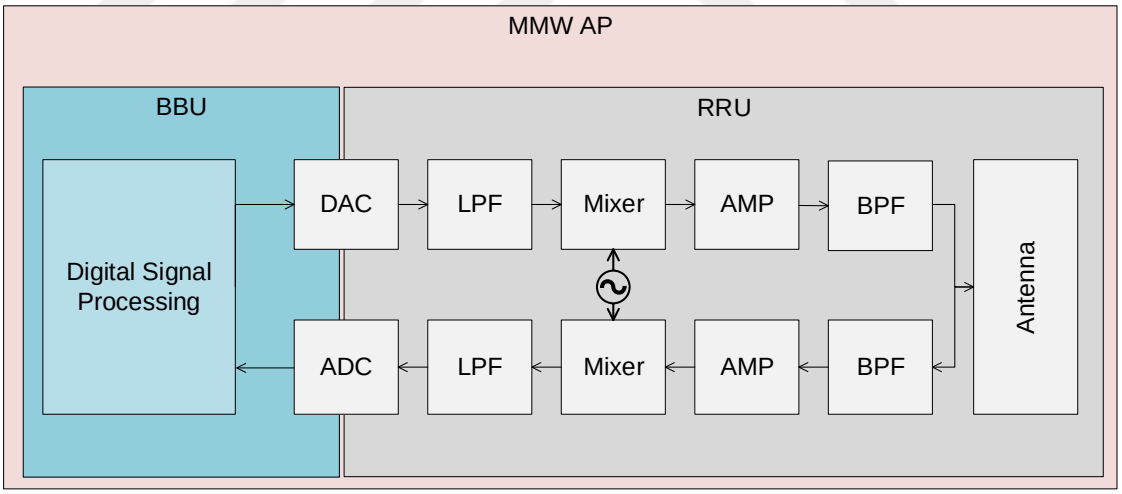

Figure 6: MMW AP unit

In DL side, the signal produced by BBU is directly fed to the input of RRU through DAC. In RRU, the analog signal is first low-pass filtered and multiplied with a carrier frequency that is produced by a local-oscillator. The resulting signal is amplified and passed through band-pass filter. It is then fed to MMW antenna for propagation to UE side. In UL side, the received electromagnetic signal is converted

to electrical signal through MMW antenna. It is passed through band-pass filter and amplified. The process is followed by multiplying with the same (or different) carrier frequency in TDD (or FDD) mode and low-pass filtering. The resulting signal is then fed to BBU through ADC for further digital processing. As in VLC network, BBU is also connected to the HG through a backhaul link which can be in different form regarding to the infrastructure conditions.

In the traditional architecture, BBU and either RRU or OFE based on technology type are integrated inside each AP. The APs perform all required digital and analog processes of wireless communication for their connected UEs. The processes are independently performed for each AP, however, an interface (e.g., X2 in LTE [86]) can be defined for coordination of APs with the aim of better network performance through handover, load balancing, interference cancellation etc.

2.2 Centralized Architecture

The concept of C-RAN architecture was first introduced by IBM [87] in which the architecture is named as "Wireless Network Cloud". Inspired from the C-RAN which provides a centralized coordination without a requirement of the interface between APs to boost the network performance and better resource utilization in an energy-efficient way, a centralized platform which includes both MMW and VLC APs is proposed in this section.

In the proposed centralized architecture (see Fig. 7), BBUs, which are locating in MMW and VLC APs in the distributed architecture, are removed from APs and shifted into a CU in which all required digital signal processing takes place. The main differences between distributed and centralized architectures are summarized in Table 5. All computational resources are also aggregated in the CU. It can be embedded into HG or can be located in a different part of the network. As a result of the shifting, VLC AP becomes a simple lighter device that includes only OFE and

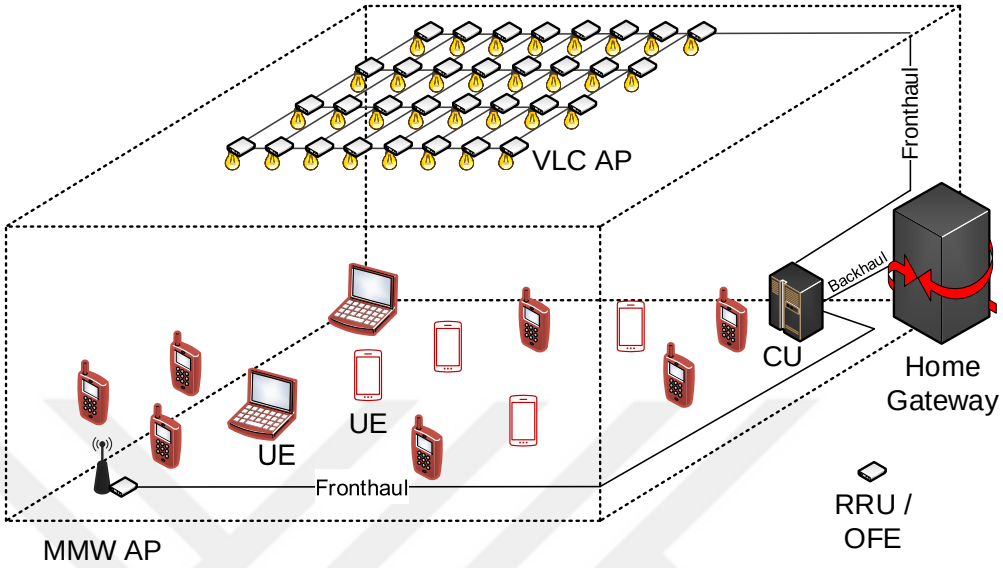

Figure 7: Proposed centralized indoor network architecture

similarly, MMW AP consists of single RRU. Separating BBUs and RRUs and moving BBUs to the CU provide cheaper and smaller-sized VLC-capable LEDs and MMW APs production as compared with those in the distributed approach. These two facts are particularly important for the market penetration of a new wireless access technology. In the proposed architecture, a link between CU and OFE/RRU, which is also known as fronthaul link, has to be deployed. Structure of CU and different technology APs in the proposed architecture is displayed in Fig. 8.

Table 5: Comparison of distributed and centralized architectures

	Distributed	Centralized
BBU Placement	Each AP has its own BBU and serves UEs using single BBU resource.	BBU resources are aggregated and virtualized in CU. They are shared among APs for on-demand usage and UEs can be served using multi BBU resources.

	Distributed	Centralized
Fronthaul Links	Since BBU and RRU/OFE are in the same hardware, no additional link is required.	It requires high capacity fronthaul links between AP and CU to transfer the produced and received waveform between BBU and RRU/OFE.
Cost	High-costed APs are deployed.	Low-costed APs are deployed. However, it requires an additional high-costed CU deployment.
Energy-Efficiency	Regardless of number of connected UEs to the APs, each AP has to be active for system reliability. It causes high energy consumption.	In the case of low number of connected UEs, a set of BBUs can be turned-off, which provides an energy saving opportunity.
Fault Tolerance	A single point failure can be compensated by other APs.	A single point failure on CU causes system breakdown.
Inter-AP Optimization and Coordination Requirements	Optimization is done using the distributed algorithms implemented in each AP. They use pegged metrics in APs and a low-latency interfaces among APs are required to transfer information.	Optimization is done using centralized algorithms implemented in CU. They use pegged metrics related to APs, which are already available in CU. Therefore, coordination and joint processing that maximize the system performance are possible without any additional requirements.
System Upgrade	Addition of a new feature is done through multiple individual connections to APs.	Addition of a new feature can be done through a single connection to CU.

The upcoming IEEE standard on VLC [88] includes multiple PHY methods including variants of O-OFDM, different MIMO technologies, and relative adaptation between them. Implementation of all and switching between them according to the

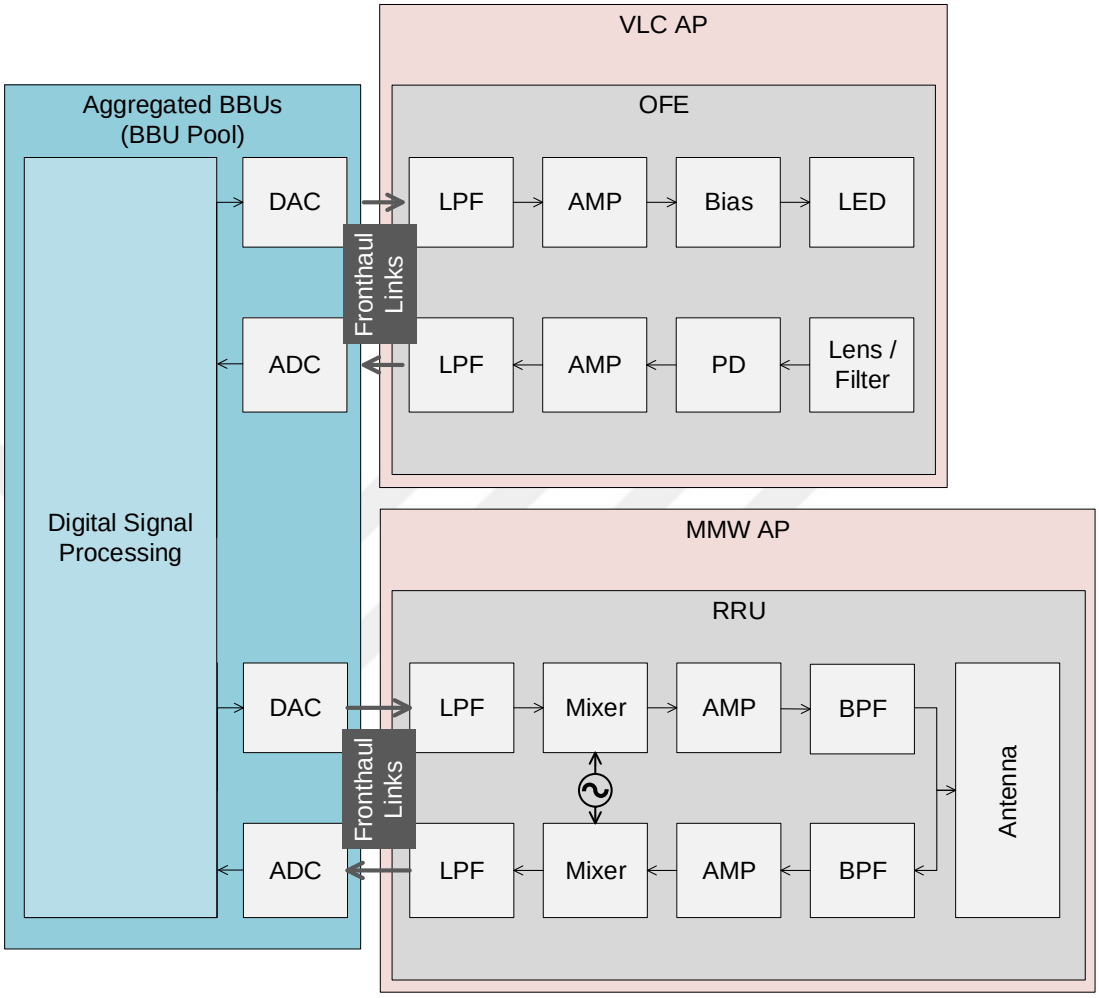

Figure 8: Structure of CU and APs in centralized architecture

varying network conditions to boost the network performance require additional computational storage and processing complexity. They can be handled with a single CU in which individual BBU resources are aggregated and virtualized for on-demand usage. Proposed architecture benefits to network performance via decreasing signal processing and power consumption for the under-utilized AP and giving more priority for over-utilized ones. Additionally, centralized awareness of channel and network indicators such as CSI, received signal level, SINR, traffic load etc. which have been already available in the distributed architecture, provides better optimization scenarios such as load balancing, handover management, interference-aware scheduling and

joint resource management etc.

The centralized processing also provides a open platform to implement advanced PHY and MAC techniques in indoor room environment in order to boost the network performance. Specifically, following use cases are run in CU and they are investigated in the rest of the dissertation:

- **SU distributed MIMO VLC system** uses individual LEDs as a single AP with distributed VLC transmitters (see Fig. 9). The signals transmitted and received through LEDs are jointly processed by the CU to serve a single UE equipped with multiple PDs. As a result of awareness of MIMO channel matrix, an ATC that is implemented in CU performs bit and power loading and adaptively selects the MIMO mode that maximizes the system performance.

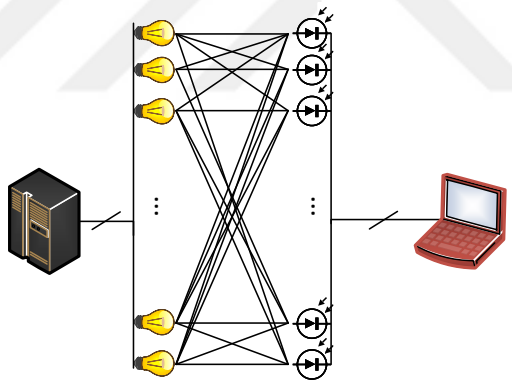

Figure 9: Use Case-1: SU distributed MIMO VLC system

- **MU massive MIMO VLC system** uses the massive number of LEDs as a single AP with distributed VLC transmitters (see Fig. 10). The signals transmitted and received through the LEDs are jointly processed by CU to serve multiple UEs through beamforming. In order to keep the DL and UL data rates at an acceptable level, a DPC that is implemented in CU further performs PA selection.

- **Hybrid MMW/VLC access system** considers each individual LED as a

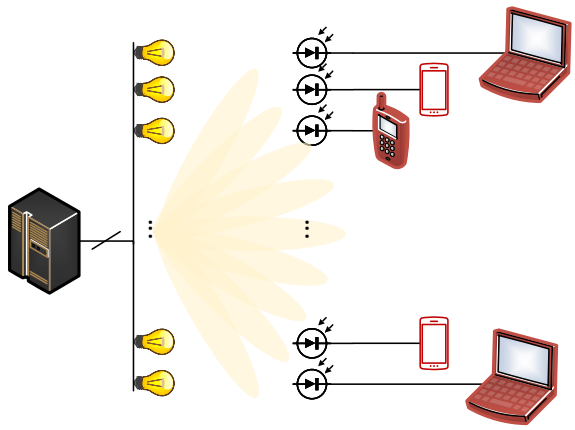

Figure 10: Use Case-2: MU massive MIMO VLC system

VLC AP with its own local coverage region (see Fig. 11) in addition to existing MMW AP that covers all indoor room environment. Under the consideration of over- and under-utilization conditions of VLC and MMW APs, an LB that is implemented in CU adaptively adjusts the handover parameters in order to increase the overall system performance as a result of awareness of global network view.

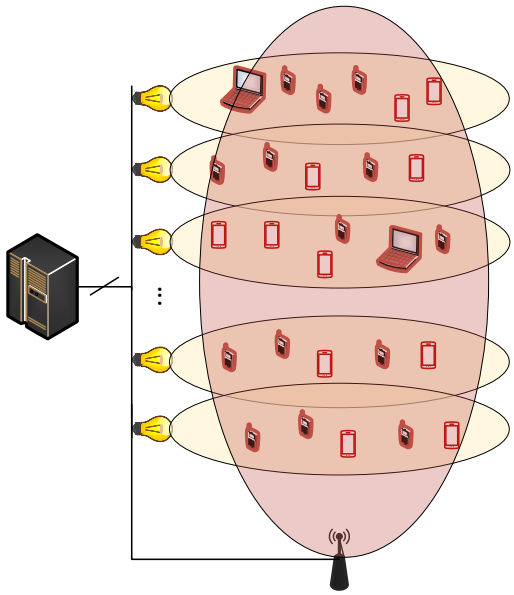

Figure 11: Use Case-3: Hybrid MMW/VLC access system

CHAPTER III

ADAPTIVE DISTRIBUTED MIMO OFDM VLC

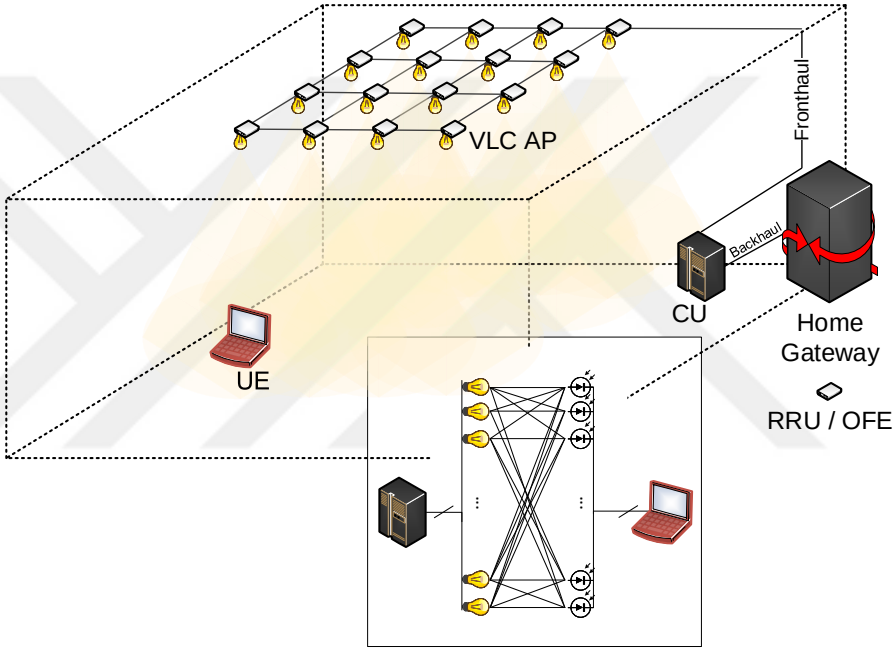

Figure 12: Distributed MIMO architecture in centralized platform

Utilizing the centralized network platform proposed in Chapter 2, an SU distributed MIMO OFDM-based VLC transmission is investigated in this chapter. The system architecture in which the distributed LEDs act as a single VLC AP with multiple distributed transmitters thanks to CU is depicted in Fig 12. The transmission system includes bit and power loading and switching between two different MIMO modes which are RC and SM in DL side.

ATC that is implemented inside the CU aims to maximize DL data rate of VLC

The content and results have been partially published in [55, 89].

transmission. For this purpose, it performs bit and power loading schemes in conjunction with MIMO switching under the consideration of DL MIMO VLC channel conditions that are measured by the UE and feedbacked to CU side. CU accordingly generates the waveform to be transmitted and forwards the transmission parameters to UE through a dedicated DL control channel for further decoding.

The remaining of the chapter is organized as following: DL system model is explained in Section 3.1. In Section 3.2, adaptive algorithms to boost the network performance are proposed and their performance results are demonstrated in Section 3.3.

3.1 Downlink System Model

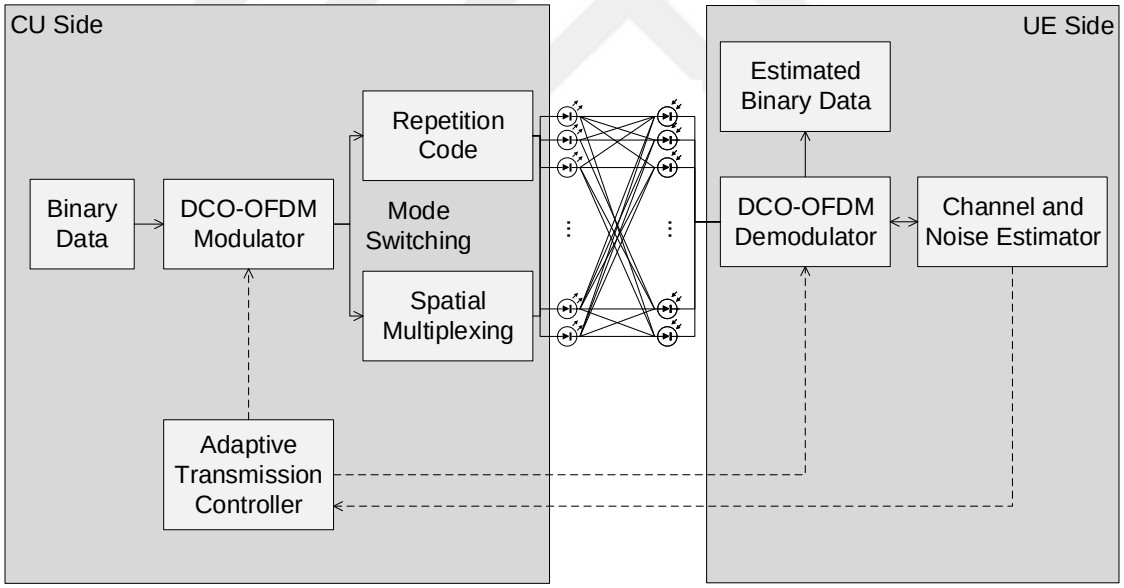

Figure 13: Adaptive SU DL MIMO-OFDM VLC system

DL system model under consideration is illustrated in Fig. 13 in which the MIMO system includes totally $N_{\text{VLC}}^{\text{LED}}$ LEDs, connected to CU through fronthaul links and locating at the ceiling, and totally $N_{\text{VLC}}^{\text{PD}}$ receiver components (e.g., PDs) available in the UE side[1]. Let i and u refer to any individual LED and PD, respectively,

[1]It is assumed that $N_{\text{VLC}}^{\text{PD}}$ is greater than or equal to $N_{\text{VLC}}^{\text{LED}}$.

where $i \in \{1, 2...N_{\text{VLC}}^{\text{LED}}\}$ and $u \in \{1, 2...N_{\text{VLC}}^{\text{PD}}\}$. Direct current biased optical OFDM (DCO-OFDM), a modified version of conventional OFDM to handle with IM/DD requirements, is employed in DL PHY. Let $\mathbf{H}^{\text{VLC}}$ denote the four-dimensional channel matrix where the dimensions are the LEDs, PDs, subcarriers, and sub-frames (or time slots). Each element of the channel matrix (e.g., channel coefficient between i^{th} LED and u^{th} PD at k^{th} subcarrier and τ^{th} sub-frame) is denoted by $H_{u,i}^{\text{VLC}-k,\tau}$ where $k \in \{0, 1..N_{\text{VLC}}^{\text{SBC}} - 1\}$, $N_{\text{VLC}}^{\text{SBC}}$ is the total number of subcarriers, $\tau \in \{0, 1..T_{\text{VLC}} - 1\}$, and T_{VLC} is the total number of sub-frames in a single DCO-OFDM frame.

The DL MIMO system utilized in the chapter is able to work in either RC or SM mode. The DCO-OFDM block diagram with RC mode where each LED is fed by the same signal is depicted in Fig. 14.

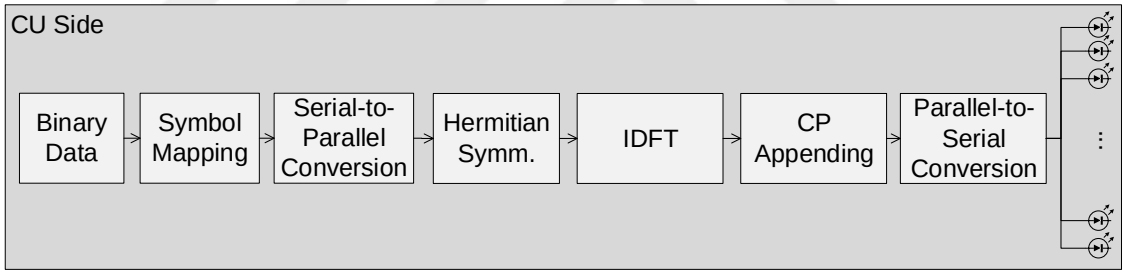

Figure 14: Block diagram of DCO-OFDM with RC MIMO mode in CU side

The bit-stream of the UE is firstly converted to complex-valued modulation symbols based on the modulation schema (e.g., binary phase-shift keying (PSK) or $M-$ary quadrature amplitude modulation (QAM) constellations) that is adaptively selected by the ATC among total of $M_{\text{MAX}} = \log_2 [\max(M)]$ different modulation schemes after allocating different electrical power to each subcarrier, denoted by $P_{\text{VLC}}^{k,\tau}$, based on channel conditions. The complex-valued symbol sequence that is transmitted by the LEDs at the τ^{th} sub-frame is denoted by $s^{1,\tau}\ s^{2,\tau}\ ...\ s^{N_{\text{VLC}}^{\text{SBC}}/2-1,\tau}$. To make the output of inverse discrete Fourier transform (IDFT) real valued, which is a constraint

of IM/DD, the sequence is re-arranged to satisfy Hermitian symmetry such as

$$\mathbf{X}^{\mathrm{VLC}-\tau} = [0\ s^{1,\tau}\ s^{2,\tau}\ ...\ s^{N_{\mathrm{VLC}}^{\mathrm{SBC}}/2-1,\tau}\ 0\ s^{N_{\mathrm{VLC}}^{\mathrm{SBC}}/2-1,\tau^*}\ ...\ s^{2,\tau^*}\ s^{1,\tau^*}]^{\mathrm{T}}, \tag{1}$$

where $[.]^{\mathrm{T}}$ denotes transpose operation and $(.)^*$ is complex conjugate operation. The output of $N_{\mathrm{VLC}}^{\mathrm{SBC}}-$IDFT can be written as

$$x^{\mathrm{VLC}-n,\tau} = \frac{1}{\sqrt{N_{\mathrm{VLC}}^{\mathrm{SBC}}}} \sum_{k=0}^{N_{\mathrm{VLC}}^{\mathrm{SBC}}-1} X^{\mathrm{VLC}-k,\tau} e^{j\frac{2\pi nk}{N_{\mathrm{VLC}}^{\mathrm{SBC}}}}. \tag{2}$$

To compensate the intersymbol interference (ISI), a cyclic prefix (CP) with the length of $N_{\mathrm{CP}-\mathrm{VLC}}$ which is selected to be longer than or equal to the multipath channel spread is appended to the beginning of the resulting sequence and the parallel streams are converted to serial. The signal is then DC-biased with bias-tee to keep the signal in dynamic range of LEDs and the biased signal drives the LEDs.

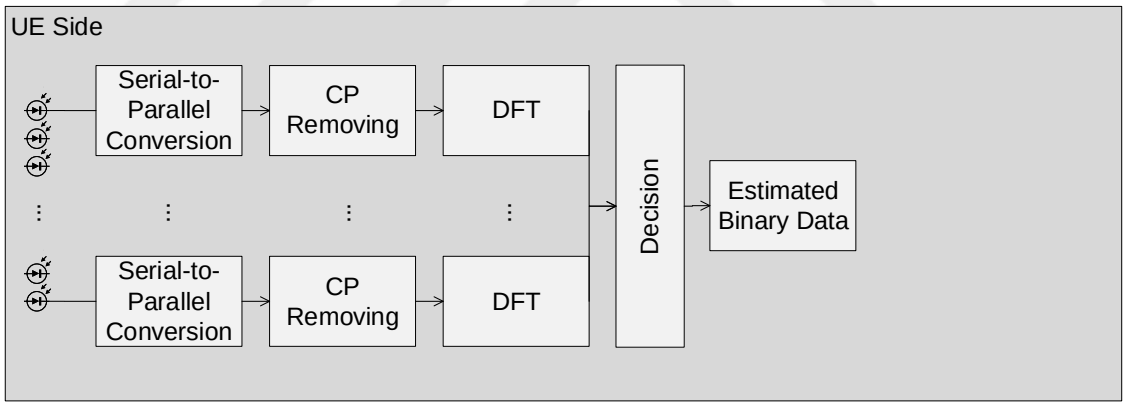

Figure 15: Block diagram of DCO-OFDM with RC MIMO mode in UE side

The block diagram of DCO-OFDM receiver with RC MIMO is depicted in Fig. 15. The time domain received signal at the u^{th} PD of a single UE, denoted by $y_u^{\mathrm{VLC}-n,\tau}$, is sampled with the period of $T_{\mathrm{S}-\mathrm{VLC}}$ and converted to discrete sequence. The serial streams are converted to parallel and the CP is removed. Then, $N_{\mathrm{VLC}}^{\mathrm{SBC}}-$point discrete Fourier transform (DFT) is applied over the resulting signal such as

$$Y_u^{\mathrm{VLC}-k,\tau} = \frac{1}{\sqrt{N_{\mathrm{VLC}}^{\mathrm{SBC}}}} \sum_{n=0}^{N_{\mathrm{VLC}}^{\mathrm{SBC}}-1} y_u^{\mathrm{VLC}-n,\tau} e^{-j\frac{2\pi nk}{N_{\mathrm{VLC}}^{\mathrm{SBC}}}}. \tag{3}$$

The output of $N_{\mathrm{VLC}}^{\mathrm{SBC}}-$DFT can be expressed in terms of transmitted sequence and channel matrix, such as,

$$Y_u^{\mathrm{VLC}-k,\tau} = R\sum_{i=1}^{N_{\mathrm{VLC}}^{\mathrm{LED}}}\sqrt{P_{\mathrm{VLC}}^{k,\tau}}X^{\mathrm{VLC}-k,\tau}H_{u,i}^{\mathrm{VLC}-k,\tau} + W_u^{\mathrm{VLC}-k,\tau}, \tag{4}$$

where R is the responsivity of the PD and $W_u^{\mathrm{VLC}-k,\tau}$ is additive white Gaussian noise (AWGN) with zero mean and variance of $\sigma_{\mathrm{VLC}}^2 = N_0 B_{\mathrm{VLC}}$ in which N_0 is noise power spectral density (PSD) and B_{VLC} is equal to $1/2T_{\mathrm{S-VLC}}$ using Nyquist rate.

Under the consideration of the fact that channel coefficients are perfectly estimated in the receiver side, Maximum-Likelihood (ML) decision rule is then applied in order to decode the transmitted symbols. The decision rule can be written as

$$\hat{X}^{\mathrm{VLC}-k,\tau} = \underset{x\in\Theta}{\operatorname{argmin}}\sum_{u=1}^{N_{\mathrm{VLC}}^{\mathrm{PD}}}\left\| Y_u^{\mathrm{VLC}-k,\tau} - xR\sum_{i=1}^{N_{\mathrm{VLC}}^{\mathrm{LED}}}\sqrt{P_{\mathrm{VLC}}^{k,\tau}}H_{u,i}^{\mathrm{VLC}-k,\tau}\right\|^2, \tag{5}$$

where Θ is the set of modulation symbols in selected modulation scheme. The resulting bit-error-rate (BER) in terms of selected modulation of M and SNR can be written as [90]

$$\mathrm{BER}(\mathrm{SNR},M) \approx \begin{cases} Q\left(\sqrt{2\mathrm{SNR}}\right) & , \quad 2-\mathrm{PSK} \\ \frac{2\left(\sqrt{M}-1\right)}{\sqrt{M}\log_2\sqrt{M}}Q\left(\sqrt{\frac{3\mathrm{SNR}}{M-1}}\right) & , \quad \text{square } M-\mathrm{QAM} \\ \frac{2}{\log_2(U\times J)}\left[\frac{U-1}{U}Q\left(\sqrt{\frac{6\mathrm{SNR}}{U^2+J^2-2}}\right)+\frac{J-1}{J}Q\left(\sqrt{\frac{6\mathrm{SNR}}{U^2+J^2-2}}\right)\right] & , \quad \text{rectangular } M=U\times J-\mathrm{QAM} \end{cases}, \tag{6}$$

where $Q(.)$ is the tail probability of standard normal distribution. The SNR at the k^{th} subcarrier and τ^{th} sub-frame can be written as

$$\mathrm{SNR}_{\mathrm{RC}}^{\mathrm{VLC}-k,\tau} = \frac{R^2 P_{\mathrm{VLC}}^{k,\tau}}{\sigma_{\mathrm{VLC}}^2}\sum_{u=1}^{N_{\mathrm{VLC}}^{\mathrm{PD}}}\left|\sum_{i=1}^{N_{\mathrm{VLC}}^{\mathrm{LED}}}H_{u,i}^{\mathrm{VLC}-k,\tau}\right|^2. \tag{7}$$

In SM mode whose block diagram is given in Fig. 16, the symbol sequence is multiplexed in the spatial domain, such as, $s_i^{1,\tau}\ s_i^{2,\tau}\ ...\ s_i^{N_{\mathrm{VLC}}^{\mathrm{SBC}}/2-1,\tau}$. Different electrical power, denoted by $P_{\mathrm{VLC}-i}^{k,\tau}$, is allocated to the k^{th} subcarrier of the i^{th} LED at τ^{th}

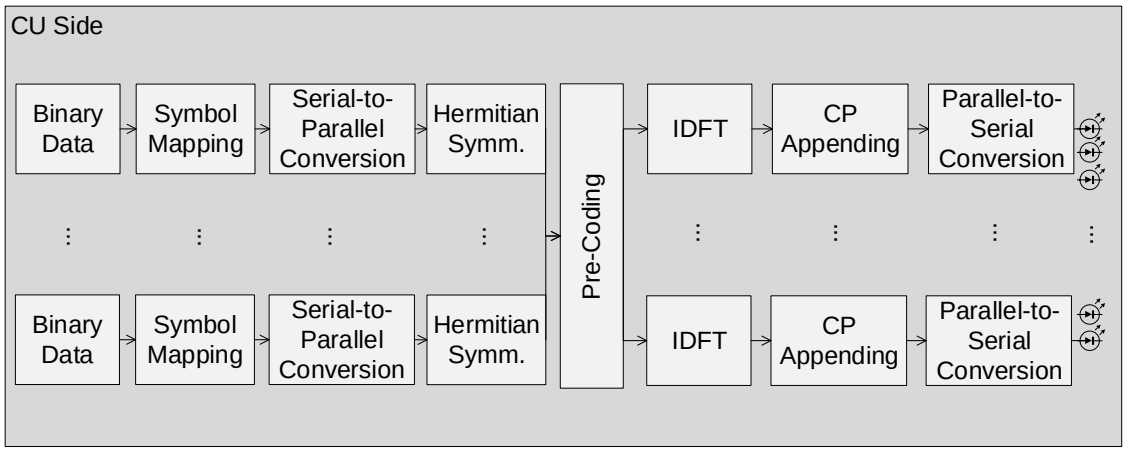

Figure 16: Block diagram of DCO-OFDM with SM MIMO mode in CU side

sub-frame as a result of ATC decision and Hermitian symmetry is imposed over the sequence as

$$\mathbf{X}_i^{\mathrm{VLC}-\tau} = [0\ s_i^{1,\tau}\ s_i^{2,\tau}\ ...\ s_i^{N_{\mathrm{VLC}}^{\mathrm{SBC}}/2-1,\tau}\ 0\ s_i^{N_{\mathrm{VLC}}^{\mathrm{SBC}}/2-1,\tau^*}\ ...\ s_i^{2,\tau^*}\ s_i^{1,\tau^*}]^{\mathrm{T}}. \tag{8}$$

As a difference from RC mode, each LED transmits different information to the receiver side. To handle with the co-channel interference, pre- and post-coding are applied before IDFT at the transmitter side and after DFT at the receiver side, respectively. The pre-coding process can be expressed as

$$\tilde{\mathbf{X}}^{\mathrm{VLC}-k,\tau} = \mathbf{V}^{\mathrm{VLC}-k,\tau}\mathbf{X}^{\mathrm{VLC}-k,\tau}, \tag{9}$$

where $\mathbf{V}^{\mathrm{VLC}-k,\tau}$ denotes unitary matrix that is obtained through SVD of channel matrix at k^{th} subcarrier and τ^{th} sub-frame, i.e.,

$$\mathbf{H}^{\mathrm{VLC}-k,\tau} = \mathbf{U}^{\mathrm{VLC}-k,\tau}\mathbf{S}^{\mathrm{VLC}-k,\tau}\mathbf{V}^{\mathrm{VLC}-k,\tau^{\mathrm{H}}}, \tag{10}$$

where $[.]^{\mathrm{H}}$ is the Hermitian operation and the input vector is in the form of

$$\mathbf{X}^{\mathrm{VLC}-k,\tau} = [X_1^{\mathrm{VLC}-k,\tau}\ X_2^{\mathrm{VLC}-k,\tau}\ ...\ X_{N_{\mathrm{VLC}}^{\mathrm{LED}}}^{\mathrm{VLC}-k,\tau}]^{\mathrm{T}}. \tag{11}$$

$N_{\mathrm{VLC}}^{\mathrm{SBC}}-$IDFT process is then applied for each i such as,

$$\tilde{x}_i^{\mathrm{VLC}-n,\tau} = \frac{1}{\sqrt{N_{\mathrm{VLC}}^{\mathrm{SBC}}}} \sum_{k=0}^{N_{\mathrm{VLC}}^{\mathrm{SBC}}-1} \tilde{X}_i^{\mathrm{VLC}-k,\tau} e^{j\frac{2\pi nk}{N_{\mathrm{VLC}}^{\mathrm{SBC}}}}. \tag{12}$$

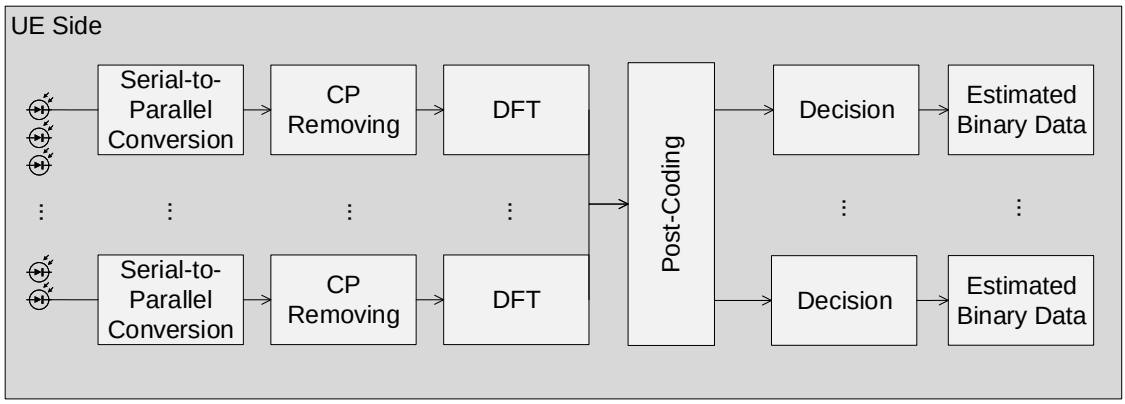

Figure 17: Block diagram of DCO-OFDM with SM MIMO mode in UE side

As in RC mode, a CP is appended and the parallel streams are converted to serial. The i^{th} signal sequence is then fed to the i^{th} LED.

In the receiver side (see Fig. 17), $N_{\text{VLC}}^{\text{SBC}}-$DFT is performed for each signal at the u^{th} PD of a single UE and the resulting signal at the k^{th} subcarrier of the τ^{th} sub-frame can be written as

$$\tilde{Y}_u^{\text{VLC}-k,\tau} = R \sum_{i=1}^{N_{\text{VLC}}^{\text{LED}}} \sqrt{P_{\text{VLC}-i}^{k,\tau}} \tilde{X}_i^{\text{VLC}-k,\tau} H_{u,i}^{\text{VLC}-k,\tau} + W_u^{\text{VLC}-k,\tau}. \tag{13}$$

The post-processing is then applied such as

$$\mathbf{Y}^{\text{VLC}-k,\tau} = \mathbf{U}^{\text{VLC}-k,\tau\text{H}} \tilde{\mathbf{Y}}^{\text{VLC}-k,\tau}, \tag{14}$$

where the input vector is in the form of

$$\mathbf{Y}^{\text{VLC}-k,\tau} = [Y_1^{\text{VLC}-k,\tau}\ Y_2^{\text{VLC}-k,\tau}\ ...\ Y_{N_{\text{VLC}}^{\text{PD}}}^{\text{VLC}-k,\tau}]^{\text{T}}, \tag{15}$$

and the resulting signal related to the i^{th} LED on the k^{th} subcarrier becomes

$$Y_i^{\text{VLC}-k,\tau} = R\sqrt{P_{\text{VLC}-i}^{k,\tau}} X_i^{\text{VLC}-k,\tau} S_{i,i}^{\text{VLC}-k,\tau} + \tilde{W}_i^{\text{VLC}-k,\tau}, \tag{16}$$

where

$$\tilde{\mathbf{W}}^{\text{VLC}-k,\tau} = \mathbf{U}^{\text{VLC}-k,\tau\text{H}} \mathbf{W}^{\text{VLC}-k,\tau}. \tag{17}$$

It should be noted that distribution of the noise does not change after multiplication by a unitary matrix. Under the consideration of perfectly known channel matrix, ML

decision rule is then applied in order to decode the transmitted symbols, which can be written as

$$\hat{X}_i^{\mathrm{VLC}-k,\tau} = \underset{x\in\Theta}{\operatorname{argmin}} \left\| Y_i^{\mathrm{VLC}-k,\tau} - xR\sqrt{P_{\mathrm{VLC}-i}^{k,\tau}} S_{i,i}^{\mathrm{VLC}-k,\tau} \right\|^2. \tag{18}$$

The resulting BER is expressed with the same formula given in Eq. 6 and SNR at the k^{th} subcarrier of the i^{th} LED becomes

$$\mathrm{SNR}_{\mathrm{SM-i}}^{\mathrm{VLC}-k,\tau} = \frac{P_{\mathrm{VLC}-i}^{k,\tau} R^2 |S_{i,i}^{\mathrm{VLC}-k,\tau}|^2}{\sigma_{\mathrm{VLC}}^2}. \tag{19}$$

3.2 Adaptive Algorithm Design

The ATC aims to boost the DL network performance in terms of data rate through proper selection of modulation order and power level at each subcarrier, that provides the highest data rate under target BER (denoted by BER_t) constraint in both RC and SM MIMO modes. In SM mode, power levels and modulation orders are also differentiated in the spatial domain. The controller then selects the MIMO mode that maximizes system data rate. For this purpose, optimization problem can be formulated for each sub-frame as

$$\max \left\{ \max_{P_{\mathrm{VLC}}^{k,\tau}, M_{\mathrm{RC}}^{\mathrm{VLC}-k,\tau}} \left(\sum_{k=1}^{N_{\mathrm{VLC}}^{\mathrm{SBC}}/2-1} \log_2 M_{\mathrm{RC}}^{\mathrm{VLC}-k,\tau} \right), \right. \tag{20}$$
$$\left. \max_{P_{\mathrm{VLC}-i}^{k,\tau}, M_{\mathrm{SM}}^{\mathrm{VLC}-k,\tau}} \left(\sum_{i=1}^{N_{\mathrm{VLC}}^{\mathrm{LED}}} \sum_{k=1}^{N_{\mathrm{VLC}}^{\mathrm{SBC}}/2-1} \log_2 M_{\mathrm{SM}-i}^{\mathrm{VLC}-k,\tau} \right) \right\}$$

such that

$$0 \le \left(\sum_{i=1}^{N_{\mathrm{VLC}}^{\mathrm{LED}}} \sum_{k=1}^{N_{\mathrm{VLC}}^{\mathrm{SBC}}/2-1} P_{\mathrm{VLC}-i}^{k,\tau} \right) \le P_{\mathrm{VLC}}^{\mathrm{MAX}} \tag{21}$$

$$\mathrm{BER}_i^{k,\tau} \le \mathrm{BER}_t \text{ or } \mathrm{BER}_i^{k,\tau} \text{ is null for SM} \tag{22}$$

$$\mathrm{BER}^{k,\tau} \le \mathrm{BER}_t \text{ or } \mathrm{BER}^{k,\tau} \text{ is null for RC} \tag{23}$$

$$P_{\mathrm{VLC}}^{k,\tau} = P_{\mathrm{VLC}-i}^{k,\tau} \; \forall \; i \text{ for RC} \tag{24}$$

where $P_{\mathrm{VLC}}^{\mathrm{MAX}}$ is the total power budget available in CU side for one DL transmission sub-frame. The first term in Eq. 20 is related to the data rate of RC, whose full-expression using the ergodic capacity defined in [91] can be written as

$$D_{\mathrm{RC}}^{\mathrm{VLC}-\tau} = \frac{N_{\mathrm{VLC}}^{\mathrm{SBC}}}{(N_{\mathrm{VLC}}^{\mathrm{SBC}} + N_{\mathrm{CP-VLC}})} \sum_{k=1}^{N_{\mathrm{VLC}}^{\mathrm{SBC}}/2-1} \Delta_{\mathrm{VLC}}^{\mathrm{SBC}} \times \log_2 M_{\mathrm{RC}}^{\mathrm{VLC}-k,\tau} \text{ bits/s}, \quad (25)$$

where $M_{\mathrm{RC}}^{\mathrm{VLC}-k,\tau}$ is the highest modulation order that satisfies the BER_t under the consideration of allocated power level (e.g., $P_{\mathrm{VLC}}^{k,\tau} = P_{\mathrm{VLC}-i}^{k,\tau} \ \forall \ i$) based on channel conditions at the k^{th} subcarrier and $\Delta_{\mathrm{VLC}}^{\mathrm{SBC}}$ is subcarrier spacing.

The second term in Eq. 20 is related to the data rate of SM, whose full-expression using the ergodic capacity defined in [91] can be written as

$$D_{\mathrm{SM}}^{\mathrm{VLC}-\tau} = \frac{N_{\mathrm{VLC}}^{\mathrm{SBC}}}{(N_{\mathrm{VLC}}^{\mathrm{SBC}} + N_{\mathrm{CP-VLC}})} \sum_{i=1}^{N_{\mathrm{VLC}}^{\mathrm{LED}}} \sum_{k=1}^{N_{\mathrm{VLC}}^{\mathrm{SBC}}/2-1} \Delta_{\mathrm{VLC}}^{\mathrm{SBC}} \times \log_2 M_{\mathrm{SM}-i}^{\mathrm{VLC}-k,\tau} \text{ bits/s}, \quad (26)$$

where $M_{\mathrm{SM}-i}^{\mathrm{VLC}-k,\tau}$ is the highest modulation order that satisfies the BER_t under the consideration of allocated power level (e.g., $P_{\mathrm{VLC}-i}^{k,\tau}$) based on channel conditions at the k^{th} subcarrier and the i^{th} LED.

The optimization problem defined in Eq. 20 is equal to the selection of MIMO mode that provides the higher data rate after individual maximization of the data rates for RC (given by Eq. 25) and SM (given by Eq. 26) is completed. For this purpose, the Hughes-Hartogs algorithm, which is originally proposed for SISO systems [61] with the aim of bit and power loading, is enhanced in this chapter. The pseudo-code of enhanced version [89] is provided in Algorithm. 1 which has two different tuning parameters denoted by N_{HH} and U_{HH}, whose values are determined after several trials, and one configuration parameter that limits the maximum number of iteration, denoted by I_{HH} during power allocation phase. The other inputs of the algorithm are total power budget, denoted by $P_{\mathrm{VLC}}^{\mathrm{MAX}}$, maximum available modulation order, denoted by M_{MAX}, and subcarrier-based SNR information parameter, denoted by γ. For RC and SM modes, the latter parameter calculation for each sub-frame can

be written as

$$\gamma_{\mathrm{RC}}^{\mathrm{VLC}-k,\tau} = \frac{\sigma_{\mathrm{VLC}}^2}{R^2 \sum_{u=1}^{N_{\mathrm{VLC}}^{\mathrm{PD}}} \left| \sum_{i=1}^{N_{\mathrm{VLC}}^{\mathrm{LED}}} H_{u,i}^{\mathrm{VLC}-k,\tau} \right|^2}, \tag{27}$$

$$\gamma_{\mathrm{SM-i}}^{\mathrm{VLC}-k,\tau} = \frac{\sigma_{\mathrm{VLC}}^2}{R^2 |S_{i,i}^{\mathrm{VLC}-k,\tau}|^2}, \tag{28}$$

and the algorithm input becomes

$$\gamma_{\mathrm{RC}}^{\mathrm{VLC},\tau} = [\gamma_{\mathrm{RC}}^{\mathrm{VLC}-1,\tau} \ \gamma_{\mathrm{RC}}^{\mathrm{VLC}-2,\tau} \ \cdots \ \gamma_{\mathrm{RC}}^{\mathrm{VLC}-N_{\mathrm{VLC}}^{\mathrm{SBC}}/2-1,\tau}]^{\mathrm{T}}, \tag{29}$$

$$\gamma_{\mathrm{SM}}^{\mathrm{VLC},\tau} = [\gamma_{\mathrm{SM}-1}^{\mathrm{VLC}-\tau} \ \gamma_{\mathrm{SM}-2}^{\mathrm{VLC}-\tau} \ \cdots \ \gamma_{\mathrm{SM}-N_{\mathrm{VLC}}^{\mathrm{LED}}}^{\mathrm{VLC}-\tau}], \tag{30}$$

where

$$\gamma_{\mathrm{SM}-i}^{\mathrm{VLC}-\tau} = [\gamma_{\mathrm{SM}-i}^{\mathrm{VLC}-1,\tau} \ \gamma_{\mathrm{SM}-i}^{\mathrm{VLC}-2,\tau} \ \cdots \ \gamma_{\mathrm{SM}-i}^{\mathrm{VLC}-N_{\mathrm{VLC}}^{\mathrm{SBC}}/2-1,\tau}]^{\mathrm{T}} \ \forall \ i. \tag{31}$$

The selection of the parameters is summarized as following:

- The DL MIMO channel matrix between transmitter and receiver and noise power for each subcarrier are estimated with the use of pilot signals at UE side. The estimated coefficients and noise power level are feedbacked to the ATC through a dedicated UL channel. It should be noted that it is assumed that channel coefficients and noise power level are perfectly estimated in UE side and the information is feedbacked through a error-free link to the CU side in this chapter[2].

- Using an enhanced version of Hughes-Hartogs algorithm, bit and power loading under the consideration of BER_t and $P_{\mathrm{VLC}}^{\mathrm{MAX}}$ is completed for both RC and SM MIMO modes.

- The MIMO mode that provides the higher data rate is then selected.

[2]More practical approach in which channel estimation and interpolation errors are included can be found in Chapter 4.

Input: $P_{\mathrm{VLC}}^{\mathrm{MAX}}, \gamma, M_{\mathrm{MAX}}, I_{\mathrm{HH}}, N_{\mathrm{HH}}, U_{\mathrm{HH}}$
Output: $\mathbf{P}_{\mathrm{VLC}}$

Let R and C denote the row and column size of γ
Reshape γ to the dimension of 1 x $(R \times C)$
$B \leftarrow \log_2[0\ 1\ ...\ M_{\mathrm{MAX}}]$
$S_T \leftarrow$ target SNR value for each order: $[0\ 1\ ...\ M_{\mathrm{MAX}}]$
$\alpha_0 \leftarrow 0$
$\beta_0 \leftarrow 0$
$\alpha_1 = (P_{\mathrm{VLC}}^{\mathrm{MAX}} + \sum_i \gamma^i)/(R \times C)$
$m \leftarrow 0$
while $m < I_{\mathrm{HH}}$ **do**
    $m \leftarrow m + 1$
    foreach i in $\{1, 2..(R \times C)\}$ **do**
        $t \leftarrow \underset{j}{\mathrm{argmax}} \left\{ S_T^j \text{ where } S_T^j < \alpha_m/\gamma_i \right\}$
        $P_{\mathrm{VLC}}^i \leftarrow \gamma_i S_T^t$
        $R_B^i \leftarrow B_t$
    $P_T^m \leftarrow \sum_i P_{\mathrm{VLC}}^i$
    $\beta_m = \sum_i R_B^i$
    if $P_{\mathrm{VLC}}^{\mathrm{MAX}} - P_T^m \geq 0$ and $P_{\mathrm{VLC}}^{\mathrm{MAX}} - P_T^m \leq N_{\mathrm{HH}}\alpha_m$ **then**
        break
    else
        if $-N_{\mathrm{HH}}\alpha_m \leq P_{\mathrm{VLC}}^{\mathrm{MAX}} - P_T^m$ and $P_{\mathrm{VLC}}^{\mathrm{MAX}} - P_T^m < 0$ **then**
            $\alpha_{m+1} = \alpha_m - N_{\mathrm{HH}} \frac{\alpha_m - \alpha_{m-1}}{\beta_m - \beta_{m-1}}$
        else
            $\alpha_{m+1} = \alpha_m + U_{\mathrm{HH}} \frac{P_{\mathrm{VLC}}^{\mathrm{MAX}} - P_T^m}{\alpha_m} \frac{\alpha_m - \alpha_{m-1}}{\beta_m - \beta_{m-1}}$
reshape $\mathbf{P}_{\mathrm{VLC}}$ with the dimension of RxC

Algorithm 1: Enhanced Hughes-Hartogs Algorithm

- The selected transmission parameters are imported to DCO-OFDM modulator available in CU side and transmitted to DCO-OFDM demodulator available in UE side through a dedicated DL control channel using a certain set of subcarriers and sub-frames of DL frame for further decoding.

It should be also noted that in the case of when available $P_{\mathrm{VLC}}^{\mathrm{MAX}}$ level is not sufficient to satisfy BER_t using even lowest modulation (e.g., 2-PSK) for any MIMO

mode then, transmitter increases the available power level to initialize the transmission. Power increment process is then followed by the transmission parameter selection.

3.3 Performance Evaluations

In this section, the performance results of proposed DL adaptive system are demonstrated after the simulation environment is explained.

3.3.1 Simulation Environment

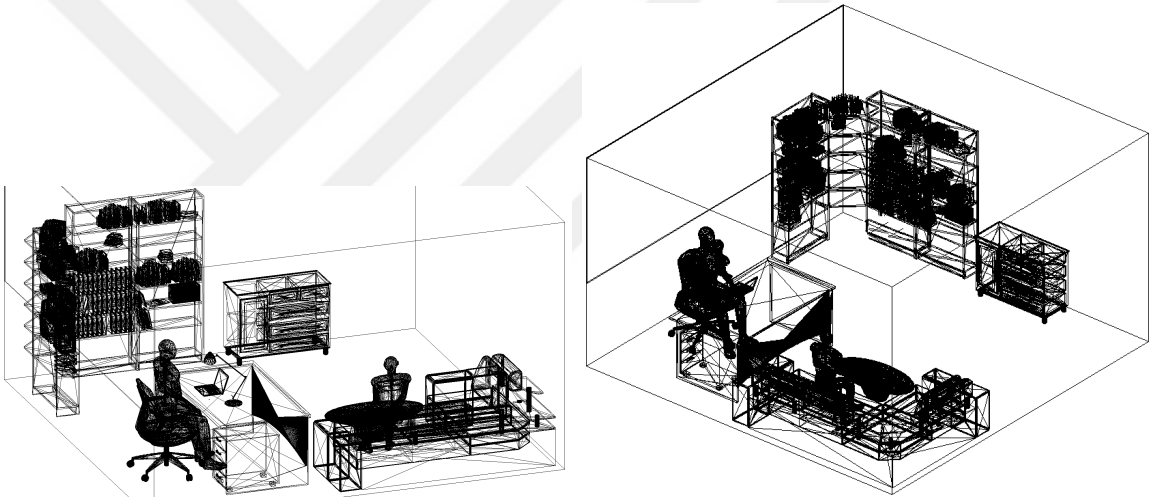

Figure 18: View of the office space under consideration

An indoor room environment with the size of 5 m $\times$ 5 m $\times$ 3 m is considered (see Fig. 18). $N_{\text{VLC}}^{\text{LED}} = N_{\text{VLC}}^{\text{PD}}$ is set to 16. The distance between two adjacent VLC LEDs is set to 1.4 m and the distance between the wall and LEDs is 0.4 m (see Fig. 19). It should be noted that, for typical indoor scenarios, the Illuminating Engineering Society (IES) Standard [92] suggests surface illumination levels between 100 lux and 1000 lux. Each LED is biased for 17 W that achieves illumination levels in the range of $365 - 612$ lux complying with the IES standard.

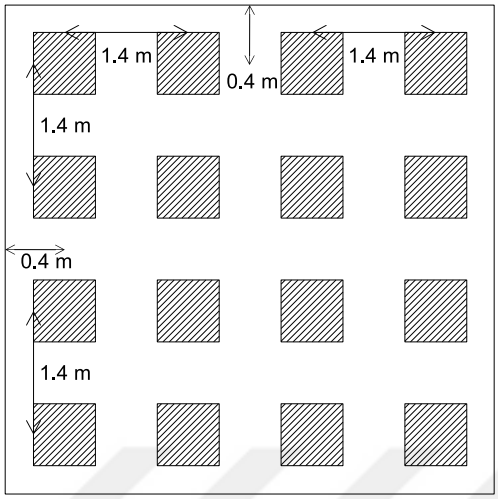

Figure 19: Arrangement of VLC LEDs

UE is considered as a laptop device with four different USB hubs, each is equipped with four PDs (see Fig. 20), each of which has a surface area of 0.07 cm^2. The separation between adjacent PDs is set to 5 cm. The channel matrix is obtained through following the ray-tracing method given in Appendix. A.1 using the specification given in Table 6. In order to extend typical modulation bandwidth (e.g., 2-3 MHz) of commercial white LR24-38SKA35 LED, blue filtering is applied at the receiver with a drawback of reducing the received optical power by 50% [93]. The UE is assumed to be fixed, thereby, the coefficients in $\mathbf{H}^{\mathrm{VLC}}$ do not vary with respect to τ.

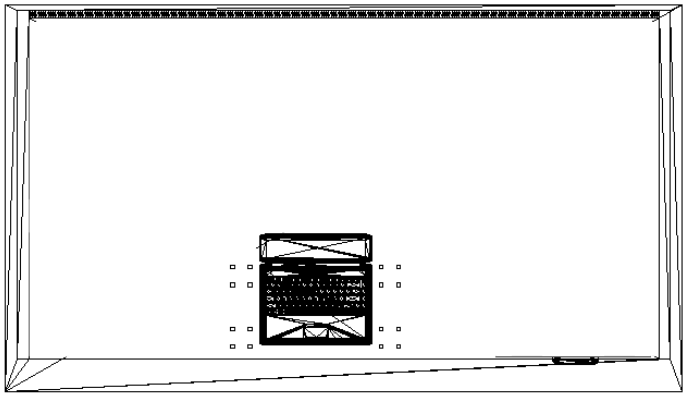

Figure 20: Top view of the desk with VLC PDs

Table 6: Indoor room model specifications

Materials	Walls: Plaster, Ceiling: Plaster, Floor: Pinewood, Desk: Pinewood,
Objects	1 desk and a chair paired with desk, 1 laptop on the desk, 1 desk light on the desk, 1 library, 1 couch, 1 coffee table, window, 2 human bodies
Object specifications	Desk: Pinewood (Height 0.88 m), Chair: Black gloss paint, Laptop: Black gloss paint Desk light: Black gloss paint, Library: Pinewood, Window: Glass Couch: Cotton, Coffee table: Pinewood Human body: Head & Hands (assumed to be absorbing), clothes (cotton), shoes (black gloss)
Luminary Specifications	Brand: LR24-38SKA35 Cree Inc. Half viewing angle: 40^{o}

Table 7: Simulation parameters of adaptive distributed MIMO OFDM VLC

Parameter	**Value**
LED cut-off frequency ($f_{3-\mathrm{dB}}$)	10 MHz
PD responsivity (R)	0.28 A/W [93]
Noise PSD (N_0)	10^{-22} W/Hz [93]
CP length in VLC sub-frame ($N_{\mathrm{CP-VLC}}$)	48
VLC system bandwidth (B_{VLC})	100 MHz
Number of sub-frames in DL frame T_{VLC}	200
Number of subcarriers in DL sub-frame ($N_{\mathrm{VLC}}^{\mathrm{SBC}}$)	1024
Subcarrier spacing in DL sub-frame ($\Delta_{\mathrm{VLC}}^{\mathrm{SBC}}$)	195.31 kHz
Target BER (BER_t)	10^{-5}
N_{HH}	4
U_{HH}	0.8
I_{HH}	150

The simulation parameters are summarized as Table 7 and 2-PSK, 4-QAM, 8-QAM, ..., 4096-QAM are defined as a set of modulation schemes. For adaptive algorithm in DL side, minimum required SNR value of each modulation order for BER_t

Table 8: Minimum required SNR levels for target BER.

SNR Levels	**Modulation Order**
-	not-used
9.59	2-PSK
12.60	4-QAM
17.29	8-QAM
19.46	16-QAM
23.54	32-QAM
25.57	64-QAM
29.53	128-QAM
31.53	256-QAM
35.47	512-QAM
37.47	1024-QAM
41.41	2048-QAM
43.41	4096-QAM

is depicted in Table 8 in which the values are calculated using Eq. 6. The minimum required SNR values are also used as S_T in Algorithm. 1. The performance results are depicted in terms of $P_{\text{VLC}}^{\text{MAX}}$ and channel coefficients at DC subcarrier, which can be written as

$$\text{SNR}_{\text{RX}} = \frac{P_{\text{VLC}}^{\text{MAX}} R^2}{(N_{\text{VLC}}^{\text{SBC}}/2 - 1) N_{\text{VLC}}^{\text{LED}} \sigma_{\text{VLC}}^2} \sum_{u=1}^{N_{\text{VLC}}^{\text{PD}}} \left| \sum_{i=1}^{N_{\text{VLC}}^{\text{LED}}} H_{u,i}^{\text{VLC}-0} \right|^2 . \tag{32}$$

3.3.2 Numerical Results

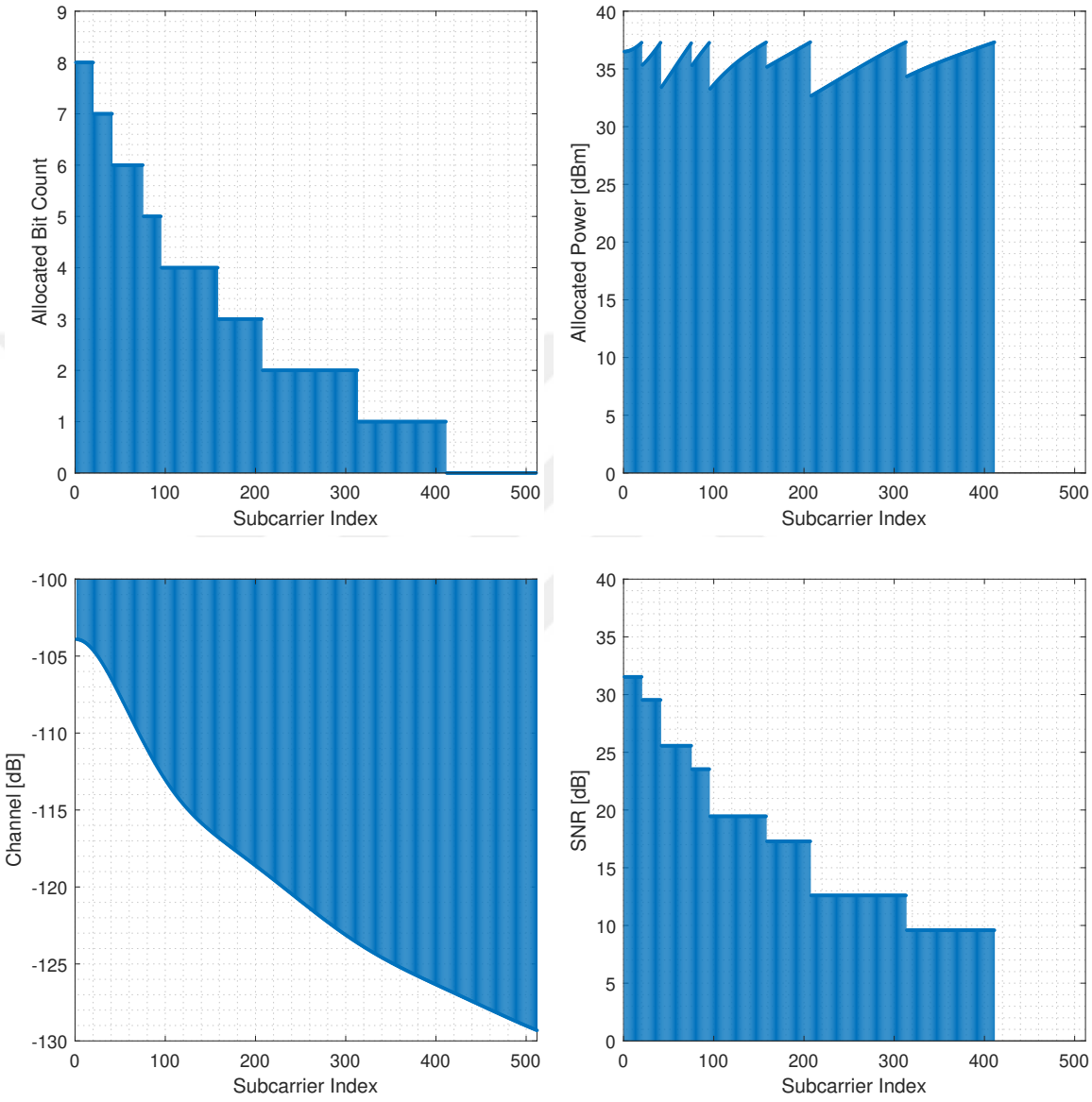

Figure 21: Bit and power loading with P_{MAX} of 74 dBm

Bit and power loading across the subcarriers as a result of enhanced Hughes-Hartogs algorithm is depicted in Fig. 21 where RC MIMO is considered and P_{MAX} is set to 74 dBm. The channel varies between approximately -104 dB and -129 dB. The results reveal that subcarrier-based SNR level with the value of 31.53 dB is achieved with power loading scheme, which yields 256-QAM deployment at the subcarriers

with the indexes between 1 and 20. As a result of relatively higher attenuation, 128-QAM is utilized in the subcarriers between 21 and 41. For the higher part of the spectrum, the order of deployed modulation is decreased, e.g., 64-QAM for the range of 42-75, 32-QAM for 76-95 etc. are selected. Additionally, the subcarriers with the indexes between 411 and 511 are not used to carry UE data for given P_{MAX} value.

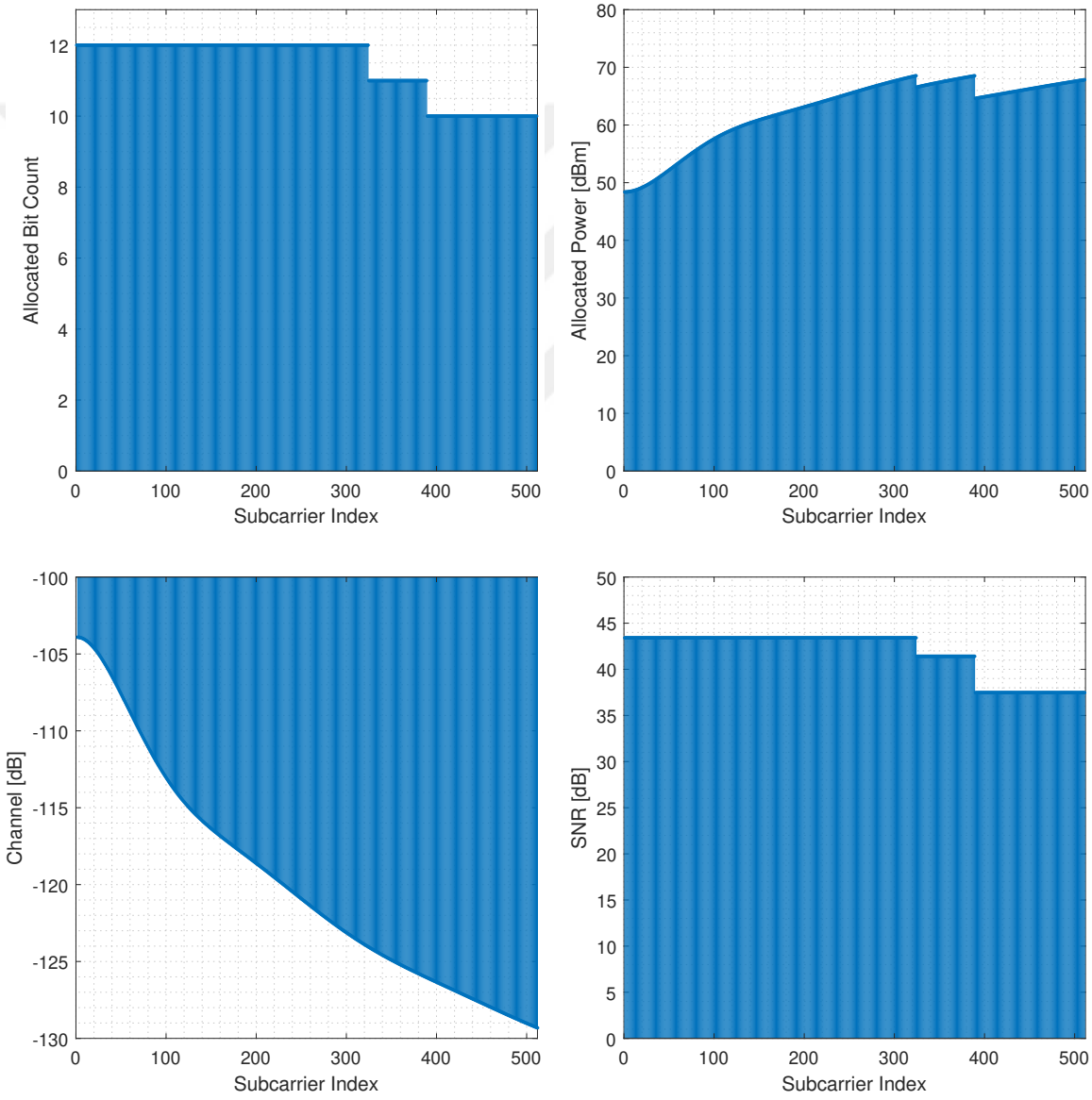

Figure 22: Bit and power loading with P_{MAX} of 104 dBm

In Fig. 22, similar analysis is conducted for increased P_{MAX} value such as 104 dBm.

It can be seen that 4096-QAM is employed in the subcarriers with the indexes between 1 and 324 as a result of obtained SNR value of 43.41 dB with power allocation algorithm. Since the channel gain is relatively higher at the low part of these subcarriers and they are already utilized with the highest available modulation order, the allocated power levels are relatively less than the values in the remaining ones.

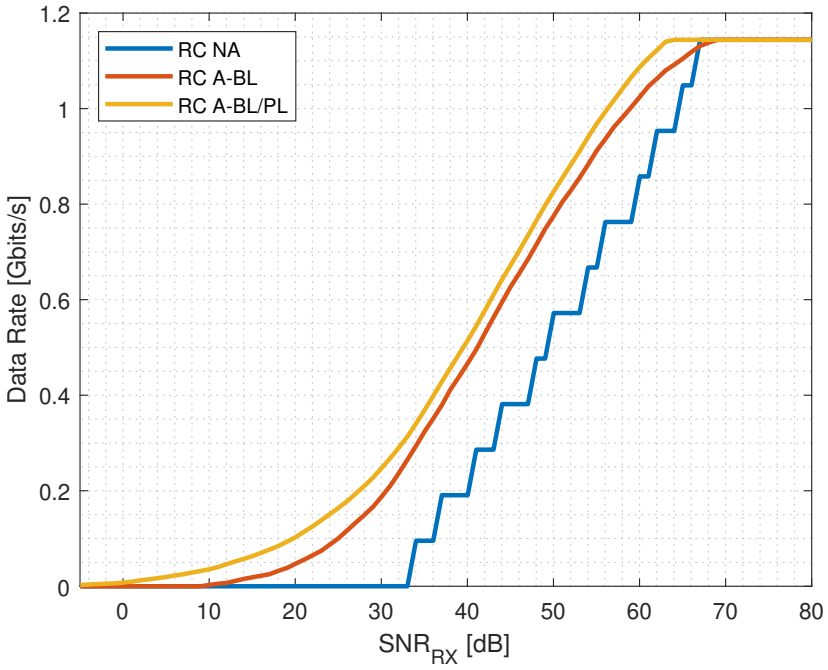

Figure 23: Data rate of DL RC MIMO mode with bit and/or power loading

The data rate performance of adaptive RC mode MIMO OFDM-based DL transmission is presented in Fig. 23. As benchmark, following scenarios are considered:

- NA transmission in which modulation order is selected based on overall BER across all subcarriers instead of evaluation per subcarrier. Therefore, the highest modulation order that satisfies the target BER is set to all of the subcarriers.

- A-BL transmission in which modulation order is subcarrier-based selected using the BER at each subcarrier with equal power allocation.

NA starts the transmission at $\mathrm{SNR_{RX}}$ level of 34.03 dB with 2-PSK deployment

across all subcarriers and the data rate of 95.33 Mbps is achieved. At this point, A-BL has the data rate of 293.84 Mbits/s as a result of independent usage of the subcarriers that satisfy the target BER constraint. The value is further increased to 340.67 Mbps with the use of power loading scheme. On the other hand, both NA and A-BL transmissions are silent for SNR_{RX} less than 10 dB and they do not transmit any information to UE side, whereas, proposed adaptive bit and loading algorithm is able to work in this SNR_{RX} region as a result of additional gain coming from power loading scheme. At the SNR_{RX} value of 10 dB, enhanced Hughes-Hartogs algorithm, depicted by A-BL/PL, provides the data rate of 35.63 Mbits/s. It should be also noted that RC mode with the use of NA and A-BL saturates at SNR_{RX} value of 67.03 dB where 4096-QAM is used at all of the subcarriers. The saturation point for A-BL/PL is 63.03 dB, where maximum achievable data rate with the value of 1.14 Gbits/s is observed.

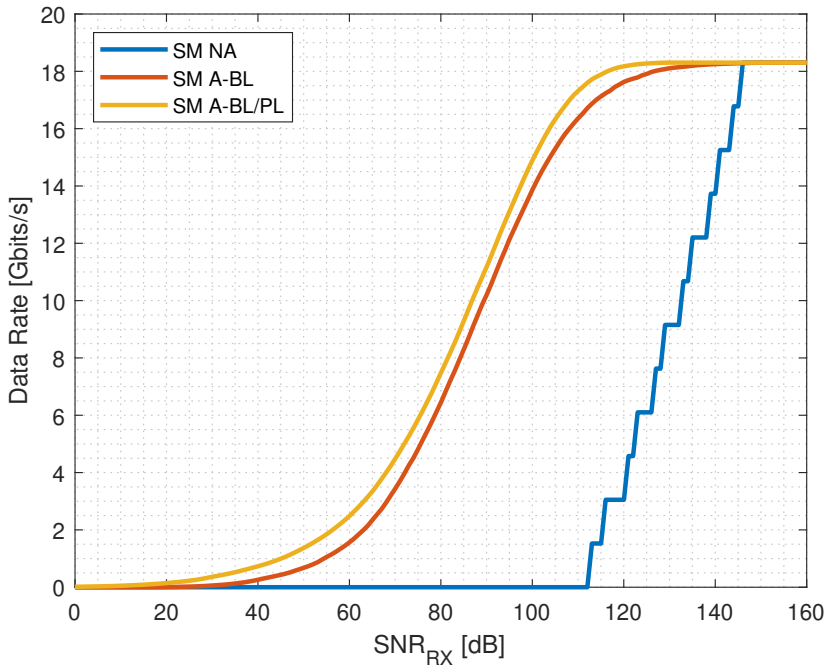

Figure 24: Data rate of DL SM MIMO mode with bit and/or power loading

The data rate performance of adaptive SM mode MIMO OFDM-based DL transmission is presented in Fig. 24. Same benchmark transmissions are considered while evaluating SM mode. As in RC mode, it can be observed that most of the gain is resulted by bit-loading (see A-BL). Numerically, NA starts the transmission at $\mathrm{SNR_{RX}}$ of 113.03 dB with the data rate of 1.52 Gbps, whereas, this level is equal to 20.03 dB for A-BL. It refers to 93 gain in terms of $\mathrm{SNR_{RX}}$ for data transmission. Furthermore, power loading with the use of enhanced Hughes-Hartogs algorithm (A-BL/PL) provides an additional gain with the amount of approximately 21 dB. It should be also noted that SM mode with the use of A-BL/PL saturates at $\mathrm{SNR_{RX}}$ value of 128.03 dB where 4096-QAM is used at all subcarriers. The saturation point for NA transmission is 146.03 dB. At this point, maximum achievable data rate with the value of 18.3 Gbits/s is observed.

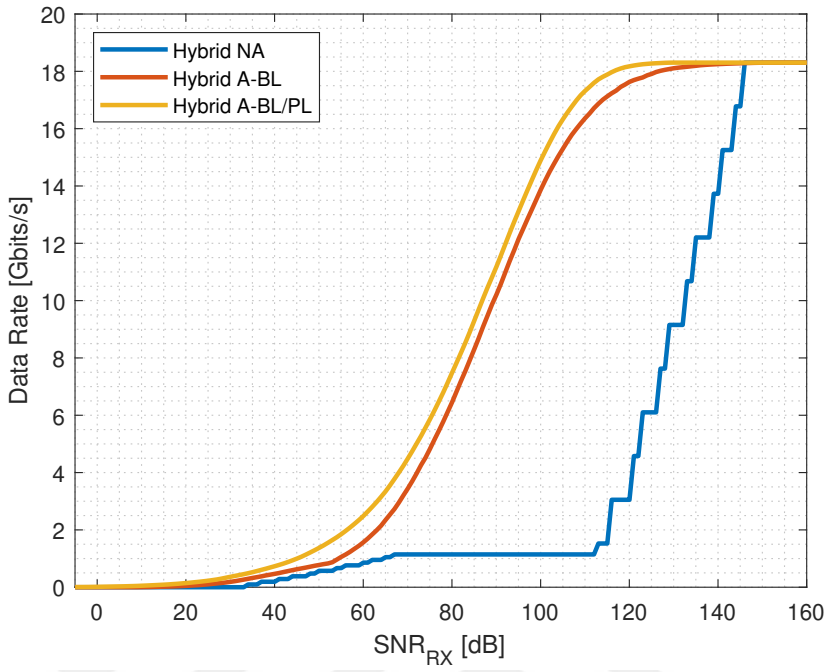

Figure 25: Data rate of adaptive DL MIMO DCO-OFDM system

The performance of the proposed adaptive system including MIMO mode switching in addition to bit and power loading is depicted in Fig. 25 as comparing with NA and A-BL systems including additional switching. It can be observed that RC mode saturates at $\mathrm{SNR_{RX}}$ value of 67.03 dB in NA system with data rate of 1.14 Gbits/s and adaptive system select RC mode until $\mathrm{SNR_{RX}}$ of 112.03 dB. However, A-BL system has a benefit from switching algorithm before saturation of RC mode. When proposed algorithm is considered, it outperforms the benchmark cases, particularly in lower $\mathrm{SNR_{RX}}$ region.

CHAPTER IV

MASSIVE MIMO OFDM-BASED VLC NETWORKS

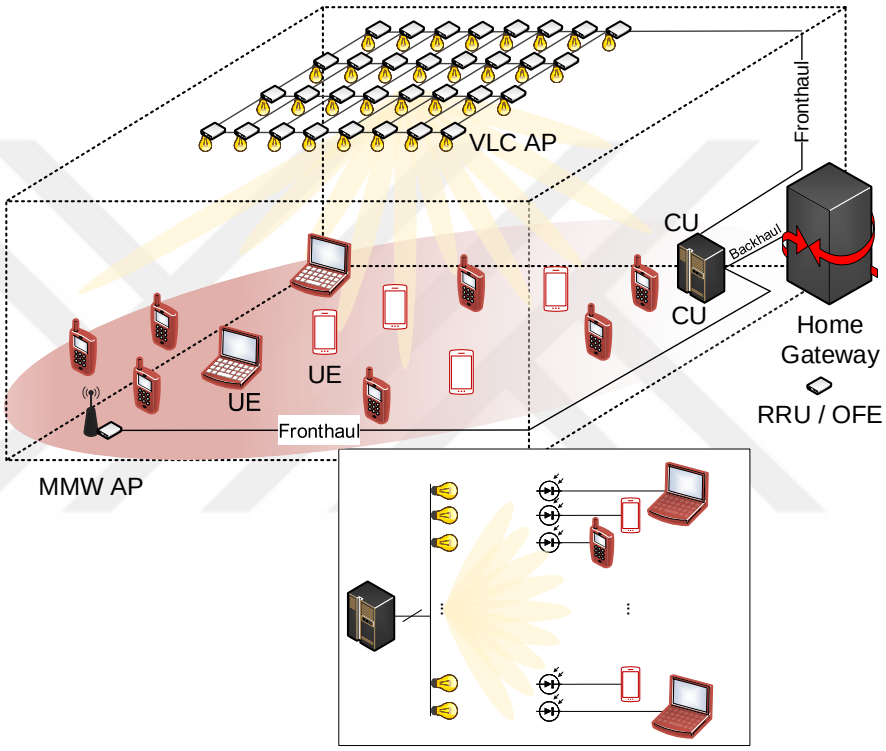

Figure 26: Massive MIMO VLC system with UL transmission in MMW

MU massive MIMO OFDM-based VLC transmission, which is another application that can be run in the centralized network platform provided in Chapter 2, is investigated in this chapter. The system architecture under the consideration of the distributed LEDs acting as a single VLC AP with large-scale distributed transmitters thanks to CU is depicted in Fig. 26. Massive MIMO is a promising technology in order to meet the requirements of the next generation wireless communication systems [94]. It has been also identified as one of the key 5G NR technologies due to supporting multiple-access and significant capacity gain improvements. As in 5G NR

technology, the performance of VLC can be further improved with the integration of massive MIMO system into the PHY.

Massive MIMO in RF networks benefits from the usage of TDD mode in which the propagation channels in both DL and UL are reciprocal. It yields to use estimated UL channel responses during pre-coding (beamforming) phase in DL transmission. On the other hand, when VLC networks are considered, UL transmission is operated in the different part of the spectrum (see product offerings from [27, 28]). It results in the fact that FDD is the only choice to separate the DL and UL transmissions. However, the propagation channels are not reciprocal in FDD and the estimated DL channel responses should be feedbacked to the CU side for beamforming purpose. It requires a necessity of an efficient DL pilot design since the UL feedback overhead increases in proportion to the number of active UEs.

In this Chapter, an MU massive MIMO OFDM-based VLC transmission building upon FDD is considered as MMW technology is imposed to UL side with the use of orthogonal frequency-division multiple access (OFDMA) to support MU transmission simultaneously. Various types of DL PAs which yield different data rates in DL and UL as a result of a trade-off between UL feedback overhead and DL channel estimation and interpolation errors are designed and their performances are investigated. In order to select a proper PA, a DPC, which is implemented in CU, is further proposed to keep the DL and UL data rates at an acceptable level based on the number of active UEs.

The remaining of the chapter is organized as following: After the transmission frame structure is explained in Section 4.1, DL and UL system models are given in Section 4.2 and Section 4.3, respectively. In Section 4.4, different DL PAs are designed and DPC mechanism is given in Section 4.5. DL channel estimation and interpolation processes are then detailed in Section 4.6. Finally, the performance results are demonstrated in Section 4.7.

4.1 Transmission Frame Structure

PHY of DL MU transmission builds upon DCO-OFDM where MU is supported using beamforming. Let $N_{\mathrm{VLC}}^{\mathrm{LED}}$ denote the number of LEDs and N denote the number of active UEs[1]. Each DL transmission frame consists of T_{VLC} ($\geq N_{\mathrm{VLC}}^{\mathrm{LED}}$) sub-frames (or time-slots) and each sub-frame has $N_{\mathrm{VLC}}^{\mathrm{SBC}}$ subcarriers. The DL frame (see Fig. 27) consists of DL pilot signals, DL data signals, and DL control signals.

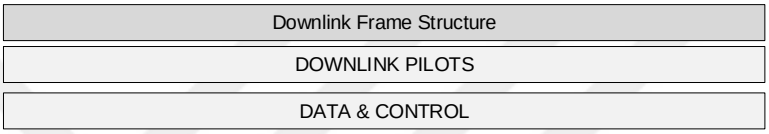

Figure 27: DL massive MIMO DCO-OFDM frame structure

In DL frame, let $N_{\mathrm{VLC}}^{\mathrm{LED-P}}$, which is less than or equal to $N_{\mathrm{VLC}}^{\mathrm{LED}}$, and $N_{\mathrm{VLC}}^{\mathrm{SBC-P}}$, which is less than or equal to $N_{\mathrm{VLC}}^{\mathrm{SBC}}$, denote the number of the LEDs and the number of subcarriers, respectively, in which the pilot signals are transmitted. The total number of DL pilot signals then becomes $N_{\mathrm{VLC}}^{\mathrm{SBC-P}} \times N_{\mathrm{VLC}}^{\mathrm{LED-P}}$ where $\times$ is scalar multiplication. Noting that the value of $N_{\mathrm{VLC}}^{\mathrm{LED-P}}$ and relatively LEDs indexes (e.g., $1, 2...N_{\mathrm{VLC}}^{\mathrm{LED}}$) can be adaptively selected by the DPC implemented in the CU based on the network dynamics in terms of the number of active UEs, that is explained in following sections.

PHY of UL MU transmission is based on OFDMA technique. Each MMW OFDMA frame consists of T_{MMW} sub-frame and each sub-frame has $N_{\mathrm{MMW}}^{\mathrm{SBC}}$ subcarriers. UL frame is divided into multiple resource blocks (RBs), each of which includes $N_{\mathrm{MMW}}^{\mathrm{RB-S}}$ consecutive subcarriers for the duration of $T_{\mathrm{MMW}}^{\mathrm{RB}}$[2]. Therefore, total number of RBs that are allocated to UEs can be expressed as

$$N_{\mathrm{MMW}}^{\mathrm{RB}} = \left\lfloor N_{\mathrm{MMW}}^{\mathrm{SBC}} / N_{\mathrm{MMW}}^{\mathrm{RB-S}} \right\rfloor \times T_{\mathrm{MMW}} / T_{\mathrm{MMW}}^{\mathrm{RB}}, \tag{33}$$

[1]It is assumed that $N_{\mathrm{VLC}}^{\mathrm{LED}}$ is greater than or equal to N.

[2]$N_{\mathrm{MMW}}^{\mathrm{RB-S}}$ should be selected to yield $\mathrm{mod}[N_{\mathrm{MMW}}^{\mathrm{SBC}}, N_{\mathrm{MMW}}^{\mathrm{RB-S}}] > 0$ to keep DC subcarrier as null and $T_{\mathrm{MMW}}^{\mathrm{RB}}$ should be selected to yield $\mathrm{mod}[T_{\mathrm{MMW}}, T_{\mathrm{MMW}}^{\mathrm{RB}}] = 0$

where $\lfloor . \rfloor$ denotes the floor operation and total number of relative null subcarriers over one sub-frame becomes

$$N_{\mathrm{MMW}}^{\mathrm{N}} = N_{\mathrm{MMW}}^{\mathrm{SBC}} - \left\lfloor N_{\mathrm{MMW}}^{\mathrm{SBC}} / N_{\mathrm{MMW}}^{\mathrm{RB-S}} \right\rfloor \times N_{\mathrm{MMW}}^{\mathrm{RB-S}}. \tag{34}$$

Each UL frame (see Fig. 28) consists of UL pilot signals, UL data signals, UL control signals, and estimated DL channel coefficients.

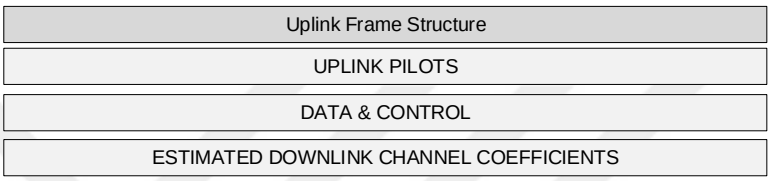

Figure 28: UL SISO OFDMA frame structure

In UL frame, let $N_{\mathrm{MMW}}^{\mathrm{SBC-P}}$ denote the number of pilot subcarriers in one RB and total number the UL pilots becomes $N_{\mathrm{MMW}}^{\mathrm{RB}} \times N_{\mathrm{MMW}}^{\mathrm{SBC-P}}$. Estimated DL channel coefficient feedback also utilizes totally $N_{\mathrm{VLC}}^{\mathrm{SBC-P}} \times N_{\mathrm{VLC}}^{\mathrm{LED-P}} \times N$ subcarriers over one UL frame.

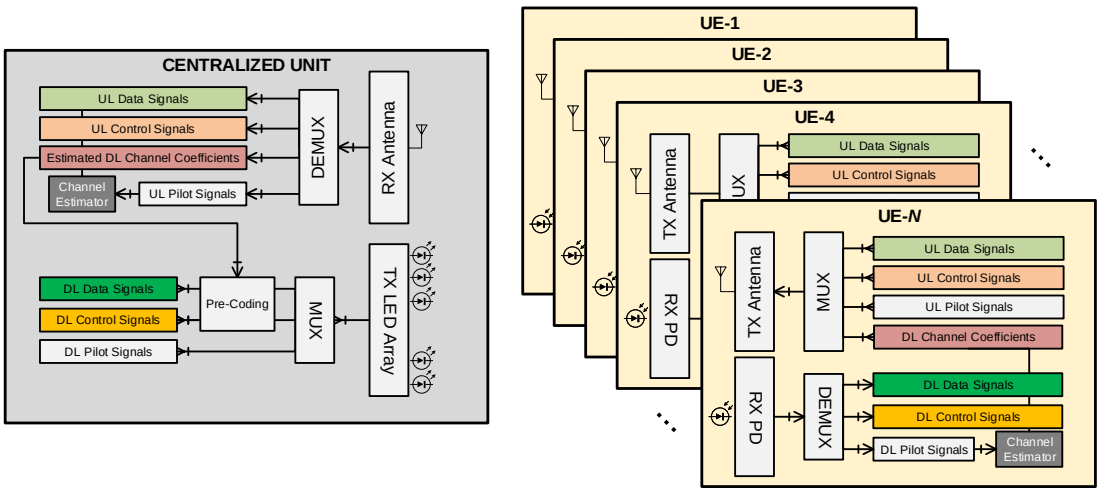

Figure 29: Transmission and reception in FDD system structure

The frame construction and deconstruction are further summarized in Fig. 29. After DL data and control signals are passed through a pre-coding process, they are

multiplexed with the DL pilot signals. The resulting signals are then transmitted to UEs. In UE side, the received signal is demultiplexed to extract DL data, control, and pilot signals. The DL channel coefficients are estimated using DL pilots and interpolated to find the coefficients in other subcarriers in which data and control signals are transmitted. The decoding process is then started over data and control signals using the estimated and interpolated channel coefficients.

In UL side, UE multiplexes UL data, control, and pilots signals with the estimated DL channel coefficients and transmits them through UL MMW link. In the receiver side of CU, the UL channel coefficients are estimated using UL pilot signals and the remaining ones are found using interpolation. UL data and control signals and estimated DL channel coefficients are then decoded. The estimated DL coefficients are further used in following pre-coding progress.

4.2 Downlink System Model

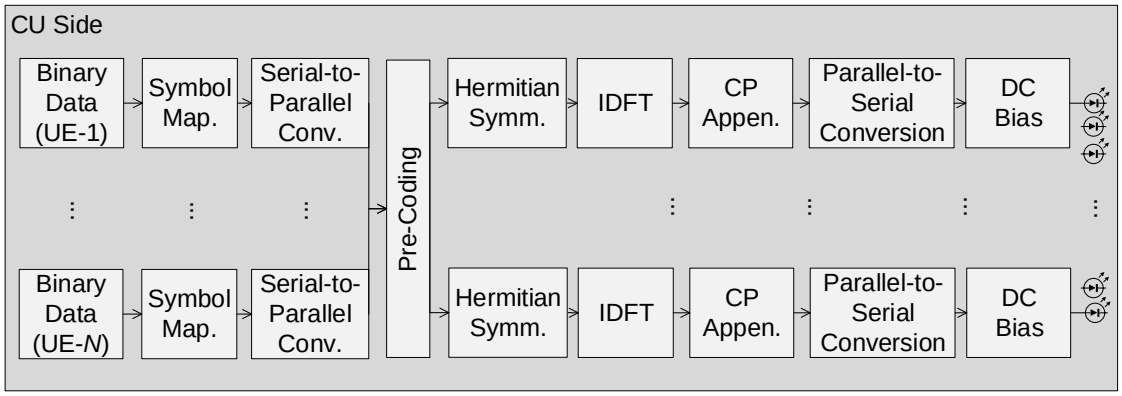

Figure 30: Block diagram of MU massive MIMO OFDM VLC in CU side

The block diagram of MU massive MIMO VLC transmitter system with DCO-OFDM is depicted in Fig. 30. As in conventional DCO-OFDM which is explained in Chapter 3, the binary information is mapped to complex-valued symbols using either $M-$ary PSK or QAM. However, this process is independently repeated for each UE's information in this chapter. Let $\mathbf{S}_u^\tau$ denote the complex-valued symbol vector for u^{th}

UE[3] for τ^{th} sub-frame. The length of the vector is equal to $\beta \times (N_{\text{VLC}}^{\text{SBC}}/2-1)$ where β is an arbitrary positive integer (e.g., $1, 2...$). $\mathbf{S}_u^{\tau}$ is then converted to totally β parallel streams, each has a length of $N_{\text{VLC}}^{\text{SBC}}/2-1$. Let $\mathbf{q}^{k,\tau}$ denote the input of pre-coding progress with the structure of

$$\mathbf{q}^{k,\tau} = [S_1^{k,\tau},\ S_2^{k,\tau},\ ...\ S_N^{k,\tau}]^{\text{T}}, \tag{35}$$

and let $\mathbf{G}^{k,\tau}$ denote the subcarrier-based pre-coding matrix generated based on estimated DL channel coefficients that is explained in following parts. The pre-coding progress that is done for each sub-frame and subcarrier can be written as

$$\mathbf{b}^{k,\tau} = \sqrt{\alpha^{k,\tau}}\mathbf{G}^{k,\tau}\mathbf{q}^{k,\tau}, \tag{36}$$

where $\alpha^{k,\tau}$ is the normalization constant and $\mathbf{b}^{k,\tau}$ is in the form of $[b_1^{k,\tau}\ b_2^{k,\tau}\ ...\ b_{N_{\text{VLC}}^{\text{LED}}}^{k,\tau}]^{\text{T}}$. The pre-coding matrix is generated with the use of global channel matrix which can be written as

$$\mathbf{H}_{\mathbf{G}}^{k,\tau} = [\mathbf{H}_1^{\text{VLC}-k,\tau^{\text{T}}},\ \mathbf{H}_2^{\text{VLC}-k,\tau^{\text{T}}}\ ...\ \mathbf{H}_{N_{\text{VLC}}^{\text{LED}}}^{\text{VLC}-k,\tau^{\text{T}}}]^{\text{T}}, \tag{37}$$

where $[.]^{\text{T}}$ denotes the transpose operation and

$$\mathbf{H}_i^{\text{VLC}-k,\tau} = [H_{1,i}^{\text{VLC}-k,\tau}\ H_{2,i}^{\text{VLC}-k,\tau}\ ...\ H_{N,i}^{\text{VLC}-k,\tau}]. \tag{38}$$

As pre-coding scheme, maximum ratio transmission (MRT), known as conjugate beamforming [15] and maximizing the signal gain at receiver side[4], is used in this chapter. Analytical expression of the pre-coding matrix is written as

$$\mathbf{G}^{k,\tau} = \mathbf{H}_{\mathbf{G}}^{k,\tau^*}, \tag{39}$$

with a normalization constant given by

$$\alpha^{k,\tau} = \frac{1}{\text{tr}(\mathbf{G}^{k,\tau}\mathbf{G}^{k,\tau^{\text{H}}})}, \tag{40}$$

[3]It is assumed that each UE has a single PD for simplicity.

[4]It should be noted that large conference rooms or public spaces such as libraries, airports, etc. in which the number of LEDs is sufficiently high benefits the channel vectors to become closer to mutually orthogonal, which yields multiplication of pre-coding matrix and channel matrix approaches a diagonal matrix leading to the optimal solution.

where $(.)^*$, $[.]^{\mathrm{H}}$, and tr(.) denote complex conjugate, Hermitian, and trace operations, respectively.

As following of DCO-OFDM procedure, Hermitian symmetry is imposed over pre-coded signal such as

$$\mathbf{X}_i^{\mathrm{VLC}-\tau} = [0,\ b_i^{1,\tau},\ b_i^{2,\tau},\ \ldots\ b_i^{N_{\mathrm{VLC}}^{\mathrm{SBC}}/2-1,\tau},\ 0,\ b_i^{N_{\mathrm{VLC}}^{\mathrm{SBC}}/2-1,\tau^*},\ \ldots\ b_i^{2,\tau^*},\ b_i^{1,\tau^*}]^{\mathrm{T}}, \tag{41}$$

where $\mathbf{X}_i$ is the input of IDFT process for the i^{th} LED. $N_{\mathrm{VLC}}^{\mathrm{SBC}}-$IDFT output can be written as

$$x_i^{\mathrm{VLC}-n,\tau} = \frac{1}{\sqrt{N_{\mathrm{VLC}}^{\mathrm{SBC}}}} \sum_{k=0}^{N_{\mathrm{VLC}}^{\mathrm{SBC}}-1} X_i^{\mathrm{VLC}-k,\tau} e^{j\frac{2\pi nk}{N_{\mathrm{VLC}}^{\mathrm{SBC}}}}. \tag{42}$$

In order to hande with ISI, a CP with the length of $N_{\mathrm{CP}-\mathrm{VLC}}$ which is selected to be longer than or equal to the multipath channel spread is appended to the beginning of $\mathbf{x}_i^{\tau}$. It is followed by parallel-to-serial conversion and DC-bias addition to shift the signal into the dynamic range of LEDs. The DC-biased signal then drives the LEDs and propagates through the optical MIMO channel to the PD of UEs.

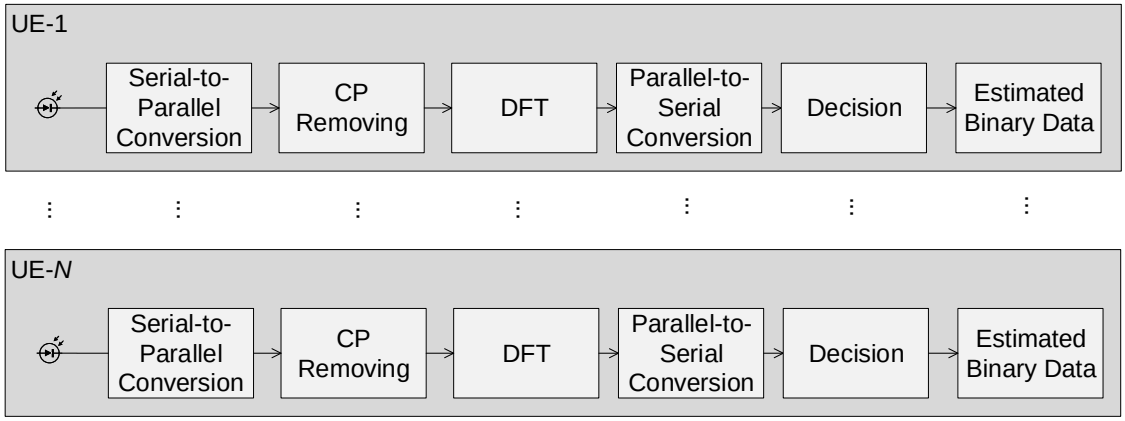

Figure 31: Block diagram of MU massive MIMO OFDM VLC in UE side

In the u^{th} UE side (see Fig. 31), the received signal is sampled with the rate of $T_{\mathrm{S}-\mathrm{VLC}}$ and converted to parallel streams with the length of $N_{\mathrm{VLC}}^{\mathrm{SBC}} + N_{\mathrm{CP}-\mathrm{VLC}}$. The CP is removed from the parallel streams and $N_{\mathrm{VLC}}^{\mathrm{SBC}}-$DFT is performed. The resulting

signal at the k^{th} subcarrier of τ^{th} sub-frame becomes

$$Y_u^{\text{VLC}-k,\tau} = R\sqrt{P_{\text{VLC}}}\mathbf{H}_u^{\text{VLC}-k,\tau}\mathbf{X}^{\text{VLC}-k,\tau} + W_u^{\text{VLC}-k,\tau} \tag{43}$$

$$= R\sqrt{\alpha^{k,\tau}P_{\text{VLC}}}\mathbf{H}_u^{\text{VLC}-k,\tau}\mathbf{G}_u^{k,\tau}q_u^{k,\tau} + R\sqrt{\alpha^{k,\tau}P_{\text{VLC}}}\mathbf{H}_u^{\text{VLC}-k,\tau}\sum_{i=1,i\neq u}^{N}\mathbf{G}_i^{k,\tau}q_i^{k,\tau} + W_u^{\text{VLC}-k,\tau}, \tag{44}$$

where

$$\mathbf{X}^{\text{VLC}-k,\tau} = [X_1^{\text{VLC}-k,\tau},\ X_2^{\text{VLC}-k,\tau},\ \ldots\ X_{N_{\text{VLC}}^{\text{LED}}}^{\text{VLC}-k,\tau}]^{\text{T}}, \tag{45}$$

$$\mathbf{H}_u^{\text{VLC}-k,\tau} = [H_{u,1}^{\text{VLC}-k,\tau},\ H_{u,2}^{\text{VLC}-k,\tau},\ \ldots\ H_{u,N_{\text{VLC}}^{\text{LED}}}^{\text{VLC}-k,\tau}], \tag{46}$$

$$\mathbf{G}_u^{k,\tau} = [G_{1,u}^{k,\tau},\ G_{2,u}^{k,\tau},\ \ldots\ G_{N_{\text{VLC}}^{\text{LED}},u}^{k,\tau}]^{\text{T}}, \tag{47}$$

R is PD responsivity, $W_u^{\text{VLC}-k,\tau}$ is the AWGN term with zero-mean and $\sigma_{\text{VLC}}^2 = N_{0-\text{VLC}}B_{\text{VLC}}$ variance where $N_{0-\text{VLC}}$ is the PSD and $B_{\text{VLC}} = 1/2T_{\text{S}-\text{VLC}}$ is VLC system bandwidth, and P_{VLC} is the electrical average DCO-OFDM signal power without DC bias term. The resulting SINR at the u^{th} UE and the k^{th} subcarrier of the τ^{th} sub-frame can be obtained as

$$\text{SINR}_u^{\text{VLC}-k,\tau} = \frac{R^2\alpha^{k,\tau}P_{\text{VLC}}\left|\mathbf{H}_u^{\text{VLC}-k,\tau}\mathbf{G}_u^{k,\tau}\right|^2}{R^2\alpha^{k,\tau}P_{\text{VLC}}\sum_{i=1,i\neq u}^{N}\left|\mathbf{H}_u^{\text{VLC}-k,\tau}\mathbf{G}_i^{k,\tau}\right|^2 + \sigma_{\text{VLC}}^2}. \tag{48}$$

4.3 Uplink System Model

The block diagram of UL SISO OFDMA-based MMW transmission is depicted in Fig. 32. Multiple access support is given by using Proportional Fair (PF) scheduler, whose analytical expression is given in Appendix. B. After scheduling algorithm is run, each UE's information is put into the subcarriers at the relevant sub-frame of allocated RBs based on its output that is also transmitted to UEs through a dedicated DL control channel. The rest of the subcarriers are filled by zero. Let $X_u^{\text{MMW}-k,\tau}$ denote the frequency-domain transmitted signal by the u^{th} UE at the k^{th} subcarrier

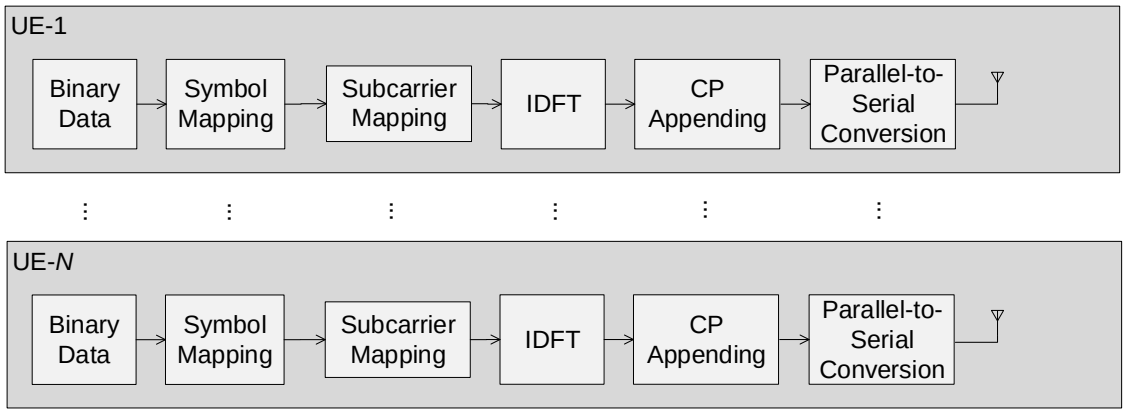

Figure 32: Block diagram of OFDMA-based UL MMW system in UE side

and including zeros for non-allocated subcarriers. The $N_{\mathrm{MMW}}^{\mathrm{SBC}}-$IDFT process is done over $X_u^{\mathrm{MMW}-k,\tau}$, e.g.,

$$x_u^{\mathrm{MMW}-n,\tau} = \frac{1}{\sqrt{N_{\mathrm{MMW}}^{\mathrm{SBC}}}} \sum_{k=0}^{N_{\mathrm{MMW}}^{\mathrm{SBC}}-1} X_u^{\mathrm{MMW}-k,\tau} e^{j\frac{2\pi nk}{N_{\mathrm{MMW}}^{\mathrm{SBC}}}}. \tag{49}$$

It is followed by CP appending with the length of $N_{\mathrm{CP}-\mathrm{MMW}}$ and parallel-to-serial conversion. The resulting signal is then propagated through MMW antenna to CU side. It should be noted that above processes are independently done in each UE.

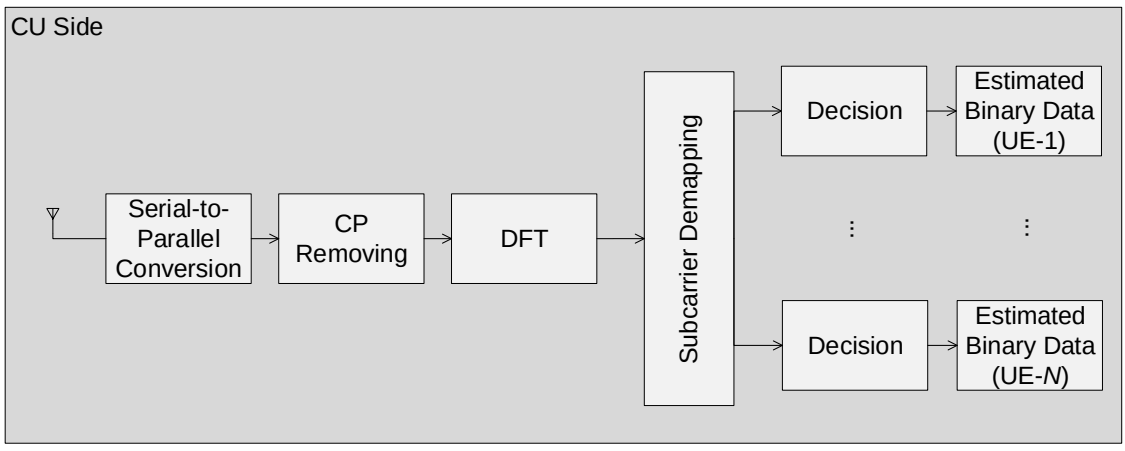

Figure 33: Block diagram of OFDMA-based UL MMW system in CU side

In CU side (see Fig. 33), the received signal is sampled with the rate of $T_{\mathrm{S}-\mathrm{MMW}}$. The sampled signal sequence is then converted to parallel streams and $N_{\mathrm{MMW}}^{\mathrm{SBC}}-$DFT

is performed over them. In frequency-domain, the received signal can be written as

$$Y^{\mathrm{MMW}-k,\tau} = \sqrt{P_{\mathrm{MMW}}} \sum_{u=1}^{N} H_u^{\mathrm{MMW}-k,\tau} X_u^{\mathrm{MMW}-k,\tau} + W^{\mathrm{MMW}-k,\tau}, \tag{50}$$

where P_{MMW} is the average OFDMA signal power across utilized subcarrier. Here, $W^{\mathrm{MMW}-k,\tau}$ is the complex zero-mean AWGN term. Its variance is given by $\sigma^2_{\mathrm{MMW}} = N_{0-\mathrm{MMW}} B_{\mathrm{MMW}}$ where $N_{0-\mathrm{MMW}}$ is the PSD and $B_{\mathrm{MMW}} = 1/T_{\mathrm{S}-\mathrm{MMW}}$ is MMW system bandwidth.

To extract the UEs' information, subcarrier de-mapping is done based on allocation information and transmitted bits of UEs are independently decoded. The UL SNR of the u^{th} UE in the k^{th} subcarrier becomes

$$\mathrm{SNR}_u^{\mathrm{MMW}-k,\tau} = \frac{P_{\mathrm{MMW}} \left| H_u^{\mathrm{MMW}-k,\tau} \right|^2}{\sigma^2_{\mathrm{MMW}}}. \tag{51}$$

4.4 Pilot Signal Design

When the practical implementations are considered for massive MIMO systems, it can be seen that optimization of DL pilot signal overhead is the major design topic as a result of high number of transmitters (LEDs in this chapter). To boost the DL network performance, DL channel estimation and interpolation errors should be minimized. The way to achieve this target is to increase the number of pilot signals. On the other hand, since DL estimated channel coefficients are feedbacked to CU side, it increases the UL feedback overhead. It should be also noted that the feedback overhead in UL increases in proportion to number of active UEs. Therefore, the number of pilots should be kept in an acceptable value under the consideration of both DL and UL system performance.

In this chapter, a metric, called as pilot overhead ratio (POR), that is the ratio of the number of subcarriers carrying the pilot signals to the number of total subcarriers excluding the nulls and Hermitian symmetry imposed ones over a DCO-OFDM/OFDMA frame is defined. The DL and UL POR values can be expressed

as

$$\mathrm{POR_{DL}} = \frac{N_{\mathrm{VLC}}^{\mathrm{SBC-P}} \times N_{\mathrm{VLC}}^{\mathrm{LED-P}}}{(N_{\mathrm{VLC}}^{\mathrm{SBC}}/2 - 1) \times T_{\mathrm{VLC}}}, \tag{52}$$

$$\mathrm{POR_{UL}} = \frac{N_{\mathrm{MMW}}^{\mathrm{RB}} \times N_{\mathrm{MMW}}^{\mathrm{SBC-P}} + N \times N_{\mathrm{VLC}}^{\mathrm{SBC-P}} \times N_{\mathrm{VLC}}^{\mathrm{LED-P}}}{(N_{\mathrm{MMW}}^{\mathrm{SBC}} - N_{\mathrm{MMW}}^{\mathrm{N}}) \times T_{\mathrm{MMW}}}. \tag{53}$$

Using the ergodic capacity defined in [91] and Eqs. 52 and 53, the achievable maximum data rate levels in DL and UL can be calculated for t^{th} frame as

$$D^{\mathrm{DL}-t} = \frac{(1 - \mathrm{POR_{DL}}) \times N_{\mathrm{VLC}}^{\mathrm{SBC}}}{(N_{\mathrm{VLC}}^{\mathrm{SBC}} + N_{\mathrm{CP-VLC}}) \times T_{\mathrm{VLC}}} \times \sum_{u=1}^{N} \sum_{k=1}^{N_{\mathrm{VLC}}^{\mathrm{SBC}}/2-1} \sum_{\tau=0}^{T_{\mathrm{VLC}}-1} \Delta_{\mathrm{VLC}}^{\mathrm{SBC}} \times \log_2(1 + \mathrm{SINR}_u^{\mathrm{VLC}-k,\tau}), \tag{54}$$

$$D^{\mathrm{UL}-t} = \frac{(1 - \mathrm{POR_{UL}}) \times N_{\mathrm{MMW}}^{\mathrm{SBC}}}{(N_{\mathrm{MMW}}^{\mathrm{SBC}} + N_{\mathrm{CP-MMW}}) \times T_{\mathrm{MMW}}} \times \sum_{u=1}^{N} \sum_{k=0}^{N_{\mathrm{MMW}}^{\mathrm{SBC}}-1} \sum_{\tau=0}^{T_{\mathrm{MMW}}-1} \varphi_u^{k,\tau} \times \Delta_{\mathrm{MMW}}^{\mathrm{SBC}} \times \log_2(1 + \mathrm{SNR}_u^{\mathrm{MMW}-k,\tau}), \tag{55}$$

where $\varphi_u^{k,\tau}$ takes the value of either 0 or 1, denotes the allocation of k^{th} subcarrier at τ^{th} sub-frame to the u^{th} UE as a result of PF scheduling algorithm running at CU, $\Delta_{\mathrm{VLC}}^{\mathrm{SBC}}$ and $\Delta_{\mathrm{MMW}}^{\mathrm{SBC}}$ denote the subcarrier spacing in DCO-OFDM/OFDMA-based VLC and MMW transmissions, respectively.

The CU has to properly choose the POR value with the aim of keeping data rates at an acceptable level for both DL and particularly UL transmission while achieving enough accuracy in DL channel estimation and interpolation processes. While choosing POR value; LED, subcarriers, and sub-frame indexes in which DL pilot signals are transmitted should be determined. The overall process is called as PA; and as in stated above, different PA selection is resulted as different POR values and network performance in both DL and UL sides as a consequence of UL feedback overhead and DL channel estimation and interpolation errors.

In this chapter, to analyze the PA selection, an indoor room environment with the size of 22.1 m × 22.1 m × 22.1 m is considered. The environment includes totally

169 LEDs uniformly locating at the ceiling (e.g., in a square grid with 13×13 array structure).

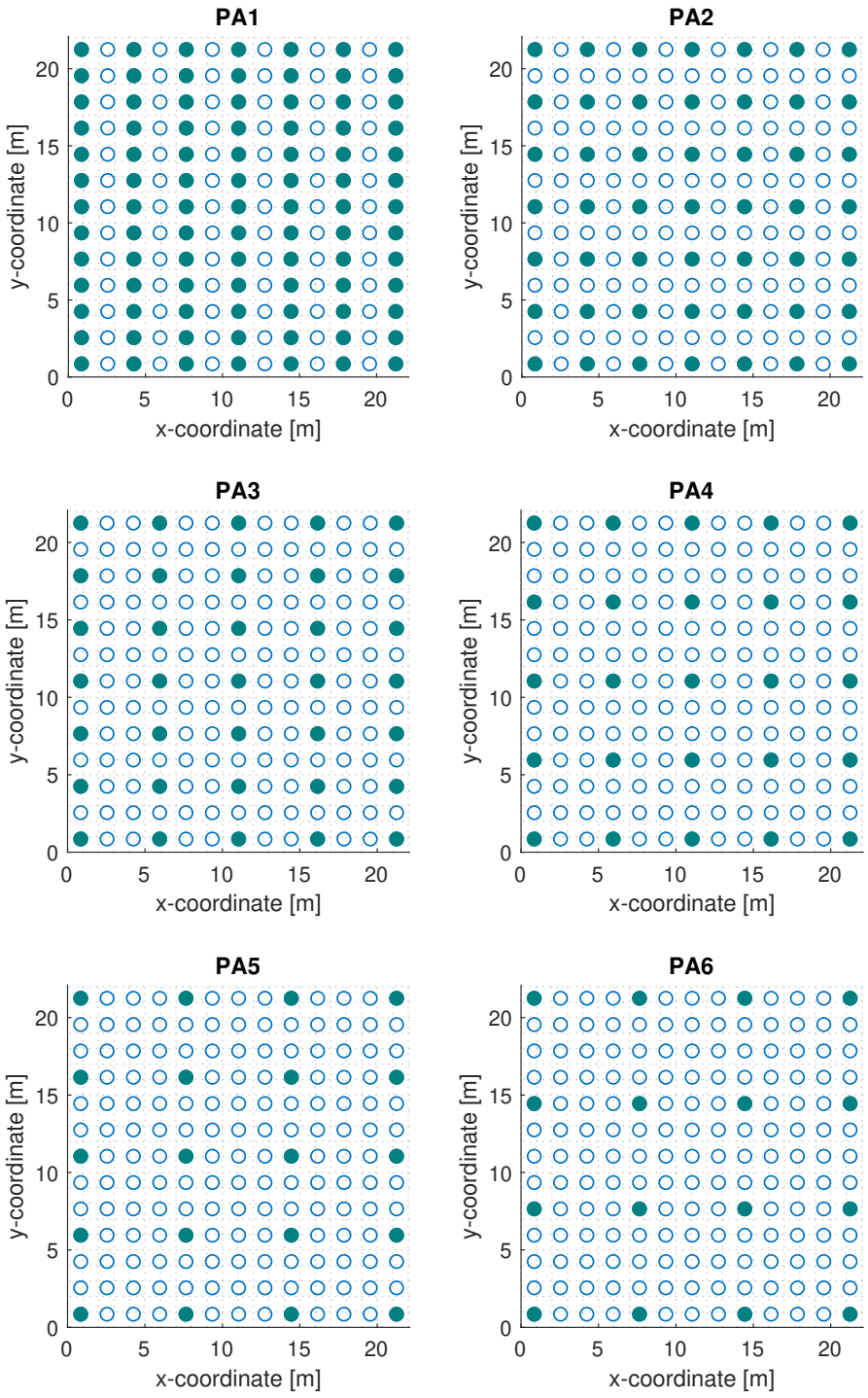

Figure 34: Different PAs for massive MIMO VLC system

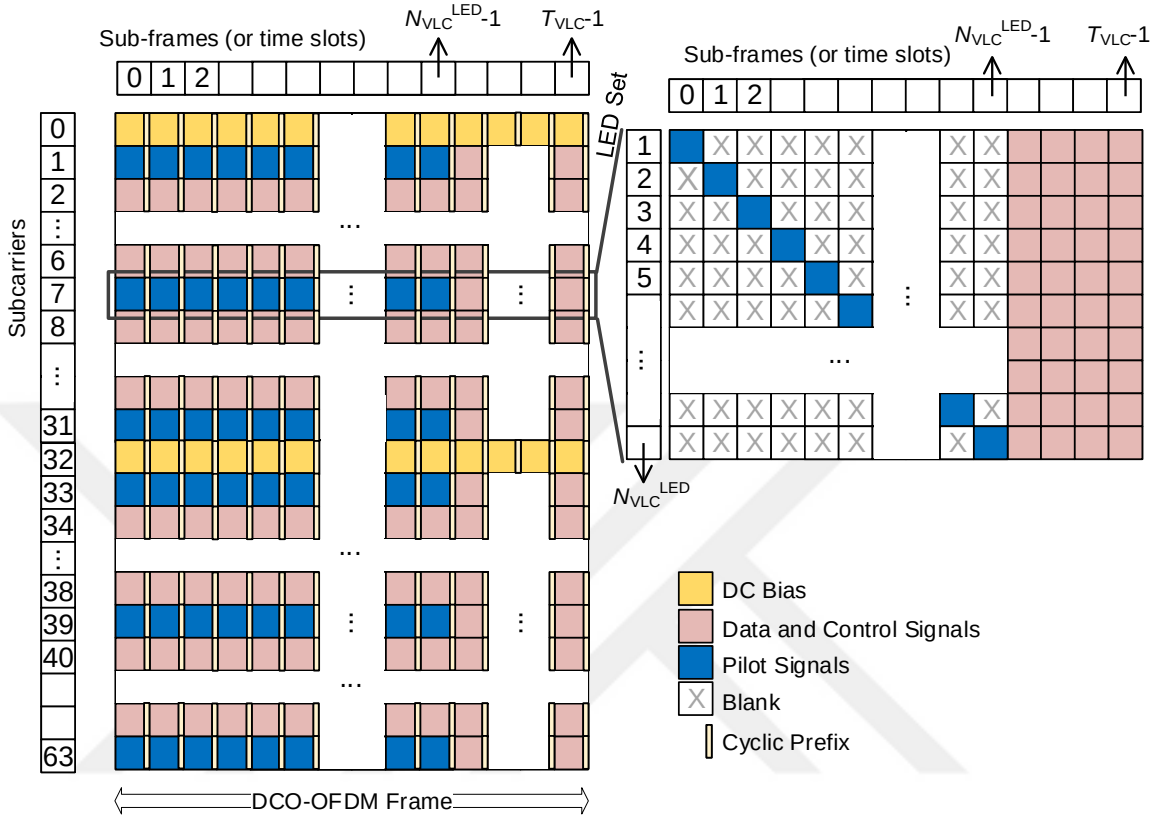

Figure 35: DCO-OFDM frame with pilots in frequency, time, and spatial domains

Totally 6 different PAs in spatial domain (LEDs layout) are considered (please see Fig. 34 where the LEDs transmit the pilots are filled by the blue color) and PA0 in which all LEDs are used for the pilot transmission is additionally introduced for benchmarking purpose. For the above schemes, a symmetrical distribution of the pilot signals across the LEDs is taken into account in the spatial domain. Additionally, the pilots are distributed in the frequency and time domains. These selections are inspired from the reference signal positioning in LTE[5]. In LTE, the pilot signals are transmitted from specific subcarriers and sub-frames. After UE estimates the channel coefficients in these specific locations, they find the remaining ones with the use of

[5]Please see Figure 6.10.1.2-1 of [95] which shows the pilot signal locations in single resource block of LTE base station with 4 transmit antennas.

interpolation. The almost same behavior in LTE as transmitting pilots in frequency, time, and spatial domain is used. On the other hand, in contrast to LTE where the pilot signals are transmitted from each transmitter, the system model in this chapter transmits the pilots from only specific transmitters (e.g., LEDs). The remaining channel coefficients in spatial domain are then interpolated with the use of room geometry.

The DCO-OFDM frame under consideration consists of $N_{\text{VLC}}^{\text{SBC}} = 64$ subcarriers and $T_{\text{VLC}} = 200$ sub-frames. Noting that one subcarrier is reserved for DC bias and half of the subcarriers are used to satisfy Hermitian symmetry, therefore, the total number of resource elements in a single DL frame becomes $31 \times 200 = 6200$. In Fig. 35 depicts DCO-OFDM frame structure with the pilot signal distribution over the time and frequency domains. In the frequency domain, subcarrier indexes of 1, 7, 13, 19, 25, and 31 are used for pilots[6] (i.e., $N_{\text{VLC}}^{\text{SBC-P}} = 6$) in all PAs and channels are assumed as static over a frame duration. It should be also noted that, as in depicted in Fig. 35, the pilot signals transmitted through the different LEDs should be orthogonal to each other and this issue is satisfied as transmitting the pilots over different sub-frames for different LEDs. For example, LED-1 uses the 0^{th} sub-frame for pilot signal transmission at the specified subcarriers. During this phase, the rest of the LEDs do not transmit any signal over this sub-frame. In a similar way, LED-2 uses the 1^{st} sub-frame and the rest do not use the subcarriers within the same sub-frame. In all of the PAs, the channel responses are estimated at the subcarriers with the index of 1, 7, 13, 19, 25, and 31. In PA0, the remaining channel response at the rest of the subcarriers and sub-frames are calculated using interpolation in the frequency and time domain. However, for other PAs, four dimensional interpolation is conduced with the addition of two-dimensional spatial domain as taking the layout

[6]It should be also noted that subcarriers with the indexes of 33, 39, 45, 51, 57, and 63 are filled by the pilot signals as a result of Hermitian symmetry.

of LED luminaries into account.

The other specifications of the PAs are summarized as

- PA0 uses all of the LEDs for pilot transmission.
- PA1 selects the LEDs through skipping one-line along the x-axis for pilot transmission.
- PA2 selects the LEDs through skipping one-line along the x-axis and one-line along the y-axis for pilot transmission.
- PA3 selects the LEDs through skipping two-line along the x-axis and one-line along the y-axis for pilot transmission.
- PA4 selects the LEDs through skipping two-line along the x-axis and two-line along the y-axis for pilot transmission.
- PA5 selects the LEDs through skipping three-line along the x-axis and two-line along the y-axis for pilot transmission.
- PA6 selects the LEDs through skipping three-line along the x-axis and three-line along the y-axis for pilot transmission.

The structure of UL OFDMA frame is depicted in Fig. 36. The RBs consist of 9 consecutive subcarriers for the duration of 5 sub-frames, i.e., $N_{\mathrm{MMW}}^{\mathrm{RB-S}} = 9$ and $T_{\mathrm{MMW}}^{\mathrm{RB}} = 5$. Totally $N_{\mathrm{MMW}}^{\mathrm{SBC-P}} = 8$ pilots are used in each RB in which each first, third, and fifth slots carry the pilots. The pilots for channel estimation purpose are arranged in a symmetrical manner and the rest of the channel coefficients are calculated using an interpolation method.

Total numbers of subcarriers and sub-frames within a single OFDMA frame are set to $N_{\mathrm{MMW}}^{\mathrm{SBC}} = 128$ and $T_{\mathrm{MMW}} = 200$, respectively. It yields totally $N_{\mathrm{MMW}}^{\mathrm{RB}} = 560$

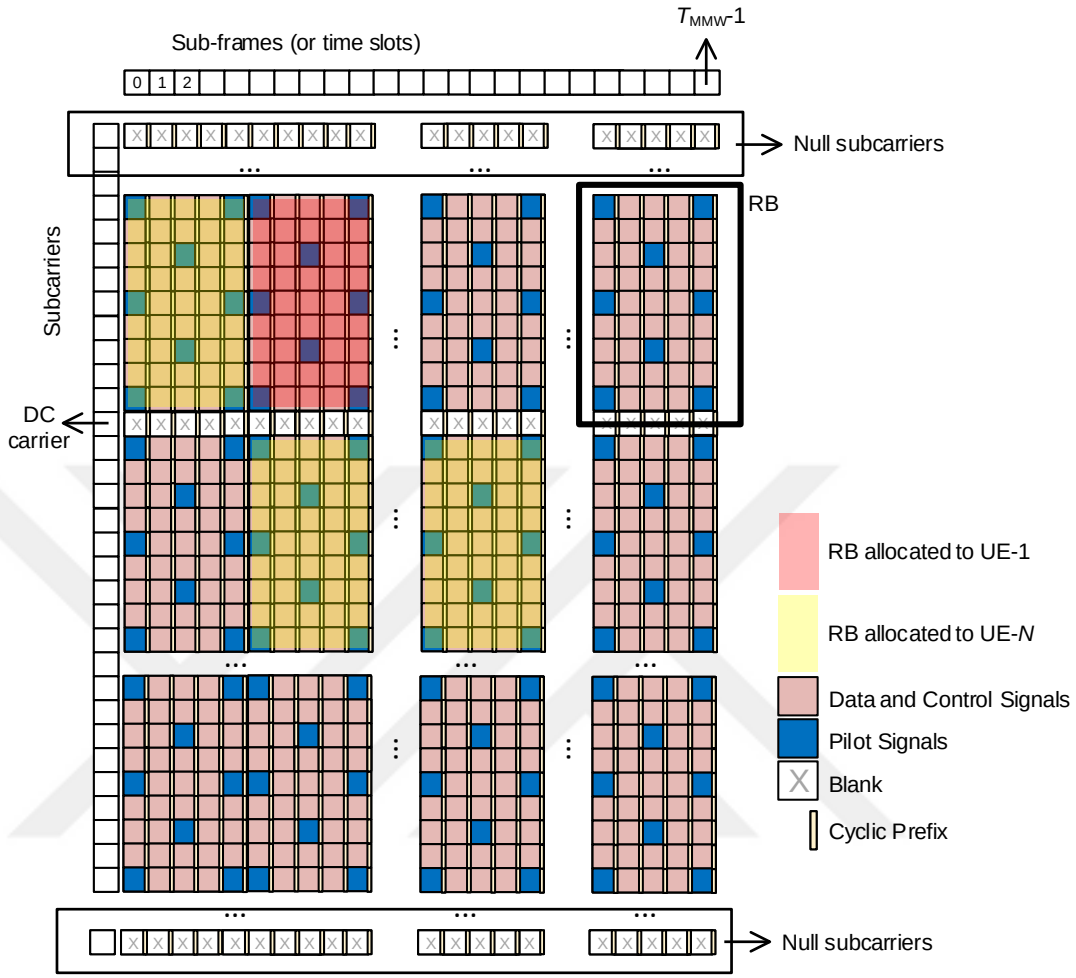

Figure 36: UL OFDMA frame with pilots in frequency and time domains

RBs and $N^{\mathrm{N}}_{\mathrm{MMW}} = 2$ null subcarrier, one of them is DC subcarrier. As an example, RBs allocated to the 1^{st} and N^{th} UE are depicted with purple and yellow color.

The resulting DL POR is given in Table 9. The highest POR is observed at PA0 as a result of all LEDs are participated in pilot transmission, whereas, the lowest POR is available with the use of PA7 that uses only 16 LEDs to carry pilots. It should be also noted that the values are not varying regarding to N in contrast to UL POR whose values are depicted in Table 10 regarding to different N up to 120.

Table 9: DL POR values for different number of UEs

PA0	PA1	PA2	PA3	PA4	PA5	PA6
16.35%	8.81%	4.74%	3.39%	2.42%	1.94%	1.55%

Table 10: UL POR values for different number of UEs

N	**PA0**	**PA1**	**PA2**	**PA3**	**PA4**	**PA5**	**PA6**
5	37.90%	28.61%	23.61%	21.94%	20.75%	20.16%	19.68%
10	58.02%	39.44%	29.44%	26.11%	23.73%	22.54%	21.59%
15	78.13%	50.28%	35.28%	30.28%	26.71%	24.92%	23.49%
20	98.25%	61.11%	41.11%	34.44%	29.68%	27.30%	25.40%
25	-	71.94%	46.94%	38.61%	32.66%	29.68%	27.30%
30	-	82.78%	52.78%	42.78%	35.63%	32.06%	29.21%
35	-	93.61%	58.61%	46.94%	38.61%	34.44%	31.11%
40	-	-	64.44%	51.11%	41.59%	36.83%	33.02%
45	-	-	70.28%	55.28%	44.56%	39.21%	34.92%
50	-	-	76.11%	59.44%	47.54%	41.59%	36.83%
55	-	-	81.94%	63.61%	50.52%	43.97%	38.73%
60	-	-	87.78%	67.78%	53.49%	46.35%	40.63%
65	-	-	93.61%	71.94%	56.47%	48.73%	42.54%
70	-	-	99.44%	76.11%	59.44%	51.11%	44.44%
75	-	-	-	80.28%	62.42%	53.49%	46.35%
80	-	-	-	84.44%	65.40%	55.87%	48.25%
85	-	-	-	88.61%	68.37%	58.25%	50.16%
90	-	-	-	92.78%	71.35%	60.63%	52.06%
95	-	-	-	96.94%	74.33%	63.02%	53.97%
100	-	-	-	-	77.30%	65.40%	55.87%
105	-	-	-	-	80.28%	67.78%	57.78%
110	-	-	-	-	83.25%	70.16%	59.68%
115	-	-	-	-	86.23%	72.54%	61.59%
120	-	-	-	-	89.21%	74.92%	63.49%

From Table 10, it can be observed that UL POR suffers from the increasing number of active UEs within an indoor room environment. Numerically, PA0 which has the highest DL POR as well gets the value of 37.9% for $N = 5$. As N is increasing, the margin to transfer data and control signals becomes very limited. Even, there is not any resource to feedback to DL channel coefficients within a single frame for $N > 20$. The limit increases to 39, 71, and 99 UEs for PA1, PA2, and PA3, respectively.

4.5 Adaptive Pilot Arrangement Selection Mechanism

The DPC aims to boost the DL network performance in terms of data rate through proper selection of DL PA among available arrangements while keeping the UL data rate at an acceptable level. For this purpose, optimization problem for t^{th} in terms

of Eqs. 54 and 55 can be formulated as

$$\max_{\text{PA0,PA1,...PA6}} \left\{ D^{\text{DL}-t} \right\} \tag{56}$$

such that

$$\beta D^{\text{DL}-t} \leq D^{\text{UL}-t} \tag{57}$$

where $\beta \in (0, 1]$ is a balance coefficient between UL and DL data rates.

4.6 Channel Estimation and Interpolation

With the use of pilot signals transmitted through the certain subcarriers over a set of LEDs and sub-frames, the channel coefficients are estimated with the use of ZF estimator. The estimated coefficients between u^{th} UE and l^{th} LED at the k^{th} subcarrier of the τ^{th} sub-frame becomes

$$\hat{H}_{u,i}^{\text{VLC}-k,\tau} = \frac{\tilde{Y}_u^{\text{VLC}-\text{P}-k,\tau}}{\tilde{X}_i^{\text{VLC}-\text{P}-k,\tau}}, \tag{58}$$

where $\tilde{X}_i^{\text{VLC}-\text{P}-k,\tau}$ is the transmitted pilot signal from i^{th} LED at the k^{th} subcarrier of the τ^{th} sub-frame and $\tilde{Y}_u^{\text{VLC}-\text{P}-k,\tau}$ is the corresponding received signal by the u^{th} UE. The estimates of channel coefficients are then transmitted to the CU through a error-free dedicated UL channel. Using the feedbacked coefficients, the remaining coefficients are then calculated using one of multi-dimensional interpolation methods. In this chapter, two different interpolation methods are considered:

- *Linear Interpolation* which constructs the new data points using a straight line

- *Cubic Interpolation* which fills the intermediate values using cubic convolution

Through one of the interpolation process, CU generates a global frequency-time DL channel matrix that includes all channel coefficients between UEs and LEDs for each subcarrier for each sub-frame. It then uses this channel matrix for pre-coding purpose. The estimated and interpolated subcarrier-based global channel matrix becomes

$$\hat{\mathbf{H}}_{\mathbf{G}}^{\text{VLC}-k,\tau} = [\hat{\mathbf{H}}_1^{\text{VLC}-k,\tau^{\text{T}}},\ \hat{\mathbf{H}}_2^{\text{VLC}-k,\tau^{\text{T}}},\ \ldots\ \hat{\mathbf{H}}_N^{\text{VLC}-k,\tau^{\text{T}}}]^{\text{T}}. \tag{59}$$

Relatively, pre-coding matrix is equal to with a normalization constant given by

$$\mathbf{G}^{k,\tau} = \hat{\mathbf{H}}_{\mathbf{G}}^{k,\tau^*}, \tag{60}$$

$$\alpha^{k,\tau} = \frac{1}{\mathrm{tr}(\mathbf{G}^{k,\tau}\mathbf{G}^{k,\tau\mathrm{H}})}. \tag{61}$$

4.7 Performance Evaluations

In this section, the performance results of MU DL massive MIMO DCO-OFDM-based VLC and UL SISO OFDMA based MMW transmissions are demonstrated after the simulation environment is explained.

4.7.1 Simulation Environment

The specifications of the indoor room environment under consideration are already given in Section 4.4. The MMW AP is located at the coordinates of $(0.5, 0.5, 0.2)$ assuming the room center is the left bottom corner of the floor.

VLC channel model between u^{th} UE and i^{th} VLC AP is generated following Eq. 86, whereas, MMW channel model between u^{th} UE and MMW AP is based on the model defined in Eq. 87 in Appendix A using the parameters specified in Tables 11 and 12. UL channel coefficients are assumed to be perfectly estimated and only UL pilot overhead issue is taken into account.

In order to evaluate the performance of the proposed system, a simulation study based on 1500 independent channel realizations each of which consists of one UL OFDMA frame (for MMW) and DL DCO-OFDM frame (for VLC) is conducted. Both frames consist of 200 sub-frames. In underlying MMW and VLC systems, sub-frames have a fixed duration of 8 us as a result of the selection of the same subcarrier spacing and CP duration. Therefore, the length of each frame is 1.6 ms. PF scheduling algorithm is run at the beginning of each frame. At the beginning of the channel realizations, UEs are uniformly distributed within indoor room environment.

Table 11: Simulation parameters of FDD massive MIMO VLC system

Parameter	**Value**
Half-intensity radiation angle ($\theta_{1/2}$)	40^{o}
Physical area of PD (A_p)	1 cm^2
Half angle of the receiver field-of-view (Θ_F)	85^{o}
3-dB cut-off frequency of LED ($f_{3-\mathrm{dB}}$)	2 MHz
PD responsivity (R)	0.28 A/W [93]
Noise PSD in VLC ($N_{0-\mathrm{VLC}}$)	10^{-22} W/Hz [93]
CP in VLC sub-frame ($N_{\mathrm{CP-VLC}}$)	16
VLC system bandwidth (B_{VLC})	5 MHz
Number of sub-frames in DL frame (T_{VLC})	200
Number of subcarrier in DL sub-frame ($N_{\mathrm{VLC}}^{\mathrm{SBC}}$)	64
Number of pilot subcarriers in DL sub-frame ($N_{\mathrm{VLC}}^{\mathrm{SBC-P}}$)	6
Number of pilot sub-frames in DL sub-frame ($N_{\mathrm{VLC}}^{\mathrm{LED-P}}$)	*varying*
Subcarrier spacing in DL sub-frame ($\Delta_{\mathrm{VLC}}^{\mathrm{SBC}}$)	156.25 kHz

Table 12: Simulation parameters of UL SISO MMW system

Parameter	**Value**
MMW reference path loss (L_{d_0})	68 dB
MMW reference distance (d_0)	1 m
MMW path loss exponent (v)	1.6
MMW shadowing standard deviation (σ_γ)	1.8
MMW Rician factor (I)	10 dB
MMW line-of-sight (LoS) fading channel (h_d)	$\sqrt{0.5 + j0.5}$
MMW transmit power (P_{MMW})	20 dBm
Noise PSD in MMW ($N_{0-\mathrm{MMW}}$)	-174 dBm/Hz
CP in MMW sub-frame ($N_{\mathrm{CP-MMW}}$)	32
MMW system bandwidth (B_{MMW})	20 MHz
Number of sub-frames in UL frame (T_{MMW})	200
Number of subcarrier in UL sub-frame ($N_{\mathrm{MMW}}^{\mathrm{SBC}}$)	128
Number of sub-frame in a single RB ($T_{\mathrm{MMW}}^{\mathrm{RB}}$)	5
Number of subcarrier in a single RB ($N_{\mathrm{MMW}}^{\mathrm{RB-S}}$)	9
Number of pilots in a single RB ($N_{\mathrm{MMW}}^{\mathrm{SBC-P}}$)	8
Number of RB in one frame ($N_{\mathrm{MMW}}^{\mathrm{RB}}$)	560
Number of null subcarrier in one UL sub-frame ($N_{\mathrm{MMW}}^{\mathrm{N}}$)	2
Subcarrier spacing in UL sub-frame ($\Delta_{\mathrm{MMW}}^{\mathrm{SBC}}$)	156.25 kHz

4.7.2 Numerical Results

In Fig. 37, DL data rates with respect to the average DCO-OFDM transmit power for different PA schemes under consideration are presented. Linear interpolation results are depicted with solid line, whereas, cubic interpolation results are displayed with dashed line. N is set to 30. Ideal case in which channel coefficients in the

spatial, frequency, and time domains are perfectly known in CU side and PA0 in which all LEDs are participated in pilot transmission and interpolation occurs in only frequency and time-domains, whereas, the channel estimation is still conducted for three domains, are taken into account as benchmark.

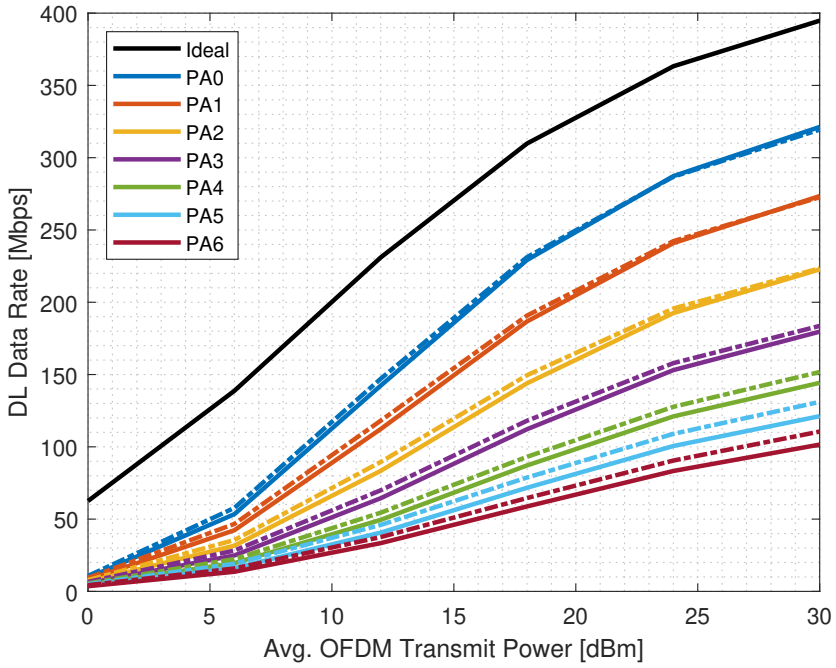

Figure 37: DL data rate of PAs for different power levels

When the power level is set to 12 dBm, ideal case achieves 230.98 Mbps. At the same level, PA0 gets the data rate values of 142.33 Mbps and 147.05 Mbps with the use of linear and cubic interpolation, respectively. The results indicate that cubic interpolation provides additional gain with respect to linear interpolation with a cost of requirement of more memory consumption and computation time. For PA1, the values are decreased to 112.29 Mbps and 118.09 Mbps, respectively. The degradation with an amount of approximately 30 Mbps is due to the interpolation error in the spatial domain. The value further decreases to 83.37 Mbps, 64.43 Mbps, 49.48 Mbps, 40.66 Mbps, and 33.38 Mbps using PA2, PA3, PA4, PA5, and PA6, respectively, with the use of linear interpolation. It can be said that DL channel estimation and

interpolation in massive MIMO VLC transmission obviously significantly affects DL data rate performance and proper selection of PA becomes critical.

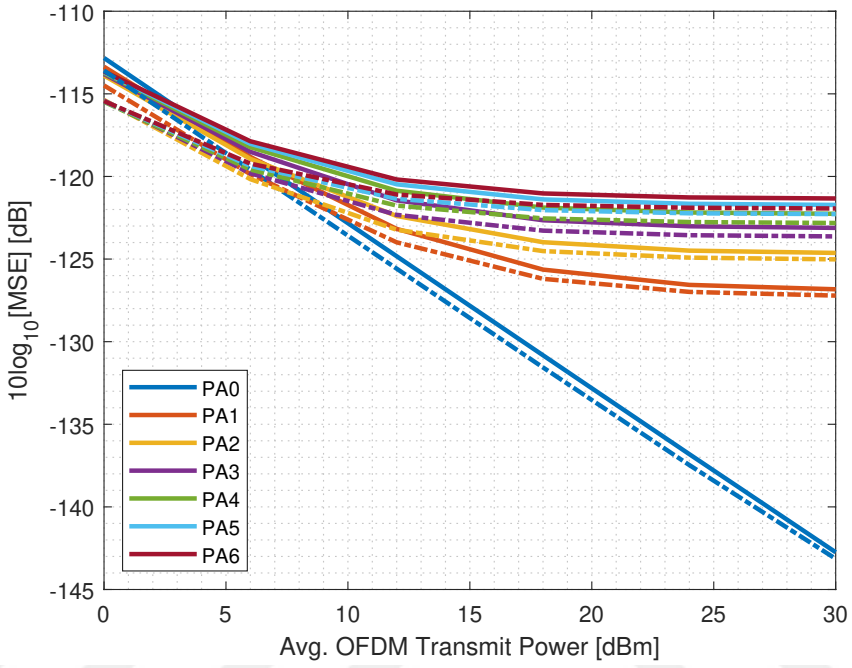

Figure 38: MSE performance of PAs under consideration

Mean squared error (MSE) performance of DL channel estimation and interpolation process is depicted in Fig. 38. The analytical expression of MSE in dB-scale can be written as

$$\text{MSE [dB]} = 10\log_{10}\frac{1}{N \times N_{\text{VLC}}^{\text{LED}} \times T_{\text{VLC}} \times N_{\text{VLC}}^{\text{SBC}}/2 - 1} \times \sum_{u=1}^{N} \sum_{i=1}^{N_{\text{VLC}}^{\text{LED}}} \sum_{\tau=0}^{T_{\text{VLC}}-1} \sum_{k=1}^{N_{\text{VLC}}^{\text{SBC}}/2-1} \left| H_{u,i}^{\text{VLC}-k,\tau} - \hat{H}_{u,i}^{\text{VLC}-k,\tau} \right|^2. \quad (62)$$

PA0 in which all LEDs are participated in pilot transmission achieves the lowest MSE and significantly outperform other PAs. It should be noted that when the transmit signal power increases, the difference between PA0 and the others becomes larger. This is because of the error floors as a consequence of interpolation error in spatial domain which is not available in PA0.

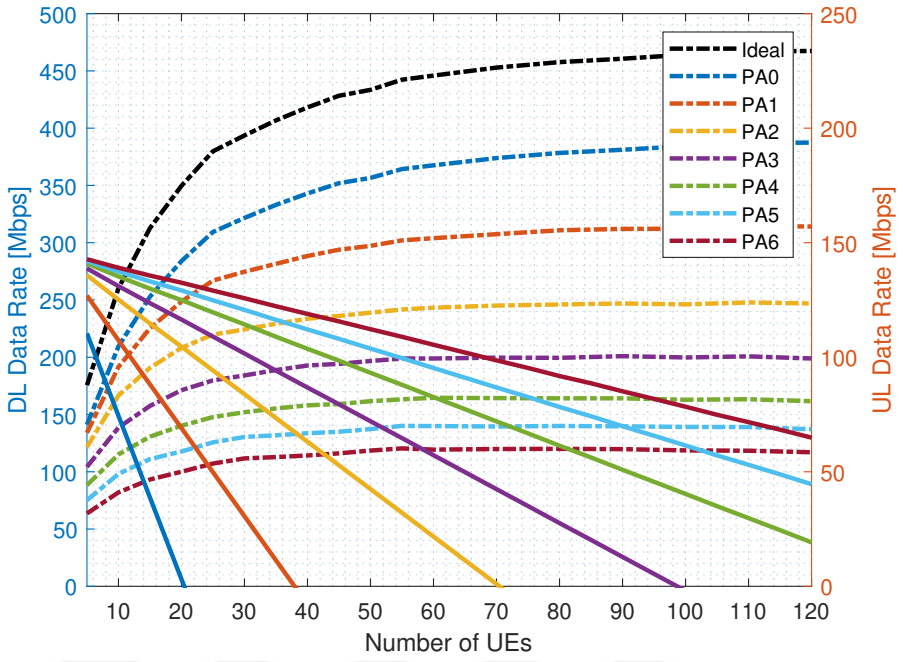

Figure 39: DL and UL data rate of PAs for different UE counts

In Fig. 39, data rate performances of DL and UL transmission regarding to the varying total number of UEs for different PA schemes under consideration are demonstrated. DL data rates are depicted with dashed line at left axis, whereas, UL data rates are given by solid line at right axis. The average transmit DCO-OFDM power in VLC network is set to 30 dBm and linear interpolation is utilized. When there are totally 5 UEs, DL data rate becomes 141.09 Mbps with the use of PA0. It then decreases to 133.99 Mbps, 121.67 Mbps, 104.26 Mbps, 88.34 Mbps, 75.09 Mbps, and 63.62 Mbps using PA1, PA2, PA3, PA4, PA5, and PA6, respectively. Relative UL values are 110.41 Mbps, 126.93 Mbps, 135.81 Mbps, 138.78 Mbps, 140.89 Mbps, 141.95 Mbps, and 142.80 Mbps, respectively. DL data rate values increase as the total number of UEs becomes larger in indoor room environment as a result of UE diversity. On the other hand, UL data rates dramatically decrease due to UL feedback overhead caused by estimated DL channel coefficient transmission. The results indicate that even though PA with lower indexes provides higher data rates, it suffers

in UL transmission when the number of UEs increases.

As in stated in Table 10, there may not any available resource to feedback to estimated DL channel coefficients to CU within a single frame. Numerically, maximum number of UEs with the use of PA0 is 20 for PA0. From the same figure, the limits of 39, 71, and 99 are obtained for PA1, PA2, and PA3, respectively. Therefore, there needs an adaptation among PAs to provide relatively sufficient data rates in both DL and UL sides.

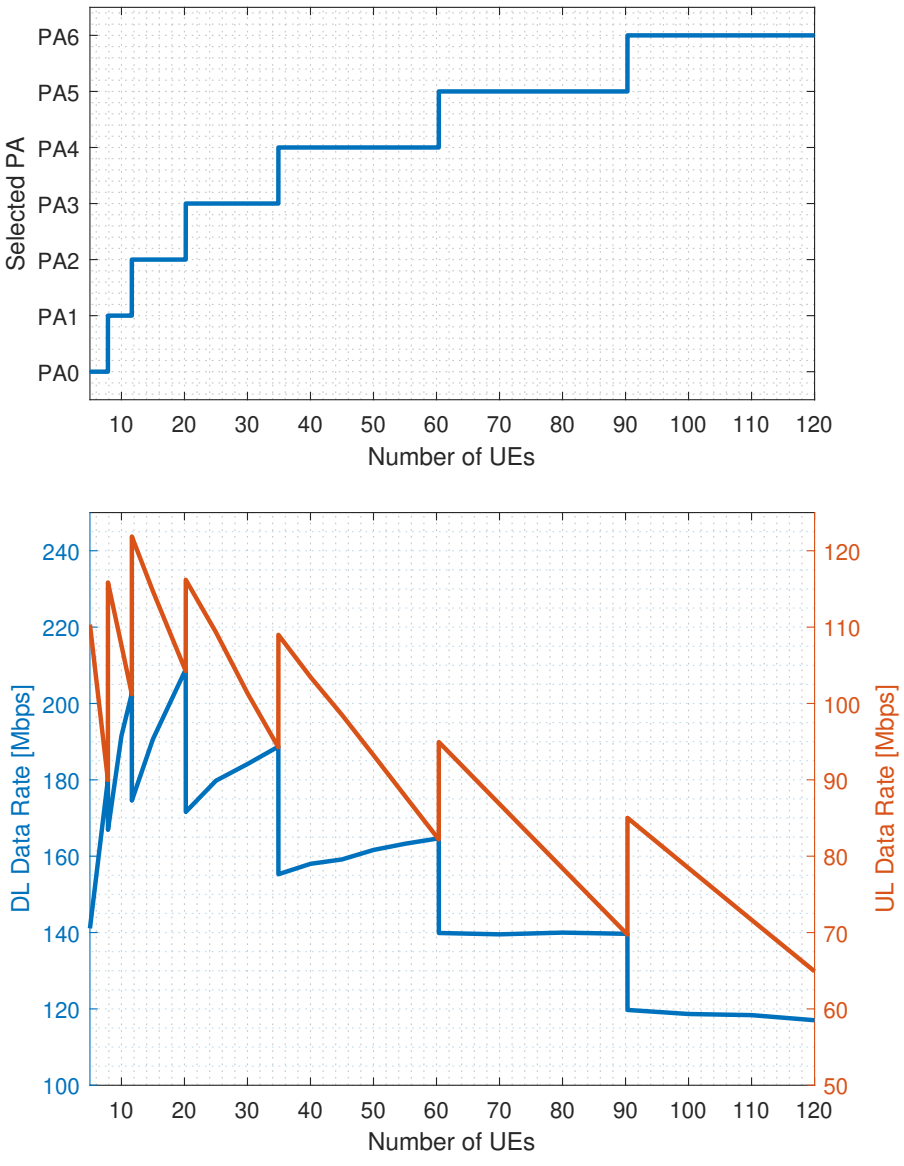

Figure 40: Selected PAs by DPC and resulting DL and UL data rates

In Fig. 40, selected PAs by DPC implemented in CU and resulting DL and UL data rate values are depicted. It is assumed that UL data rate should not be less than the half of the data rate in DL side such as $\beta = 0.5$ in Eq. 57. In this case, when there are totally less than 6 UEs, all of the PAs can be selected since all of them satisfy the constraint. However, since PA0, providing the highest DL data rate, should be selected. When the number is between 6 and 12; PA1, PA2 ... PA6 satisfy the constraint, but, PA1 achieves the highest data rate value. Therefore, it should be selected as PA scheme by CU. For the range between 12 and 20, PA2; 20 and 35, PA3; 35 and 60, PA4; 60 and 90, PA5; and for the remaining cases, PA6 can be selected by CU to keep the data rate balance at an acceptable level.

CHAPTER V

HYBRID MMW/VLC ACCESS NETWORKS

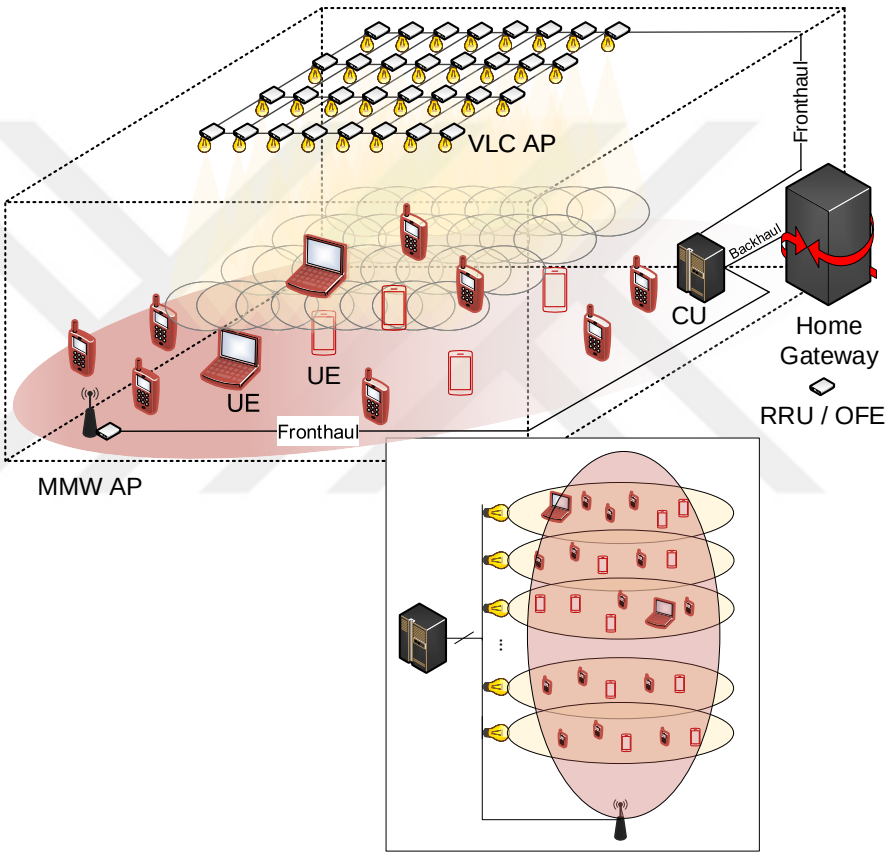

Figure 41: Centralized hybrid MMW/VLC access system architecture

In this chapter, a HetNet architecture including multiple VLC APs, each of which has a single LED, and a single MMW AP utilized in DL transmission is considered. The architecture is run over the centralized platform defined in Chapter 2 (see Fig. 41). In order to boost DL data rate performance through offloading the UEs from over-utilized APs to under-utilized ones, an adaptive vertical and horizontal handover mechanism is designed. The MMW network is the primary technology for

UE connection and UEs are then offloaded to the VLC network, which is considered as a complementary (or secondary) technology in the over-utilization cases.

In the conventional AP selection or offloading algorithms, the signal measurements from each AP for each UE are periodically obtained, then an optimization algorithm is run to find the best UE-AP mapping. However, it causes huge signalling overhead in UL side and huge battery consumption in UE. The designed handover mechanism that is inspired from the event-based reporting process of LTE [85] does not require this-type of periodical reporting. UE sends a measurement report to CU through serving AP to connect the adjacent AP if an offset-enhanced SINR level associated with the adjacent AP exceeds that of serving AP.

In contrast to the conventional distributed architectures in which each AP has its own functionality, the centralized architecture under consideration allows better optimization of the network configuration parameters as well as the management of the applications as a result of awareness of the global view of each AP. The offset variable is defined as technology-specific and tuned on-the-fly by an LB implemented in CU. Instead of using periodical reporting, LB has rule-set based algorithms which uses the number of connected UEs and data rates as inputs. Adaptive tuning of the offset variables aims to improve the network performance through the vertical handover while minimizing signaling overhead.

The remaining of the chapter is organized as following: DL system models for MMW and VLC networks are given in Section 5.1. VLC AP identification for handover is briefly described in Section 5.2. An adaptive handover mechanism is then proposed in Section 5.3. Finally, the performance results are demonstrated in Section 5.4.

5.1 Downlink System Model

PHY of DL MMW transmissions is based on OFDMA and PHY of DL VLC transmission builds upon its optical modified version, direct current biased optical OFDMA (DCO-OFDMA). Let $N_{\mathrm{VLC}}^{\mathrm{AP}}$ denote the number of VLC APs (e.g., LEDs), whereas, a single MMW AP is used, and N denote the number of active UEs within an indoor room environment under consideration. DL MMW transmission frame consists of T_{MMW} OFDMA sub-frames, each of which includes $N_{\mathrm{MMW}}^{\mathrm{SBC}}$ subcarriers, and DL VLC transmission frame consists of T_{VLC} DCO-OFDMA sub-frames, each of which includes $N_{\mathrm{VLC}}^{\mathrm{SBC}}$ subcarriers. The analytical expressions of OFDMA-based MMW and DCO-OFDMA-based VLC transmissions in DL side are defined in the rest of the section.

5.1.1 MMW Transmission

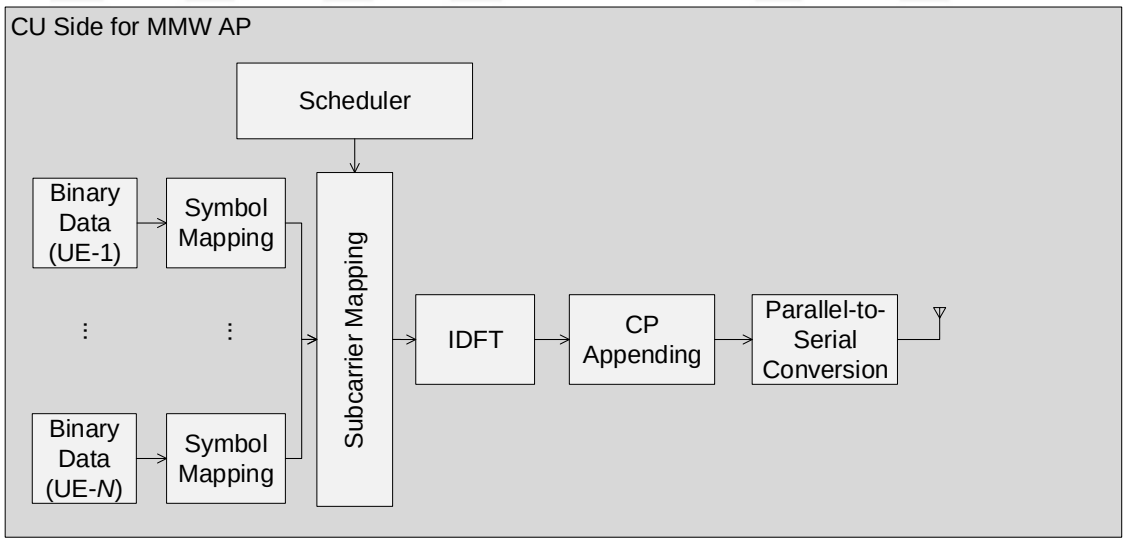

Figure 42: Block diagram of DL OFDMA transmission in CU side

The block diagram of DL OFDMA in MMW transmitter is depicted in Fig. 42. In the MMW transmitter available in CU side, the binary information of each UE is mapped to complex-valued symbols using either $M-$ary PSK or QAM. This progress

is repeated for each individual UE that is connected to MMW network. Based on the output of running PF scheduling algorithm[1], whose analytical expression is given in Appendix. B, the mapped symbols are put into the allocated subcarriers at specific sub-frames. The scheduling information is then forwarded to UEs for further decoding process through a dedicated DL control channel. The sequence including mapped symbols for τ^{th} OFDMA sub-frame, e.g.,

$$\mathbf{X}_0^{\text{MMW}-\tau} = [s_0^{0,\tau}\ s_0^{1,\tau}\ s_0^{2,\tau}\ ...\ s_0^{N_{\text{MMW}}^{\text{SBC}}-1,\tau}]^{\text{T}}, \tag{63}$$

where $[.]^{\text{T}}$ denotes transpose operation, is converted to parallel and passed through $N_{\text{MMW}}^{\text{SBC}}-$IDFT. The output can be written as

$$x_0^{\text{MMW}-n,\tau} = \frac{1}{\sqrt{N_{\text{MMW}}^{\text{SBC}}}} \sum_{k=0}^{N_{\text{MMW}}^{\text{SBC}}-1} X_0^{\text{MMW}-k,\tau} e^{j\frac{2\pi nk}{N_{\text{MMW}}^{\text{SBC}}}}. \tag{64}$$

In order to handle with ISI, a CP with the length of $N_{\text{CP}-\text{MMW}}$ which is selected to be longer than or equal to the multipath channel spread is appended to the beginning of $\mathbf{x}_0^{\text{MMW}}$. It is followed by parallel-to-serial conversion and resulting signal is then propagated through the MMW antenna.

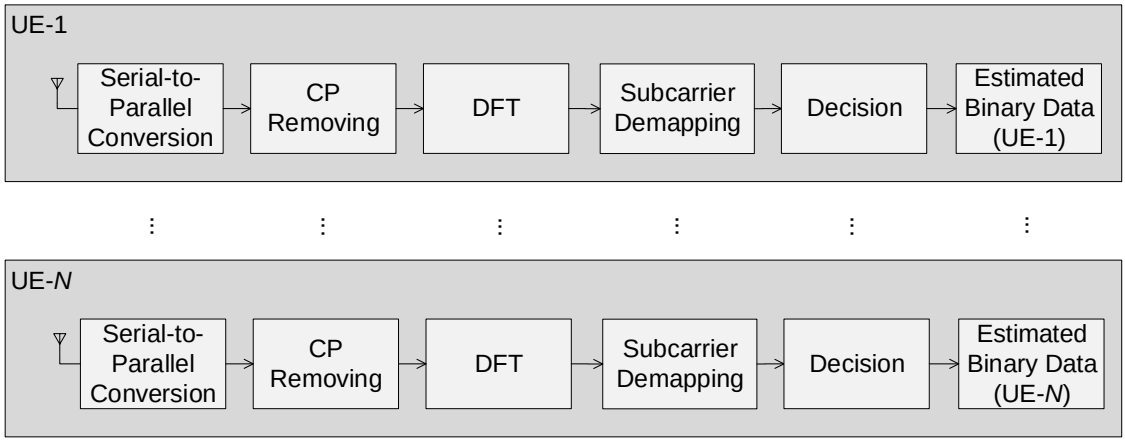

Figure 43: Block diagram of DL OFDMA transmission in UE side

[1]In this chapter, one MMW RB consists of one subcarrier over one sub-frame in contrast to the frame structure in Chapter 4 and two null subcarriers are used for each MMW sub-frame.

In the u^{th} UE (see Fig. 43), the received signal is sampled with the rate of $T_{\text{S-MMW}}$ and converted to the parallel streams with the length of $N_{\text{MMW}}^{\text{SBC}} + N_{\text{CP-MMW}}$. The CP is removed from the parallel streams and $N_{\text{MMW}}^{\text{SBC}}-$DFT is performed. The resulting signal at the k^{th} subcarrier and τ^{th} OFDMA sub-frame becomes

$$Y_u^{\text{MMW}-k,\tau} = \sqrt{P_{\text{MMW}}} H_{u,0}^{\text{MMW}-k,\tau} X_0^{\text{MMW}-k,\tau} + W_u^{\text{MMW}-k,\tau}, \tag{65}$$

where P_{MMW} is the average OFDMA signal power, $H_{u,0}^{\text{MMW}-k,\tau}$ is the MMW channel coefficients between u^{th} UE and MMW AP at k^{th} subcarrier and τ^{th} OFDMA sub-frame, and $W_u^{\text{MMW}-k,\tau}$ is complex-valued zero-mean AWGN term whose variance is given by $\sigma_{\text{MMW}}^2 = N_{0-\text{MMW}} B_{\text{MMW}}$ where $N_{0-\text{MMW}}$ is the MMW noise PSD and $B_{\text{MMW}} = 1/T_{\text{S-MMW}}$ is MMW system bandwidth in DL transmission side.

To extract the information, each UE performs subcarrier de-mapping based on allocation information obtained through the dedicated DL control channel and their own transmitted bits are decoded. Under the assumption of that channel coefficients are perfectly known in UE side, then optimal decision rule, ML, can be written as

$$\hat{X}_{u,0}^{\text{MMW}-k,\tau} = \underset{x \in \Theta}{\text{argmin}} \left\| Y_u^{\text{MMW}-k,\tau} - x\sqrt{P_{\text{MMW}}} H_{u,0}^{\text{MMW}-k,\tau} \right\|^2, \tag{66}$$

where Θ is the set of modulation symbols of selected modulation scheme. The resulting SNR of u^{th} UE at k^{th} subcarrier and t^{th} OFDMA sub-frame becomes

$$\text{SNR}_{u,0}^{\text{MMW}-k,\tau} = \frac{P_{\text{MMW}} \left| H_{u,0}^{\text{MMW}-k,\tau} \right|^2}{\sigma_{\text{MMW}}^2}. \tag{67}$$

5.1.2 VLC Transmission

The block diagram of DL DCO-OFDM in VLC transmitter is depicted in Fig. 44. In VLC transmitter available in CU side, binary information of each UE is mapped to complex-valued symbols using either $M-$ary PSK or QAM. As in MMW side, this progress is repeated for each individual UE information and the mapped symbols are inserted to the allocated subcarriers and specific sub-frames regarding to the output of

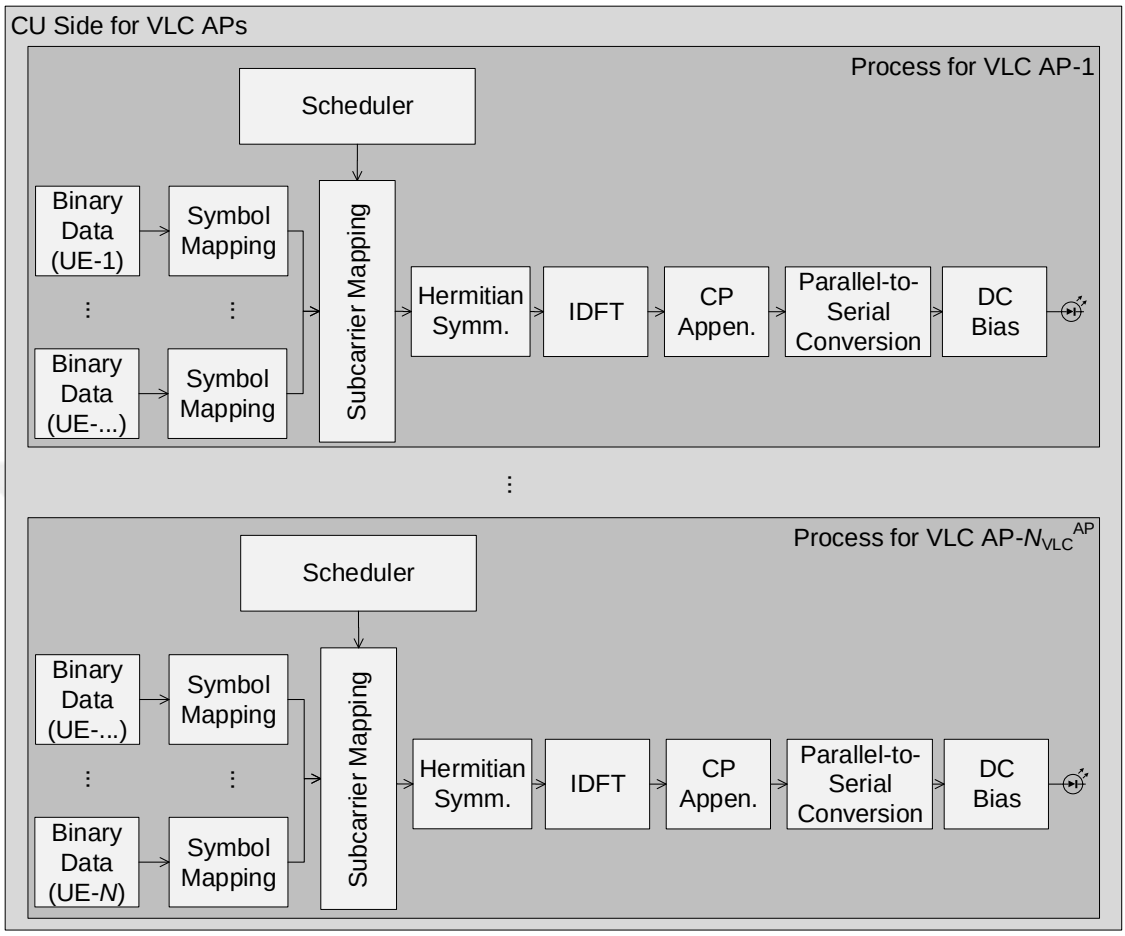

Figure 44: Block diagram of DL DCO-OFDMA transmission in CU side

running scheduling algorithm[2], whose analytical expression is given in Appendix. B. It should be noted that since there are multiple VLC APs (e.g., LEDs), each has its own UE group. Therefore, following process is done for each individual VLC AP whose index is denoted by $i \in \{1, 2...N_{\text{VLC}}^{\text{AP}}\}$[3]. The mapped signal sequence becomes $s_i^{1,\tau}\ s_i^{2,\tau}\ ...\ s_i^{N_{\text{VLC}}^{\text{SBC}}/2-1,\tau}$. To make the output of IDFT real valued, which is a constraint of IM/DD, the sequence is re-arranged to satisfy Hermitian symmetry such as

$$\mathbf{X}_i^{\text{VLC}-\tau} = [0\ s_i^{1,\tau}\ s_i^{2,\tau}\ ...\ s_i^{N_{\text{VLC}}^{\text{SBC}}/2-1,\tau}\ 0\ s_i^{N_{\text{VLC}}^{\text{SBC}}/2-1,\tau^*}\ ...\ s_i^{2,\tau^*}\ s_i^{1,\tau^*}]^{\text{T}}, \tag{68}$$

where $(.)^*$ denotes complex conjugate operation. It is converted to parallel and passed

[2]In this chapter, VLC RB consists of one subcarrier over one sub-frame.
[3]$i = 0$ refers to MMW AP.

through $N_{\mathrm{VLC}}^{\mathrm{SBC}}-$IDFT. The output can be written as

$$x_i^{\mathrm{VLC}-n,\tau} = \frac{1}{\sqrt{N_{\mathrm{VLC}}^{\mathrm{SBC}}}} \sum_{k=0}^{N_{\mathrm{VLC}}^{\mathrm{SBC}}-1} X_i^{\mathrm{VLC}-k,\tau} e^{j\frac{2\pi nk}{N_{\mathrm{VLC}}^{\mathrm{SBC}}}}. \tag{69}$$

In order to handle with ISI, a CP with the length of $N_{\mathrm{CP-VLC}}$ is appended to the beginning of $\mathbf{x}_i^{\mathrm{VLC}}$. It is followed by parallel-to-serial conversion and DC bias addition. The resulting signal is then propagated through i^{th} LED.

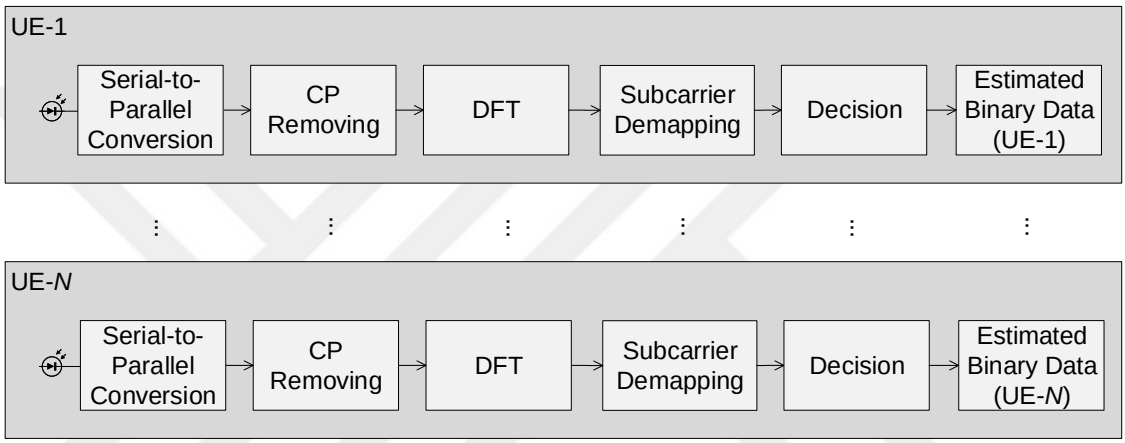

Figure 45: Block diagram of DL DCO-OFDMA transmission in UE side

In the u^{th} UE side (see Fig. 45) which is connected to the i^{th} LED, the received signal is sampled with the rate of $T_{\mathrm{S-VLC}}$ and converted to parallel streams with the length of $N_{\mathrm{VLC}}^{\mathrm{SBC}}+N_{\mathrm{CP-VLC}}$. The CP is removed from parallel streams and $N_{\mathrm{VLC}}^{\mathrm{SBC}}-$DFT is performed. The resulting signal at the k^{th} subcarrier of the τ^{th} sub-frame becomes

$$\begin{aligned} Y_u^{\mathrm{VLC}-k,\tau} =& R\sqrt{P_{\mathrm{VLC}}} H_{u,i}^{\mathrm{VLC}-k,\tau} X_i^{\mathrm{VLC}-k,\tau} + \\ & R\sqrt{P_{\mathrm{VLC}}} \sum_{j=1,j\neq i}^{N_{\mathrm{VLC}}^{\mathrm{AP}}} H_{u,j}^{\mathrm{VLC}-k,\tau} X_j^{\mathrm{VLC}-k,\tau} + W_u^{\mathrm{VLC}-k,\tau}, \end{aligned} \tag{70}$$

where R is the PD responsivity, $H_{u,i}^{\mathrm{VLC}-k,\tau}$ is the channel coefficient between u^{th} UE and i^{th} VLC AP at k^{th} subcarrier and τ^{th} DCO-OFDMA sub-frame, P_{VLC} is the average DCO-OFDMA signal power without bias term, $W_u^{\mathrm{VLC}-k,\tau}$ is complex-valued zero-mean AWGN term whose variance is given by $\sigma_{\mathrm{VLC}}^2 = N_{0-\mathrm{VLC}} B_{\mathrm{VLC}}$ where $N_{0-\mathrm{VLC}}$ is VLC noise PSD and $B_{\mathrm{VLC}} = 1/2T_{\mathrm{S-VLC}}$ is VLC system bandwidth in DL side.

To extract the information, each UE performs subcarrier de-mapping based on the allocation information obtained through the dedicated DL control channel and their own transmitted bits are decoded. Under the assumption of that channel coefficients are perfectly known in UE side, optimal decision rule, ML, can be written as

$$\hat{X}_u^{k,\tau} = \underset{x\in\Theta}{\operatorname{argmin}} \left\| Y_{u,i}^{\mathrm{VLC}-k,\tau} - x\sqrt{P_{\mathrm{VLC}}} H_{u,i}^{\mathrm{VLC}-k,\tau} \right\|^2, \tag{71}$$

where Θ is the set of modulation symbols of selected modulation scheme. The resulting SINR of the u^{th} UE at the k^{th} subcarrier and the τ^{th} DCO-OFDMA sub-frame becomes

$$\mathrm{SINR}_{u,i}^{\mathrm{VLC}-k,\tau} = \frac{R^2 P_{\mathrm{VLC}} \left| H_{u,i}^{\mathrm{VLC}-k,\tau} \right|^2}{R^2 P_{\mathrm{VLC}} \sum_{j=1,j\neq i}^{N_{\mathrm{VLC}}^{\mathrm{AP}}} \left| H_{u,j}^{\mathrm{VLC}-k,\tau} \right|^2 + \sigma_{\mathrm{VLC}}^2}. \tag{72}$$

5.2 Identification of VLC APs

Physical AP identity is a crucial parameter to identify the VLC APs operating at the same spectrum within an indoor room environment by UE. The identity is then used for specific management functions such as handover management defined in Section 5.3. CU allocates a numerical value to each AP. Based on the allocated value, AP periodically broadcast a specific signal sequence from a pre-defined subcarrier and sub-frame set. The UEs first listen these part of the DCO-OFDMA frame and identify the APs whose signals can be received.

The signal sequence is produced using Walsh Code. The UEs extract each AP identity through multiplication of each possible pre-defined Walsh Code sequence. The resulting sequences are summed and the identity giving the highest value is related to the best AP, which can be serving or adjacent. In similar way, second-best, third-best APs are identified by finding second and third highest values.

The identities should be allocated to APs in an effective way as a result of the fact that total number of distinct sequences may be less than total number of VLC APs. Specifically, the adjacent APs that have higher handover probability with each

other should not be allocated with the same identity. For this purpose, an identity allocation algorithm is proposed and given in Algorithm 2. The inputs of the proposed algorithm is $N_{\text{VLC}}^{\text{AP}}$ and available identity values, each of which refers to a unique Walsh Code, denoted by $\mathbf{C}$ (e.g., $[1, 2, 3...]^{\text{T}}$), whereas, the output is the allocated identities for each AP, denoted by $\mathbf{I}$ (e.g., $[1, 2, 8, 5..5, 2]^{\text{T}}$).

Input: $N_{\text{VLC}}^{\text{AP}}$,$\mathbf{C}$
Output: $\mathbf{I}$
$\mathbf{I} \leftarrow -1$
for $i \in \{1, 2...N_{\text{VLC}}^{\text{AP}}\}$ **do**
  $S_i^x \leftarrow$ x-coordinate of i^{th} AP
  $S_i^y \leftarrow$ y-coordinate of i^{th} AP
  initialize Δ as null
  if $I_i = -1$ **then**
    for $c \in \mathbf{C}$ **do**
      initialize δ as null
      for $t \in \{1, 2...N_{\text{VLC}}^{\text{AP}}\}$ **do**
        if $I_t == c$ **then**
          add c to δ
      $d \leftarrow \infty$
      counter $\leftarrow 0$
      for $t \in \delta$ **do**
        counter $\leftarrow$ counter $+ 1$
        $S_t^x \leftarrow$ x-coordinate of t^{th} AP
        $S_t^y \leftarrow$ y-coordinate of t^{th} AP
        d(counter) $\leftarrow \sqrt{(S_i^x - S_t^x)^2 + (S_i^y - S_t^y)^2}$
      $\Delta(c) \leftarrow \min(d)$
    $t \leftarrow \text{argmax}_c(\Delta_c)$
    $I_i \leftarrow C_t$

Algorithm 2: VLC AP identity allocation

The algorithm aims to allocate the code whose re-use distance is the highest one to the AP under consideration. For this purpose, at the beginning of the algorithm, all allocated codes to the APs are cleaned up (e.g., setting to an unknown code, -1). For an AP in order, minimum re-use distance of each code is calculated. Then, the code that gives the highest minimum re-use distance is allocated to this AP. For the following AP, same procedure is done under the consideration of the previous

allocations.

5.3 Adaptive Handover Mechanism

In the conventional AP selection algorithms, the signal measurements from each AP for UE are periodically obtained, then an optimization algorithm is run to find the best UE-AP mapping. However, it causes huge signalling overhead in UL side and huge battery consumption in UE. In contrast to the conventional algorithms, an event-based vertical and horizontal handover procedure is defined in this chapter. The proposed handover is initiated by CU after receiving a measurement report from UE side. The report content is given as

- SINR level measured from serving AP
- The highest (offset-enhanced) SINR level measured from adjacent AP
- The physical identity of this adjacent AP

The report is transmitted by UE to CU if an offset enhanced SINR level of the adjacent AP is greater than SINR level associated with serving AP. The offset variable is denoted by $O_{\mathrm{A}\rightarrow\mathrm{B}}$ where A and B represent the technology of serving and adjacent APs. For example, if $O_{\mathrm{MMW}\rightarrow\mathrm{VLC}}$ is set to 3 dB, then UEs connected to MMW network compare the SINR level measured from MMW AP with SINR level measured from VLC AP plus 3 dB. Similarly, if $O_{\mathrm{VLC}\rightarrow\mathrm{MMW}}$ is set to 3 dB, then UEs connected to VLC network compare the SINR level measured from VLC AP with SINR level measured from MMW AP plus 3 dB. The complete progress is given in Algorithm. 3. The offset variable makes the handover harder or easier via narrowing or extending the virtual coverage region of the APs and it is tuned on-the-by an LB implemented in CU.

After measurement reports are received by CU, it initiates the handover procedure to setup a connection between relevant UE and adjacent AP. For this purpose, CU

Input: Received Signal
Output: Measurement Report Transmission
Measure SINR from each AP in the coverage
Calculate $\text{SINR}_{\text{MAX}}^{\text{VLC}}$ as max(SINR of adjacent VLC APs)
if UE is served by VLC AP **then**
    Read $O_{\text{VLC}\rightarrow\text{MMW}}$ from received signal
    Calculate SINR_{MAX} as max($\text{SINR}_{\text{MAX}}^{\text{VLC}}$, SINR of MMW AP+$O_{\text{VLC}\rightarrow\text{MMW}}$)
    if SINR of serving AP < SINR_{MAX} **then**
        send measurement report
else
    Read $O_{\text{MMW}\rightarrow\text{VLC}}$ from received signal
    if SINR of serving AP < $\text{SINR}_{\text{MAX}}^{\text{VLC}} + O_{\text{MMW}\rightarrow\text{VLC}}$ **then**
        send measurement report

Algorithm 3: Measurement Report Transmission Decision

uses a neighbor relation table (NRT) that is prepared for each AP. In NRT, the physical identities and global identities[4] of the adjacent APs exist. CU first finds the AP that UE will be connected to using NRT and performs handover. It should be also noted that NRT content should be updated after every physical identity allocation and the identities in each NRT should be unique. After handovers, CU performs PF scheduling for each individual AP under the consideration of its own UE group.

The aim of proposed handover parameter tuning algorithm is to maximize overall system data rate through proper selection of AP for each UE. Based on well-known ergodic capacity definition [91], the achievable data rate for u^{th} VLC UE connected to i^{th} VLC AP at single DCO-OFDMA frame, denoted by D_u^{VLC}, can be written as

$$D_{u,i}^{\text{VLC}-t} = \frac{N_{\text{VLC}}^{\text{SBC}}}{(N_{\text{VLC}}^{\text{SBC}} + N_{\text{VLC}-\text{CP}}) \times T_{\text{VLC}}} \sum_{k=0}^{N_{\text{VLC}}^{\text{SBC}}-1} \sum_{\tau=0}^{T_{\text{VLC}}-1} \times \Delta_{\text{VLC}}^{\text{SBC}} \times \log_2 \left(1 + \frac{\varphi_{u,i}^{k,\tau} w_{u,i}^t R^2 P_{\text{VLC}} \left| H_{u,i}^{\text{VLC}-k,\tau} \right|^2}{R^2 P_{\text{VLC}} \sum_{j=1,j\neq i}^{N_{\text{VLC}}^{\text{AP}}} \left| H_{u,j}^{\text{VLC}-k,\tau} \right|^2 + \sigma_{\text{VLC}}^2} \right), \quad (73)$$

where $\times$ denotes scalar multiplication, $\varphi_{u,i}^{k,\tau}$ takes the value of either 0 or 1 and denotes

[4]It denotes the unique identity within an indoor room environment. When a new VLC AP is deployed within the indoor room environment, it cannot be configured with an existing value.

whether the k^{th} subcarrier of the i^{th} VLC AP is assigned to the u^{th} UE at the τ^{th} DCO-OFDMA sub-frame based on running PF algorithm output, $w_{u,i}^{t}$ denotes the selected APs for the u^{th} UE at the t^{th} frame and it takes value of either 0 (i.e., not-connected) or 1 (i.e., connected)[5], and $\Delta_{\text{VLC}}^{\text{SBC}}$ denotes the subcarrier spacing in DCO-OFDMA frame.

Similarly, the achievable data rate for u^{th} MMW UE at a single OFDMA frame, denoted by D_{u}^{MMW}, can be written as

$$D_{u,0}^{\text{MMW}-t} = \frac{N_{\text{MMW}}^{\text{SBC}}}{(N_{\text{MMW}}^{\text{SBC}} + N_{\text{MMW-CP}}) \times T_{\text{MMW}}} \sum_{k=0}^{N_{\text{MMW}}^{\text{SBC}}-1} \sum_{\tau=0}^{T_{\text{MMW}}-1} \times \Delta_{\text{MMW}}^{\text{SBC}} \times \log_2 \left(1 + \frac{\varphi_{u,0}^{k,\tau} w_{u,0}^{t} P_{\text{MMW}} \left| H_{u,0}^{\text{MMW}-k,\tau} \right|^2}{\sigma_{\text{MMW}}^2} \right), \tag{74}$$

where $\varphi_{u,0}^{k,\tau}$ takes the value of either 0 or 1 and denotes whether the k^{th} subcarrier of MMW AP is assigned to the u^{th} UE at the τ^{th} OFDMA sub-frame based on running PF algorithm output and $\Delta_{\text{MMW}}^{\text{SBC}}$ denotes the subcarrier spacing in DCO-OFDMA frame. Therefore, the overall system data rate at the t^{th} transmission frame, denoted by $D^{\text{HYB}-t}$, becomes

$$D^{\text{HYB}-t} = \sum_{u=1}^{N_{\text{VLC}}} \sum_{i=1}^{N_{\text{VLC}}^{\text{AP}}} D_{u,i}^{\text{VLC}-t} + \sum_{u=1}^{N_{\text{MMW}}} D_{u,0}^{\text{MMW}-t}, \tag{75}$$

where N_{VLC} and N_{MMW} denote number of UEs connected to VLC and MMW network, respectively. It can be also extracted that both PF algorithm and proposed handover algorithm work at the beginning of each OFDMA and DCO-OFDMA transmission frame.

Mathematically speaking, this optimization problem for each t^{th} frame can be

[5]It should be also noted that $w_{u,0}^{t}$ indicates the connected to MMW AP.

formulated as

$$\max_{O^t_{\mathrm{MMW}\to\mathrm{VLC}}, O^t_{\mathrm{VLC}\to\mathrm{MMW}}} \left\{D^{\mathrm{HYB}-t}\right\} \tag{76}$$

such that

$$w^t_{u,i} = \begin{cases} 1 & \text{if } i = \underset{j}{\mathrm{argmax}}(\gamma^{t-1}_{u,j} + |w^{t-1}_{u,j} - 1|O^t_{u,j}) \\ 0 & \text{else} \end{cases} \tag{77}$$

$$O^t_{u,i} = \begin{cases} O^t_{\mathrm{MMW}\to\mathrm{VLC}} & \text{if } w^{t-1}_{u,0} = 1 \\ O^t_{\mathrm{VLC}\to\mathrm{MMW}} & \text{if } w^{t-1}_{u,0} = 0 \text{ and } j = 0 \\ 0 & \text{else} \end{cases} \tag{78}$$

with the initial conditions ($t = 0$) of

$$w^0_{u,0} = 1 \tag{79}$$

$$w^0_{u,i} = 0 \; \forall \; i \in \{1, 2...N^{\mathrm{AP}}_{\mathrm{VLC}}\} \tag{80}$$

where $\gamma^{t-1}_{u,j}$ denotes the average SINR value measured from the u^{th} UE connected to the i^{th} AP at the t^{th} frame. Since the PF scheduling algorithm, which decides the values in φ, is deterministic, the only variable that should be selected by the system with the aim of maximizing overall system data rate is $O_{\mathrm{MMW}\to\mathrm{VLC}}$ and $O_{\mathrm{VLC}\to\mathrm{MMW}}$. To adjust these parameters each t^{th} frame, the observation based tuning algorithm is proposed and given in Algorithm 4.

The offset tuning mechanism includes a number of decision rule-sets where the overall system data rate (D^{HYB}), individual data rate of MMW link, denoted by D^{MMW}, and the number of UEs connected to VLC and MMW networks (N_{VLC} and N_{MMW}, respectively) are taken as inputs. At the beginning of the algorithm, the UEs are connected to the MMW network (see Eq. 79). The aim is to offload the UEs from MMW AP to VLC APs in the case of when the ratio of the number of UEs connected to the MMW network to the total number of UEs in the system (e.g., it is 1 at the beginning) is greater than or equal to a threshold level, denoted by

Input: D_{MMW},D_{HYB},N_{MMW},N_{TH},$O_{\mathrm{VLC}\to\mathrm{MMW}}$,$O_{\mathrm{MMW}\to\mathrm{VLC}}$
Output: $O_{\mathrm{VLC}\to\mathrm{MMW}}$,$O_{\mathrm{MMW}\to\mathrm{VLC}}$

```
if t > 0 then
    if D^{t-1}_MMW ≤ D^t_MMW and D^{t-1}_HYB ≤ D^t_HYB then
        if O^{t-1}_{MMW→VLC} < O^t_{MMW→VLC} and N_TH ≤ N_MMW then
            Decrease O_{VLC→MMW} with Δ
            Increase O_{MMW→VLC} with Δ
        else
            if O^{t-1}_{MMW→VLC} > O^t_{MMW→VLC} then
                Increase O_{VLC→MMW} with Δ
                Decrease O_{MMW→VLC} with Δ
            else
                Approach O_{VLC→MMW} to 0 dB
                Approach O_{MMW→VLC} to 0 dB
    if D^{t-1}_MMW > D^t_MMW and D^{t-1}_HYB > D^t_HYB then
        if O^{t-1}_{MMW→VLC} > O^t_{MMW→VLC} and N_TH ≤ N_MMW then
            Decrease O_{VLC→MMW} with Δ
            Increase O_{MMW→VLC} with Δ
        else
            if O^{t-1}_{MMW→VLC} < O^t_{MMW→VLC} then
                Increase O_{VLC→MMW} with Δ
                Decrease O_{MMW→VLC} with Δ
            else
                Approach O_{VLC→MMW} to 0 dB
                Approach O_{MMW→VLC} to 0 dB
else
    if N_TH ≤ N_MMW then
        Decrease O_{VLC→MMW} with Δ
        Increase O_{MMW→VLC} with Δ
    else
        Increase O_{VLC→MMW} with Δ
        Decrease O_{MMW→VLC} with Δ
```

Algorithm 4: Proposed Adaptive Offset Tuning

N_{TH}, which is decided based on a linear function of N. For this purpose, N_{MMW} and N_{TH} are checked. If the condition satisfies, then $O_{\mathrm{MMW}\to\mathrm{VLC}}$ will be increased with a pre-defined Δ value. The increment of $O_{\mathrm{MMW}\to\mathrm{VLC}}$ narrows the virtual coverage of MMW AP and make the handover from MMW to VLC network easier for the UEs locating at coverage edges. $O_{\mathrm{VLC}\to\mathrm{MMW}}$ will be also decreased with the same

amount in order to avoid from ping-pong handovers[6]. It should be noted that N_{TH} value should be carefully selected in order to maximize the overall system data rate. Specifically, larger value of N_{TH} limits the maximization of data rate since it restricts the offloading process, however, smaller values are resulted by no more UE connected to MMW network, that causes degradation on system level data rate.

The first offloaded UEs are the ones with worse MMW channel conditions as a result of locating at coverage borders and relatively lower data rate values are observed at these type of UEs. Since PF scheduling algorithm allocates more resource elements in terms of subcarriers at each sub-frame to this-type of UEs as a result of fairness issue among serving UEs, offloading process benefits the rest of the UEs through allocation of more resource elements, which results in higher data rate on both overall system and individual MMW network. On the other hand, there are two cases that cause a degradation on overall system data rate:

- Insufficient increment on the data rates of remaining UEs in MMW network
- Offloading of the UEs with good MMW channel conditions due to higher offset values

To handle with above two cases, proposed adaptive algorithm always checks the both overall system data rate and individual MMW network data rate in conjunction with the number of connected UE balance between two networks in terms of N_{TH}. If N_{MMW} is still equal to or greater than N_{TH} and following three conditions are satisfied:

- $O_{\mathrm{MMW}\rightarrow\mathrm{VLC}}$ is increased at the previous step
- D^{MMW} increased or remains the same as comparing with previous step
- D^{HYB} increased or remains the same as comparing with previous step

[6]A handover request from VLC to MMW network after offloading to VLC network

then $O_{\mathrm{MMW}\rightarrow\mathrm{VLC}}$ will be again increased. The reason of why same action is repeated is the assumption of that proposed algorithm tunes the offset variables in a correct-way. Similarly, If following three conditions are satisfied:

- $O_{\mathrm{MMW}\rightarrow\mathrm{VLC}}$ is decreased at the previous step
- D^{MMW} increased or remains the same as comparing with previous step
- D^{HYB} increased or remains the same as comparing with previous step

then $O_{\mathrm{MMW}\rightarrow\mathrm{VLC}}$ will be again decreased as a result of same assumption. On the other hand, if following three conditions are satisfied:

- $O_{\mathrm{MMW}\rightarrow\mathrm{VLC}}$ is increased at the previous step
- D^{MMW} decreased as comparing with previous step
- D^{HYB} decreased as comparing with previous step

then, $O_{\mathrm{MMW}\rightarrow\mathrm{VLC}}$ will be now decreased. Herein, the reason of why opposite action is taken into account is the fact that proposed algorithm tunes the offset variable is a wrong-way, in other words, previous assumption is not correct. In similar way, if following four conditions are satisfied:

- N_{MMW} is still equal to or greater than N_{TH}
- $O_{\mathrm{MMW}\rightarrow\mathrm{VLC}}$ is decreased at the previous step
- D^{MMW} decreased as comparing with previous step
- D^{HYB} decreased as comparing with previous step

then, $O_{\mathrm{MMW}\rightarrow\mathrm{VLC}}$ will be now increased due to the wrong assumption as in previous case. Noting that new UEs can participate in indoor room environment or decide to start data transfer or even some UEs may drop due to such links failures in addition

to their natural mobility conditions. All of these yields a data rate fluctuation and lead a improper comparisons for current and previous values. Therefore, in order to keep the system active and check the network behaviour regarding to different offset values, both $O_{\mathrm{MMW}\rightarrow\mathrm{VLC}}$ and $O_{\mathrm{VLC}\rightarrow\mathrm{MMW}}$ are tried to reach 0 dB through increment or decrement with the amount of Δ in the case of when any of the rule-sets defined above does not satisfy.

5.3.1 Decisions of Adaptive Handover Algorithm Inputs

In the following, the reason of why each of the metrics is used or not is explained:

- *Overall system data rate*: The main aim of the proposed handover algorithm is to maximize overall system data rate value. This is done through tuning the offset variable which is used in handover algorithm. The offset variable is tuned based on observations of whether an increment in offset parameter brings an increment in the overall system data rate or whether a decrement in offset parameter brings an increment in the data rate

- *Data rate of MMW network*: Increment of $O_{\mathrm{MMW}\rightarrow\mathrm{VLC}}$ narrows the virtual coverage of MMW APs and helps to offload UEs to VLC APs. The firstly offloaded UEs are the ones which have worse channel conditions. Since PF scheduler allocates more resources to UEs with worse channel conditions (with the aim of fairness among UEs), the offloading process can benefit the remaining UEs with allocation of more resources and results in higher data rates in MMW network. On the other hand, when the offloaded UEs (to VLC network) cannot achieve sufficiently high data rates, system data rate will decrease. Additionally, offloading of UEs with good channel conditions due to higher offset values may cause a degradation in MMW network. In order to avoid from such cases, the proposed algorithm observes the data rate of MMW network in addition to the overall system data rate. In the case that degradation of both MMW network

and overall system data rate are observed, the last change on offset is rollbacked.

- *Data rate of VLC network*: This metric is not used because UE will have lower data rate when it is offloaded to VLC network as a result of interference issue between VLC APs. On the other hand, even though VLC data rate is decreased, data rates in MMW network and overall system can still increase if firstly offloaded UEs are the ones with worse channel conditions.

- *Number of MMW and VLC UEs*: At the beginning of the algorithm, since there is no recorded data rate related to the previous time slot and the offset was not adjusted yet, any data rate variations cannot be observed. Therefore, the algorithm checks the number of connected UEs to each technology. If the number of connected UEs to MMW is greater than or equal to a pre-defined threshold level, $O_{\mathrm{MMW}\rightarrow\mathrm{VLC}}$ is increased and $O_{\mathrm{VLC}\rightarrow\mathrm{MMW}}$ is decreased. It should be also noted that MMW network provides higher data rate values than VLC network for the scenario under consideration. Therefore, to maximize the overall system data rate, at least one UE should be kept in MMW network. For this purpose, the number of connected UEs in MMW network is used in the Algorithm 4.

5.3.2 Algorithm Complexity

In this chapter, a simple and practical handover mechanism that compares an offset enhanced SINR levels obtained through different APs is proposed. The system basically tunes the offset parameter based on the obtained and recorded data rate values and the number of connected UE to each MMW and VLC technologies. The requirements of the proposed algorithm are summarized in Table 13 that indicated the total complexity of O(n) where n denotes the number of UEs within an indoor room environment.

Table 13: Requirements and Big-O of adaptive handover algorithm

Operation Type	**Item**	**Big-O**
Store	Recording the last offset values	O(1)
Store	Recording the last overall system data rate	O(1)
Store	Recording the last MMW data rate	O(1)
Store	Recording the current overall system data rate	O(1)
Store	Recording the current MMW data rate	O(1)
Comparison	Value comparisons in each time slot for each UE	O(n)

5.4 Performance Evaluations

In this section, the performance results of hybrid MMW/VLC access network architecture with an adaptive handover mechanism are demonstrated after the simulation environment is explained.

5.4.1 Simulation Environment

An indoor room environment with the dimensions of 14 m $\times$ 14 m $\times$ 3 m is considered. The environment under consideration includes one MMW AP, whose location is set to (6.5 m, 0.5 m, 0.2 m) assuming the room center is the below left corner of floor and 32 VLC APs that are uniformly located in a rectangular grid in the ceiling. Commercially available luminaries from Cree (LR24-38SKA35) are used as VLC AP and operated at 73 lumens per watt efficacy, referring the fact that the average illumination level is 533 lx in order to satisfy typical illumination requirements for workplaces [96].

Table 14: Simulation parameters of VLC network in hybrid access

Parameter	**Value**
Half-intensity radiation angle ($\theta_{1/2}$)	40^{o}
Physical area of PD (A_p)	1 cm^2
Half angle of the receiver field-of-view (Θ_F)	85^{o}
3-dB cut-off frequency of LED ($f_{3-\mathrm{dB}}$)	2 MHz
PD responsivity (R)	0.28 A/W [93]
Noise PSD in VLC ($N_{0-\mathrm{VLC}}$)	10^{-22} W/Hz [93]
VLC system bandwidth (B_{VLC})	5 MHz
Number of subcarrier in VLC AP ($N_{\mathrm{VLC}}^{\mathrm{SBC}}$)	64
Number of sub-frames (T_{VLC})	30
Subcarrier spacing ($\Delta_{\mathrm{VLC}}^{\mathrm{SBC}}$)	156.25 kHz
CP in VLC ($N_{\mathrm{CP-VLC}}$)	16
DCO-OFDM transmit power (P_{VLC})	30 dBm

Table 15: Simulation parameters of MMW network in hybrid access

Parameter	**Value**
MMW reference path loss (L_{d_0})	68 dB
MMW reference distance (d_0)	1 m
MMW path loss exponent (v)	1.6
MMW shadowing standard deviation (σ_γ)	1.8
MMW Rician factor (I)	10 dB
MMW LoS fading channel (h_d)	$\sqrt{0.5 + j0.5}$
Noise PSD in MMW ($N_{0-\mathrm{MMW}}$)	-174 dBm/Hz
MMW system bandwidth (B_{MMW})	80 MHz
Number of subcarrier in MMW sub-frame ($N_{\mathrm{MMW}}^{\mathrm{SBC}}$)	512
Number of sub-frames (T_{MMW})	30
Subcarrier spacing ($\Delta_{\mathrm{MMW}}^{\mathrm{SBC}}$)	156.25 kHz
CP in MMW sub-frame ($N_{\mathrm{CP-MMW}}$)	128
MMW transmit power (P_{MMW})	20 dBm

VLC channel model between the u^{th} UE and the i^{th} VLC AP is generated following Eq. 86, whereas, MMW channel model between the u^{th} UE and MMW AP is based on the model defined in Eq. 87 in Appendix A, respectively. The VLC-related and MMW-related parameters are given in Table 14 and 15, respectively.

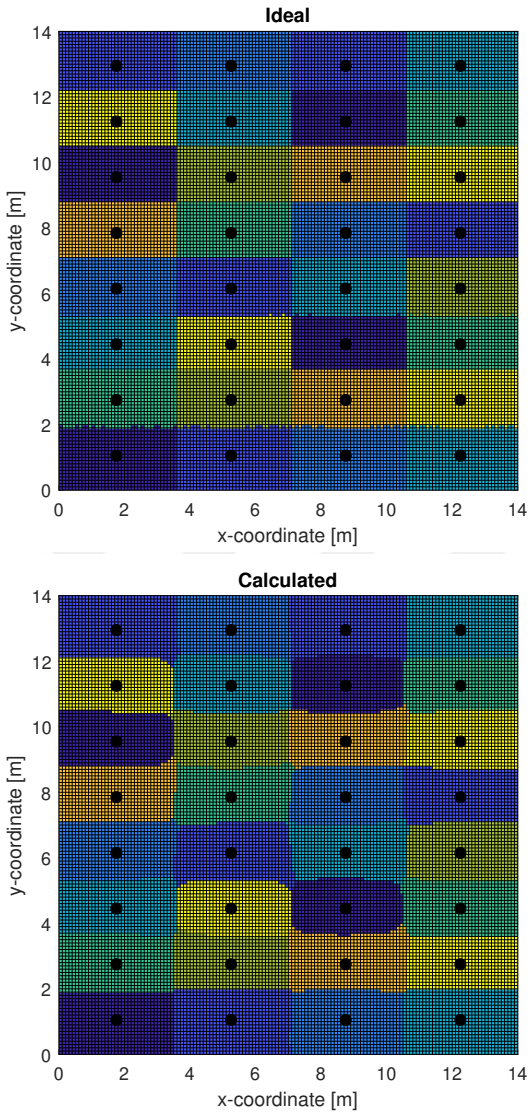

Figure 46: Serving AP identities

For an indoor room environment under consideration, calculated serving AP and second-best AP identities are depicted in Figs. 46 and 47 where each color denotes the different identity with existing (ideal) allocation for 8 distinct sequences. The black points denote the locations of VLC APs. The results show that UEs are able to perfectly identify the APs in VLC network.

In Fig. 48, the SINR for stand-alone VLC network and SNR[7] for stand-alone

[7]It should be noted that since there is a single MMW AP, SNR is equal to SINR value.

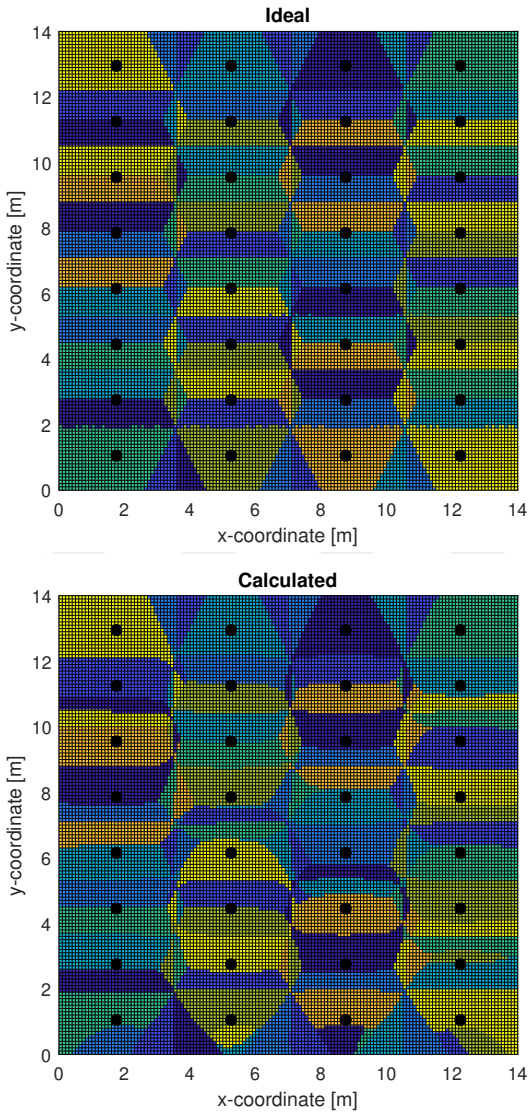

Figure 47: Second best AP identities

MMW network is depicted under the consideration of the utilized channel models. The color bars display the SINR/SNR value in dB-scale in which yellow color shows the better network quality whereas blue color indicates relatively low quality. When stand-alone MMW network is considered, it can be observed that SNR levels are in the range of approximately 23 dB and 50 dB. On the other hand, for stand-alone VLC network, the range is between -5 dB and 22 dB, which is relatively low with respect to the values in MMW network. The main reason of this difference is the inter AP

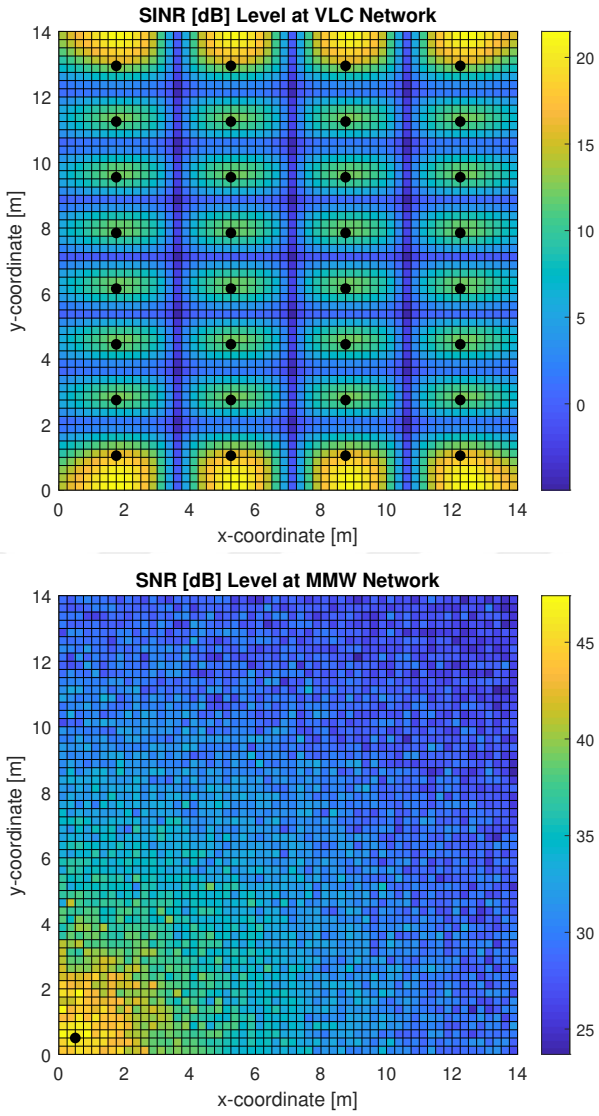

Figure 48: SINR values of UEs connected to VLC and MMW APs

interference in VLC network, which does not exist in MMW network. When pure SINR comparison is taken into account (e.g, setting offset variables to 0 dB), all UEs are connected to MMW AP and this situation yields non-usage of VLC network in which totally 32×5 MHz= 160 MHz bandwidth is not utilized, whereas, MMW network bandwidth with the value of 80 MHz is shared between all active UEs within the indoor room environment under consideration.

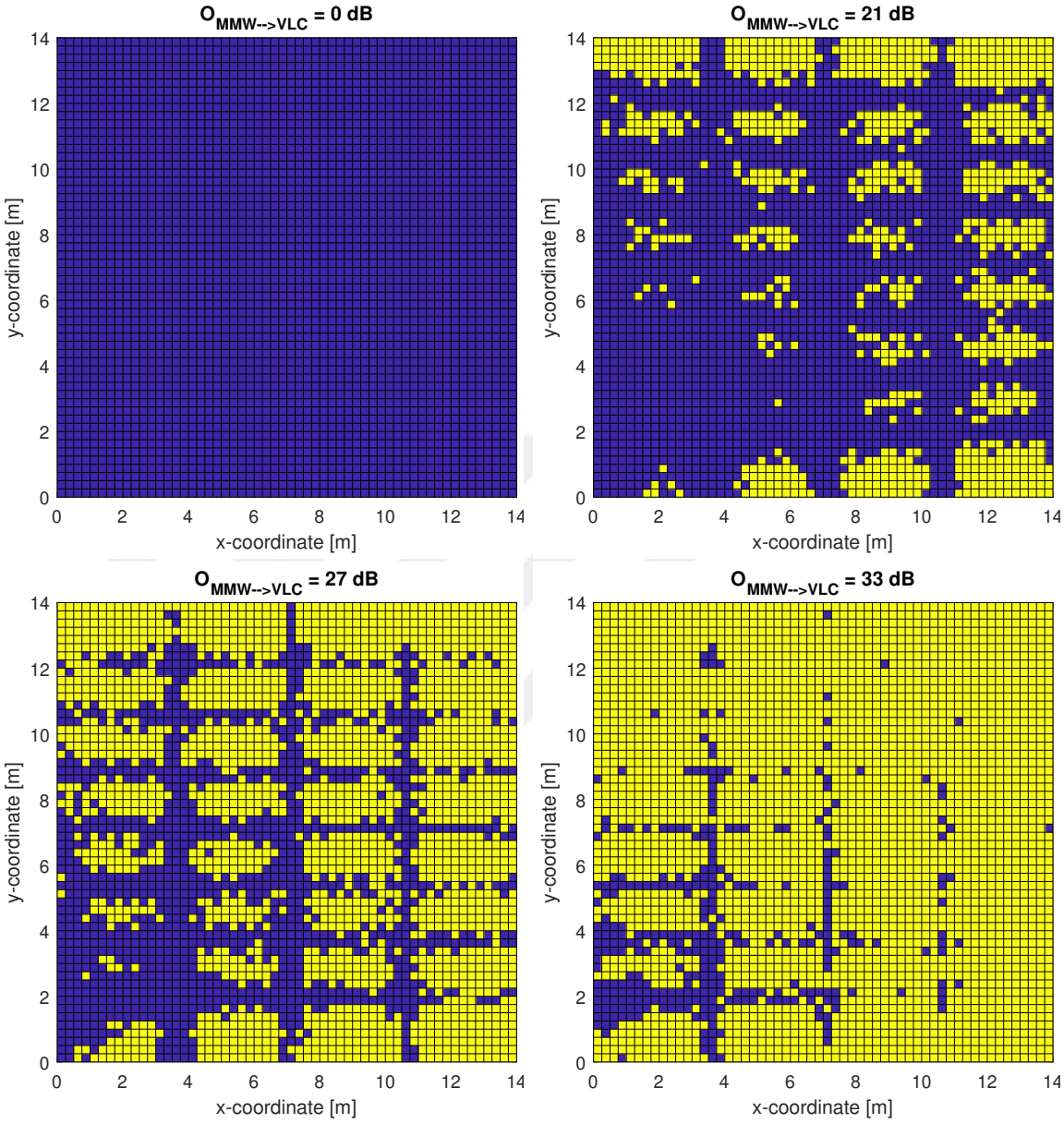

Figure 49: Selected APs with respect to different offset values

The locations in which UEs are connected to whether MMW or VLC APs regarding to the different offset variable values are depicted in Fig. 49 where yellow color indicates the VLC connection and blue color indicates the MMW connection. In the initial case (e.g., $O_{\mathrm{MMW}\rightarrow\mathrm{VLC}} = 0$ dB), as in explained in previous paragraph, all UEs are connected to MMW AP. The situation yields an imbalance between MMW and VLC networks. The value is increased to 21 dB, 27 dB, and 33 dB, respectively, it

can be seen that relatively more UEs are started to be offloaded/connected to VLC network APs. When the offset parameter is further increased, there will not be any UEs connected to MMW AP, which is resulted by a data rate degradation in the overall system performance due to relatively low SINR values at VLC network and unused bandwidth of MMW network. There is a UE balance that should be kept with the proposed algorithm with the aim of maximizing overall system performance.

5.4.2 Numerical Results

In the following, the system performance in terms of usage of different Δ and N_{TH} are depicted. It is followed by demonstration of signalling overhead reduction. Then, the data rate performance in terms of different UEs counts as comparing with stand-alone MMW and VLC network performance and a benchmark algorithm that directly offloads the UEs based on their data rates is investigated. The capacity limitation in fronthaul and backhaul links are further analyzed and individual UE data rate statistics are presented at the end of chapter.

In order to evaluate the performance of the proposed system, a simulation study based on 1500 independent channel realizations each of which consists of 100 time intervals is conducted. An interval includes one OFDMA frame (for MMW) and DCO-OFDMA frame (for VLC). Both frames consist of 30 sub-frames. In underlying MMW and VLC systems, sub-frames have a fixed duration of 8 us as a result of the selection of the same subcarrier spacing and CP duration. Therefore, the length of each time interval is 0.24 ms. Both PF scheduling algorithm and proposed offset tuning algorithm are run at the beginning of each time interval. At the beginning of the channel realizations, UEs are uniformly distributed within indoor room environment and then randomly selected set of UEs are moved with the velocity of 10 cm/s following random walk procedure.

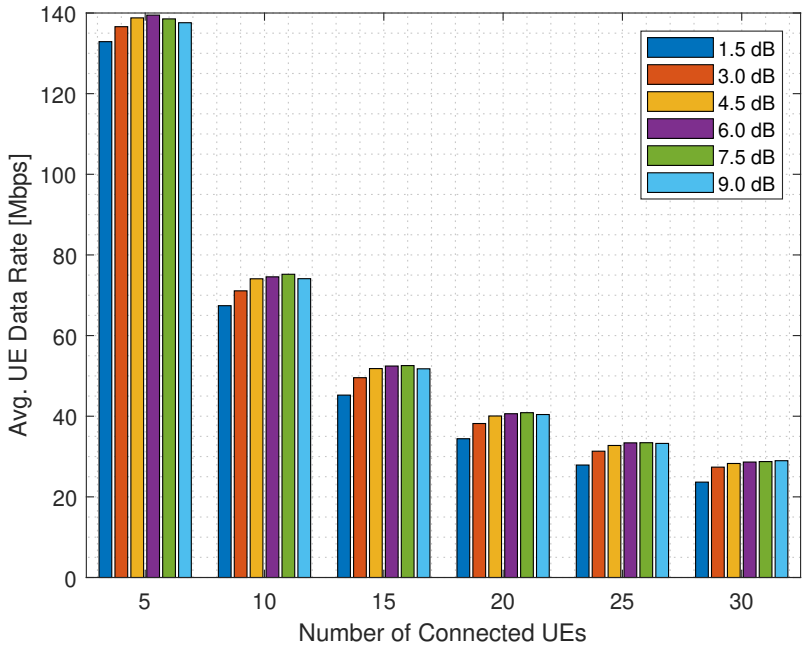

Figure 50: Effect of different Δ values over average UE data rate

The effect of the selection of Δ values on auto-tuning algorithm is demonstrated in Fig. 50 where N_{TH} is set to $0.33N$. The data rate values are obtained by taking the average of instantaneous data rates at each time slots within each channel realization. When the number of UEs is set to 5, the hybrid MMW/VLC system achieves the highest data rate with the value of 139.5 Mbps using $\Delta = 6$ dB. In this case, lowest value becomes 132.9 Mbps with the use of $\Delta = 1.5$ dB and the difference between the highest and lowest values is 6.6 Mbps. For $N = 10$, the highest data rate is obtained with the use of $\Delta = 7.5$ dB, whereas, the difference to the lowest value is 7.8 Mbps. When $N = 15$, $N = 20$, and $N = 25$ are considered, usage of $\Delta = 7.5$ dB becomes optimal. For these cases, the difference becomes 7.3 Mbps, 6.4 Mbps, and 5.5 Mbps, respectively. However, Δ of 9 dB gives the highest value for $N = 30$. Herein, the difference to the lowest value is equal to 5.3 Mbps.

The results reveal that using of different Δ values provides different data rate

performance regarding to the number of connected UE within an indoor room environment. This Δ value is a design parameter which can be optimized in practical systems, however, the performance difference of the systems in which different Δ are used becomes negligible as number of UEs increases after $N \geq 10$.

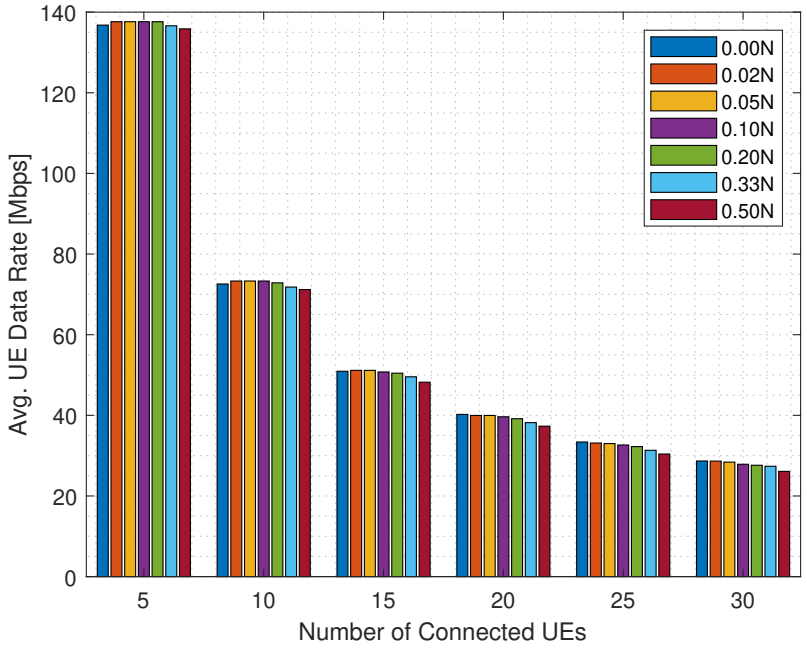

Figure 51: Effect of different N_{TH} values over average UE data rate

In Fig. 51, the effect of N_{TH} selection on the performance of the proposed adaptive hybrid system is depicted using Δ of 3 dB. Numerical N_{TH} values for different N are depicted in Table 16.

Table 16: N_{TH} values for different N

	$N = 5$	$N = 10$	$N = 15$	$N = 20$	$N = 20$	$N = 30$
$0.00N$	0	0	0	0	0	0
$0.02N$	0.10	0.20	0.30	0.40	0.50	0.60
$0.05N$	0.25	0.50	0.75	1.00	1.25	1.50
$0.10N$	0.50	1.00	1.50	2.00	2.50	3.00
$0.20N$	1.00	2.00	3.00	4.00	5.00	6.00
$0.33N$	1.65	3.30	4.95	6.60	8.25	9.90
$0.50N$	2.50	5.00	7.50	10.00	12.50	15.00

It can be observed that $N_{\mathrm{TH}} = \lceil 0.02N \rceil = \lceil 0.05N \rceil = \lceil 0.10N \rceil = \lceil 0.20N \rceil$[8] gives the highest data rate with the value of 137.3 Mbps for $N = 5$. The achievable data rates are equal to each other as a result of our proposed algorithm compares the number of UEs connected to MMW network using "greater than or equal to" operator and the condition returns the same results for integer-valued N_{MMW}. At this point, lowest data rate is resulted with the use of $N_{\mathrm{TH}} = 0.5N$. It gets the value of 135.8 Mbps, where the difference is 1.5 Mbps. When there are totally $N = 10$ UEs, the highest data rate with the value of 73 Mbps is achieved using $N_{\mathrm{TH}} = \lceil 0.02N \rceil = \lceil 0.05N \rceil = \lceil 0.10N \rceil$, whereas, lowest value becomes 71.19 Mbps. Herein, the difference is 1.8 Mbps. For $N = 15$, $N_{\mathrm{TH}} = \lceil 0.02N \rceil = \lceil 0.05N \rceil$ provides the highest data rate value with a difference to the lowest value of 2.9 Mbps. For $N \geq 20$, similar to previous cases, lower N_{TH} values give the higher data rates, however, the difference between the highest and lowest values has a downward trend. Numerically, the values become 2.8 Mbps, 2.7 Mbps, and 2.5 Mbps, respectively, for $N = 20$, $N = 25$, and $N = 30$.

The results reveal that using of different N_{TH} values provides different data rate performance regarding to the number of connected UE within an indoor room environment. Lower N_{TH} values provide higher data rates, however, the performance difference of the systems in which different N_{TH} are used becomes negligible as number of UEs increases.

[8] $\lceil . \rceil$ denotes the ceiling operation.

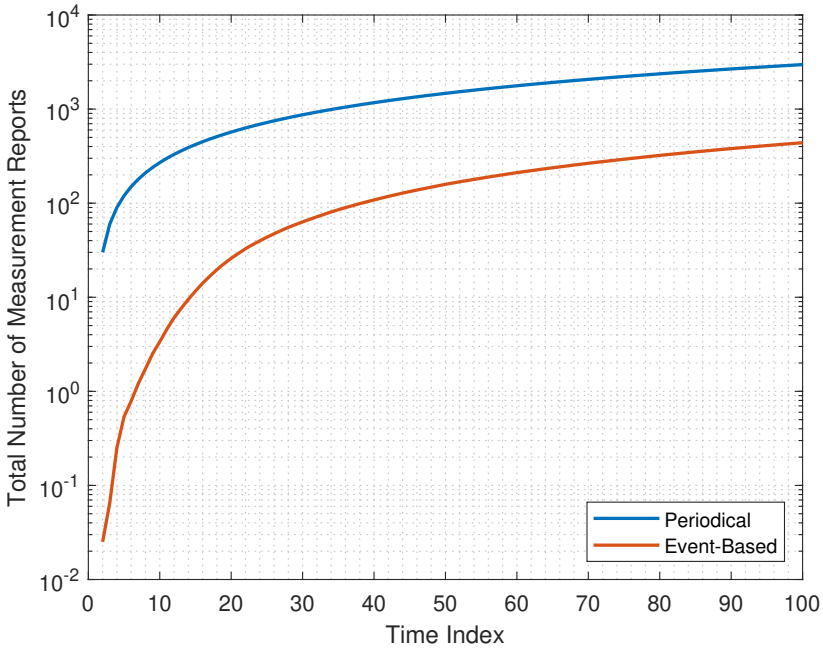

Figure 52: Cumulative measurement report count with respect to time

The reduction in signalling overhead is demonstrated in Fig. 52 where cumulative summation of the measurement report counts in the case of periodical and proposed event-based reporting is included. At the end of each channel realization, when event-based reporting is used, averagely 438.91 measurement reports are sent by UEs over 100 time slots under consideration. This is a significant reduction over periodical reporting that requires a total of $100 \times 30 = 3000$ reports. Hence, improvement in signaling overhead can be quantified as 85.37%.

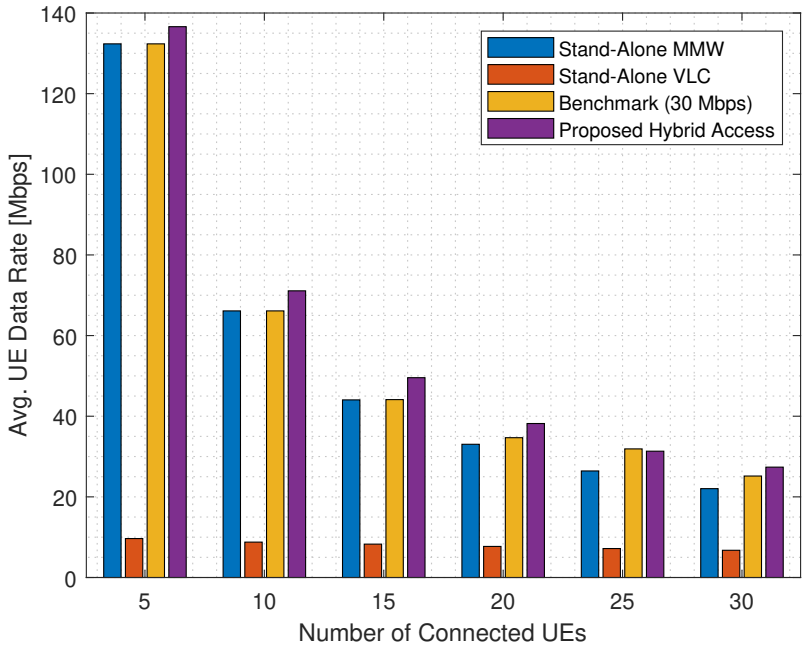

Figure 53: Average UE data rate with respect to different number of UEs

In Fig. 53, average UE data rate with respect to the number of UEs is presented with the use of $N_{\text{TH}} = 0.33N$ and $\Delta = 3$ dB. As benchmarks, the performances of stand-alone MMW and VLC networks are included. In addition, another benchmark scheme, in which UEs are initially connected to MMW network and they are offloaded to VLC network if their data rates are less than 30 Mbps, is considered.

When the number of UEs is set to 5, stand-alone MMW network provides an average of 132.3 Mbps data rate per UE, whereas 9.66 Mbps data rate is obtained in stand-alone VLC network. The hybrid VLC/MMW system achieves a data rate of 136.6 where the improvement 3.25% with respect to stand-alone MMW) comes from offloading some UEs to VLC network. For 10 UEs, stand-alone MMW and VLC networks respectively provide data rates of 66.12 Mbps and 8.78 Mbps while the hybrid system achieves 71.1 Mbps data rate. This indicates a 7.53% improvement with the use of our proposed adaptive system over stand-alone MMW network. The improvement further increases in proportion to the number of UEs. For example,

improvements of 12.51%, 15.59%, 18.58%, and 24.18% are respectively obtained for 15, 20, 25 and 30 UEs.

It can be further noted that our algorithm outperforms the benchmarking algorithm if the number of UEs is less than or equal to 20. For $N = 25$, the benchmarking algorithm yields a better performance. For $N = 30$, the trend once again changes in favor of our algorithm. This is as a result of the fact the data rate threshold in the benchmark scheme is a design parameter which needs to be optimized with respect to the number of UEs while our proposed algorithm dynamically adapts itself to handle with the varying conditions.

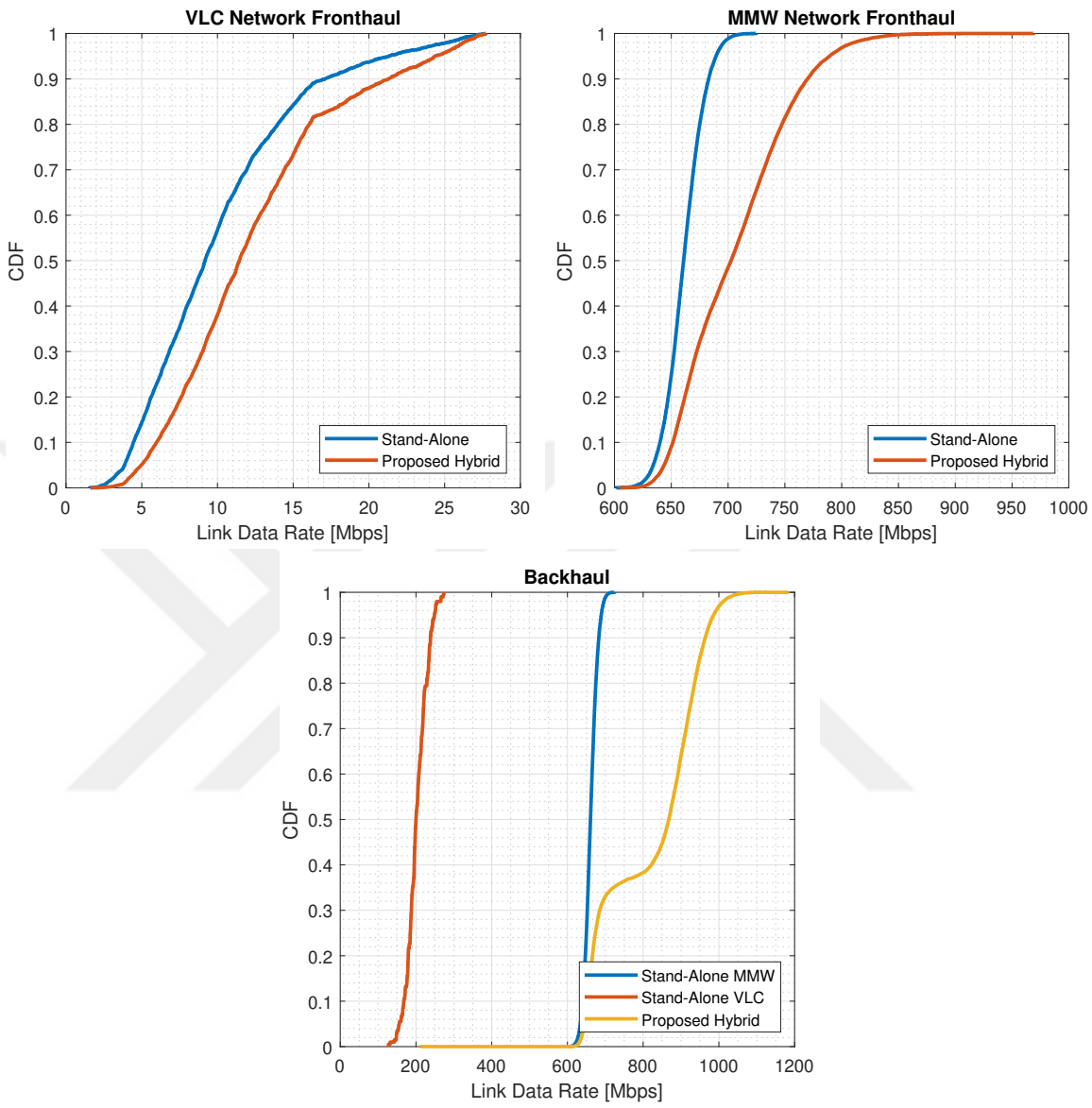

Figure 54: CDF of required capacity on fronthaul and backhaul links

In Fig. 54, the required capacity of fronthaul and backhaul links in the practical implementation of such a centralized system is pointed out through plotting cumulative distribution function (CDF) using 1500 channel realization. For $N = 30$ UEs, it can be calculated that the fronthaul link in stand-alone MMW network needs a capacity of 689.15 Mbps to satisfy data rate requirements of 95% of the UEs. For stand-alone VLC network, this value should be 21.64 Mbps. Under the assumption

of the same packet structure in both fronthaul and backhaul links, the capacity requirement of backhaul link is the same with fronthaul for MMW network, whereas, it becomes 249.26 Mbps for VLC network. In proposed hybrid architecture, fronthaul link for MMW AP and VLC APs should be at least 788.21 Mbps and 24.39 Mbps, respectively, whereas, the capacity of backhaul link should be 986.33 Mbps to handle the requirement of the same amount of UEs. Such capacities can be easily handled in today's backhaul/fronthaul wireline technologies.

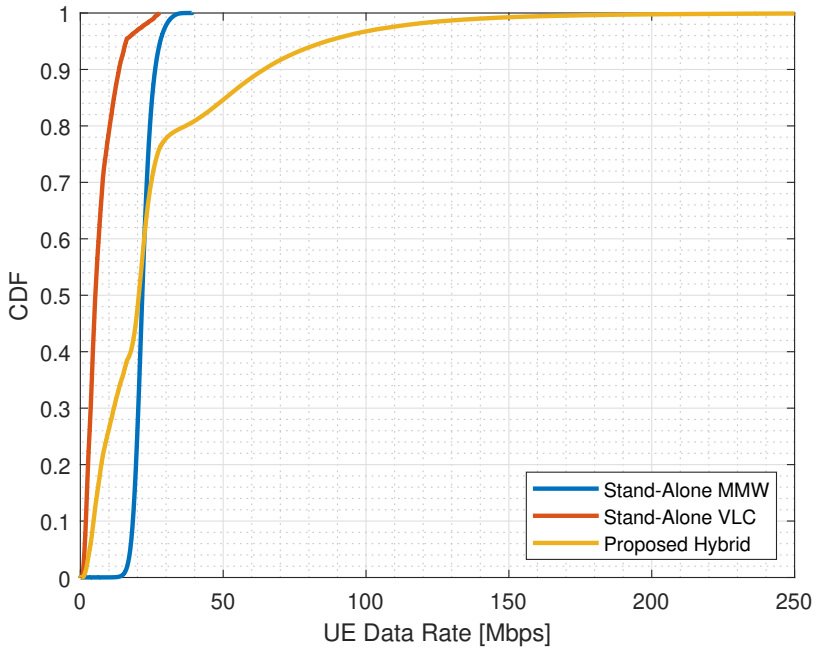

Figure 55: CDF of UE data rate values

The CDF of UE data rates in stand-alone MMW, stand-alone VLC, and proposed hybrid MMW/VLC networks are depicted in Fig. 55. In stand-alone MMW network, the probability of UEs that are experienced with a data rate greater than 30 Mbps is 0.02. This value is nearly 0 for stand-alone VLC network. However, when hybrid architecture is considered, it can be observed that UEs achieve greater than 30 Mbps data rate value with a probability of 0.23.

When outage probability is considered for the data rate of 3 Mbps, the results reveal that almost each UE in stand-alone MMW network receives the data with a rate of more than 3 Mbps. Therefore, the value is nearly 0. When stand-alone VLC network is considered, the probability becomes 0.24. However, in hybrid architecture, only 4% of the connected UEs experience with less than 3 Mbps data rate.

CHAPTER VI

CONCLUSION

In this dissertation, advanced physical layer features including adaptive transmission, OFDM, MIMO, and massive MIMO with beamforming technique and integration with the existing MMW network through an adaptive handover mechanism are investigated with the aim of boosting the network performance regarding to the varying network conditions. The deployment of these techniques, particularly MIMO scenarios, requires a centralized platform in contrast to the conventional distributed architecture. For this purpose, a centralized platform including MMW and VLC APs is proposed in Chapter 2 as emphasizing the differences from the distributed network architectures. The proposed architecture benefits from global awareness of APs conditions and coordinates the transmitted and received signals across MMW and VLC APs.

In Chapter 3, an adaptive SU distributed MIMO VLC system in which the LEDs locating at the ceiling for illumination acts as MIMO elements is investigated. DCO-OFDM is employed in the PHY of DL transmission which operates at visible light spectrum. An ATC that performs bit and power loading in conjunction with MIMO mode switching is proposed and implemented in CU in order to increase DL data rate while satisfying the target BER constraint. The results reveal that a significant performance improvement is obtained using the adaptive transmission in which the parameters are selected regarding to the channel conditions.

In Chapter 4, an MU massive MIMO VLC system in which the massive number of LEDs locating at the ceiling for illumination acts as MIMO elements is considered. The system utilizes FDD for DL and UL separation and MMW-based transmission is

employed in UL side. In order to enable an efficient DL channel estimation and interpolation while ensuring acceptable DL and UL overhead levels, the DL pilot signals are send through only over a certain number of LEDs, subcarriers, and sub-frames. The DL channel coefficients are then estimated by the UEs with the use of these pilots. In addition to the frequency and time domain interpolation, spatial interpolation is also performed by taking the benefit of the indoor room geometry and LED deployment layout with the aim of generating global channel matrix which is further used for pre-coding/beamforming purpose. Various PAs in spatial, frequency, and time domains are explored and the resulting data rates are analyzed for both DL and UL transmissions under the consideration of the DL channel estimation and interpolation errors and UL feedback overhead issues. The results reveal that higher number of DL pilot signals improve the DL data rate even through the high POR as a result of less channel estimation and interpolation errors, whereas, UL POR dramatically increases in proportion to the increase in active UE numbers. The situation is resulted by an imbalance between the data rates in DL and UL transmission. In order to handle with the imbalance condition, an DPC is proposed and implemented in CU. DPC performs an adaptation of DL pilot signals regarding to active UE numbers to get balanced DL and UL data rate performance.

In Chapter 5, a centralized hybrid MMW/VLC access network in which an event-triggered handover algorithm is used is proposed. VLC network is considered as complementary (or secondary), whereas, MMW network is selected as primary for the UE connection. In contrast to the conventional handover algorithms that require the periodical reporting of the received signal levels from each AP for each UE, the proposed scheme does not need this information. Instead, it uses only the measurement reports that are sent from UE and whose triggering conditions are determined using data rates and number of connected UEs metrics which are already pegged for debugging and further analysis purposes. The proposed method including an SINR

comparison with the technology-specific offset enhancement in UE side minimizes the signalling overhead as a result of event-based measurement report transmission and reduces the UE battery consumption. The offset variables are auto-tuned by a proposed LB that is also implemented in CU. The tuning mechanism is based on the number of connected UEs and data rates as inputs. Tuned offset variables are then broadcasted to the UEs. The results revel that a proper offloading of some UEs to the VLC network and demonstrate that a significant improvements in the average data rates are obtained especially when the number of UEs increases.

APPENDIX A

CHANNEL MODELS

A.1 Ray Tracing Assisted VLC Channel Model

Following the method defined in [97], a non-sequential ray-tracing method can be used to extract the VLC channel model between the u^{th} UE and the i^{th} LED. The model generation includes three main phases.

- In the first phase, three-dimensional indoor room environment with room objects is generated in Zemax®. The reflection parameters of the surface materials and the indoor room objects are then imported to the software tool. The locations of LED as a VLC transmitter and PD as UE receiver are also specified. In the case of multiple LEDs and PDs, they are independently specified from each other.

- In the second phase, a non-sequential ray-tracing method, which is a feature of Zemax®, is utilized to calculate the received optical power from each LED to each PD. In this phase, in addition to LoS component (in the case of when PD directly sees LED), ray-tracing method provides non-LoS components as a result of reflection from the objects and surfaces. At the end of the phase, Zemax® produces an output reports including power level at each PD and path length from each ray.

- In the last phase, the produced report is imported to MATLAB® and the channel model is expressed as

$$h_{u,i}^{\text{RAY}}(t) = \sum_{i=1}^{Z} P_i \delta(t - \tau_i), \tag{81}$$

where P_i is the optical power of the i^{th} ray, τ_i is the propagation time of the i^{th} ray, $\delta(t)$ is the Dirac delta function, and Z is the number of rays received at the PD.

The obtained VLC channel responses in the dissertation for 1^{st}, 2^{nd}, 3^{rd}, and 4^{th} USB hub are demonstrated in Figs. 56, 57, 58, and 59 with the use of indoor room model defined in Section 3.3.1.

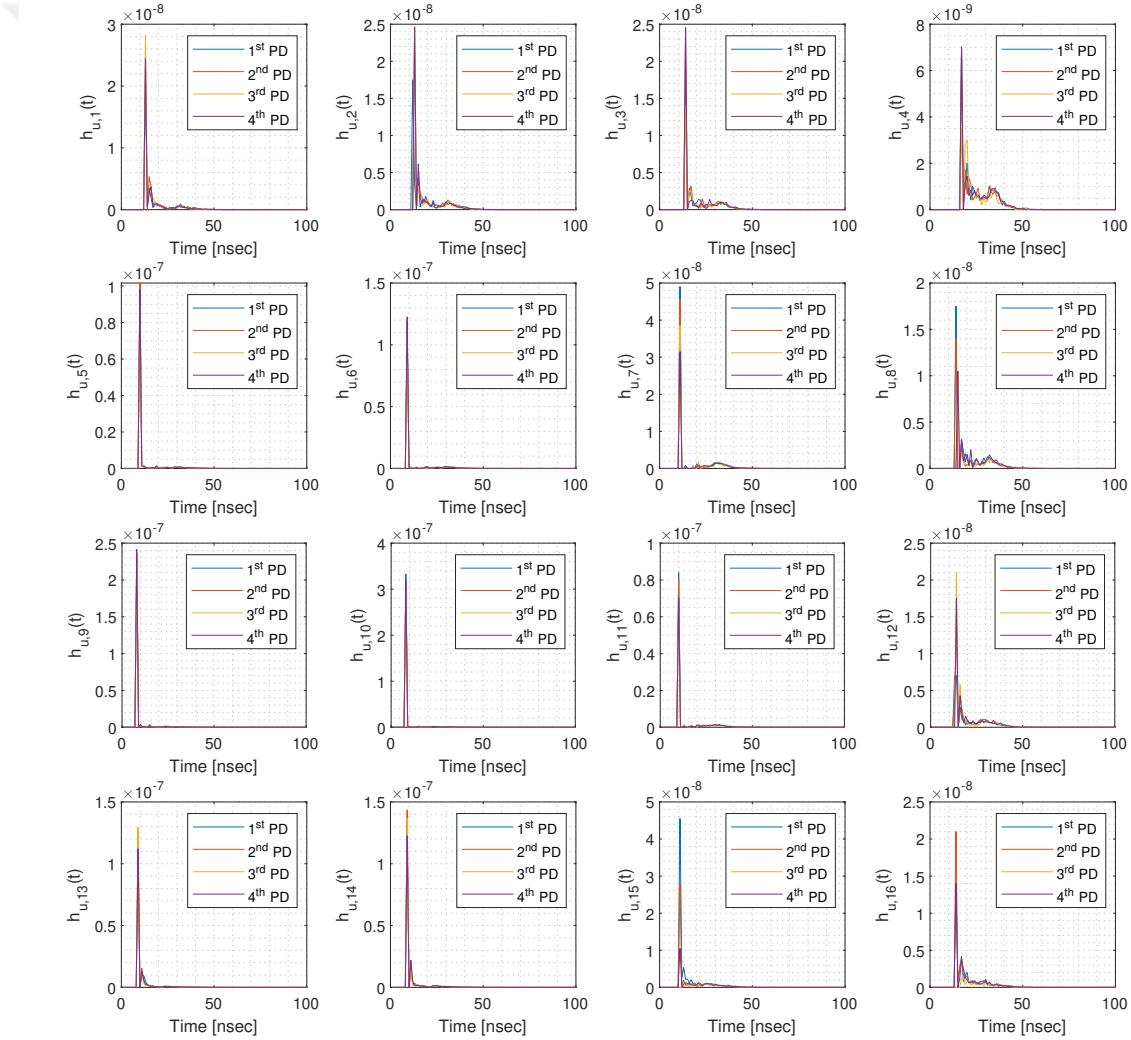

Figure 56: VLC channel responses for 1^{st} USB hub

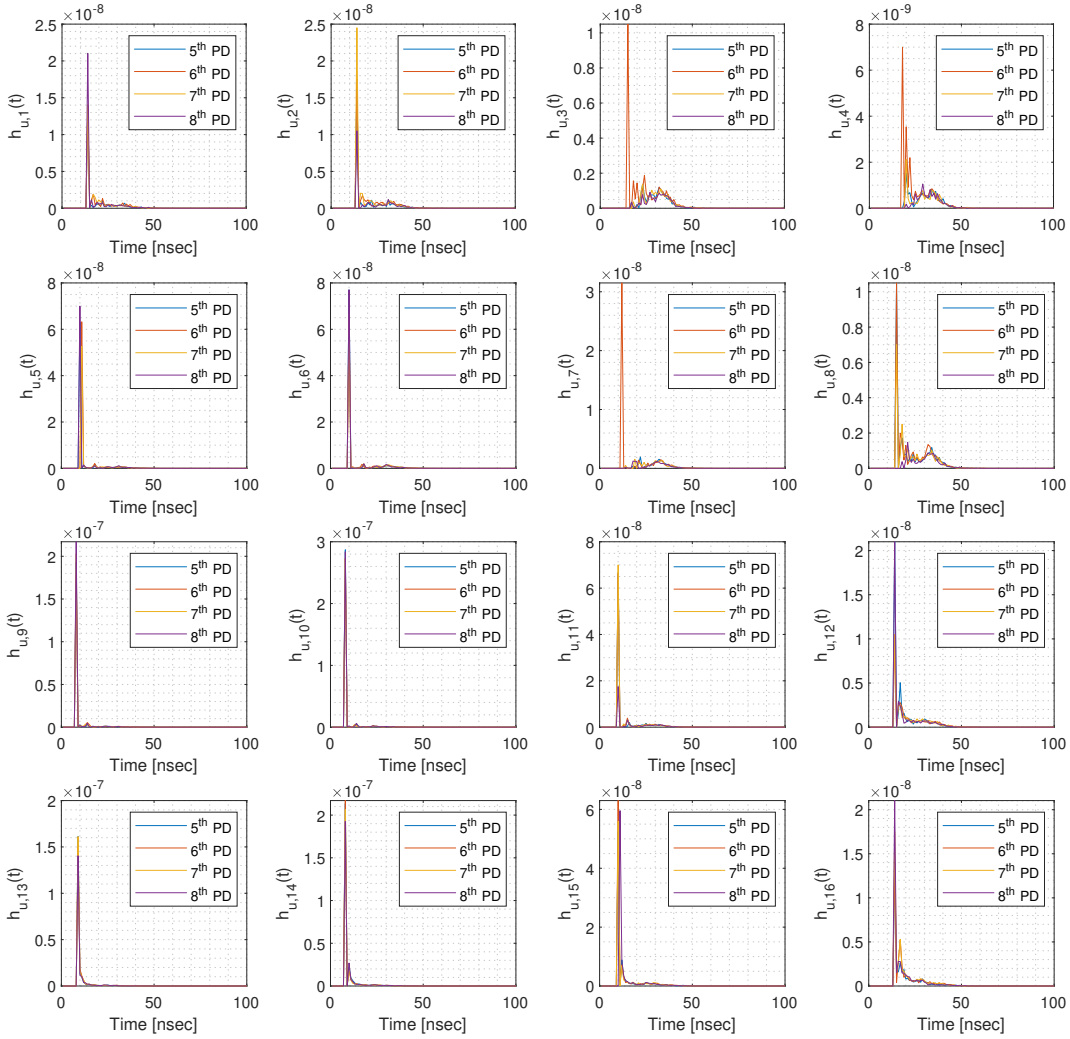

Figure 57: VLC channel responses for 2nd USB hub

A.2 LoS VLC Channel Model

In the case of MU scenarios in which UEs are randomly located for a huge ($> 10^3$) number of channel realization, extracting of VLC channel model for each UE using ray-tracing method defined in A.1 becomes harder. Therefore, analytical LoS based channel model is utilized in Chapter 4 and Chapter 5 in which MU transmission is considered. The analytical expression of the LoS component of the VLC channel

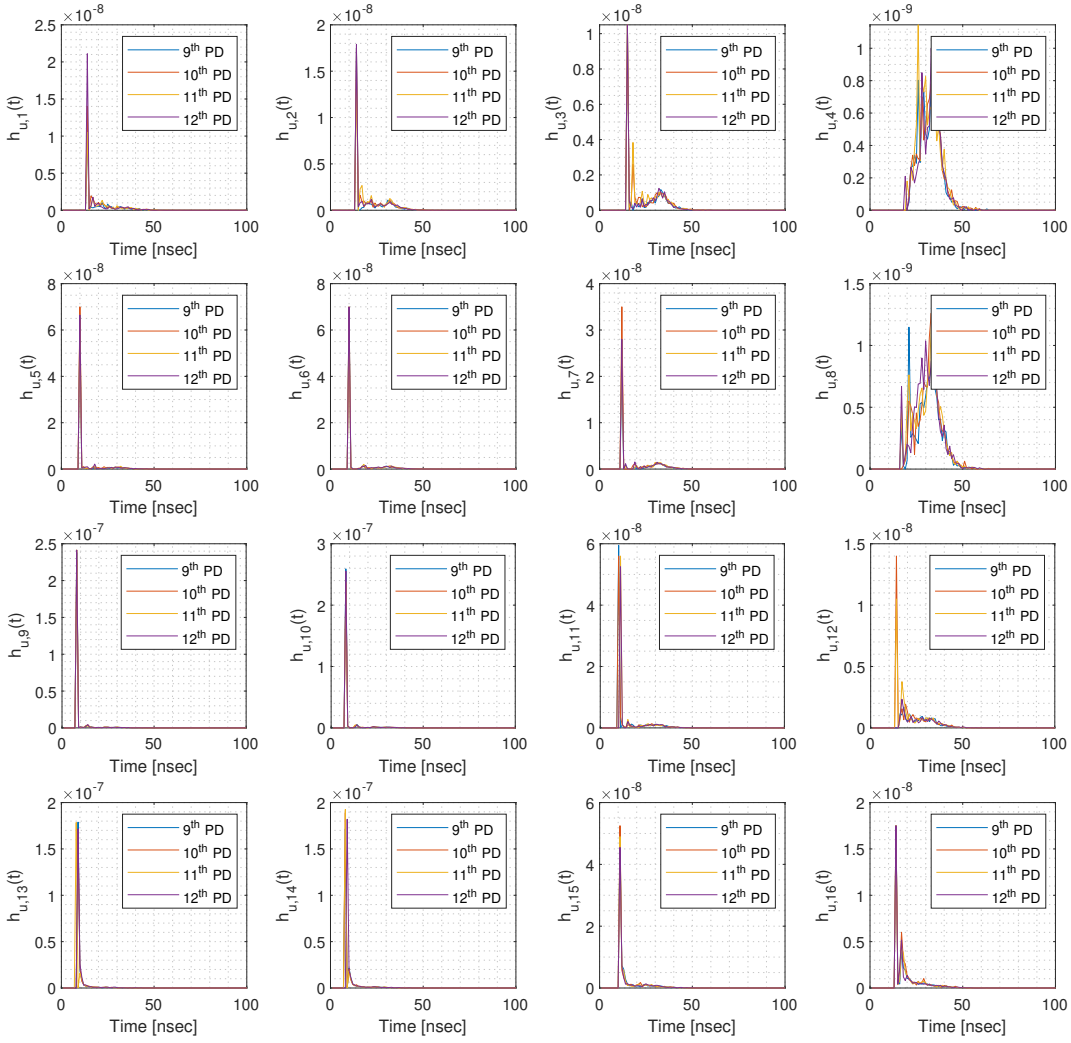

Figure 58: VLC channel responses for 3rd USB hub

model [98] between the u^{th} UE and the i^{th} LED can be written as

$$h_{u,i}^{\text{LoS}} = \begin{cases} \frac{(m+1)A_p}{2\pi d_{u,i}^2 \sin^2(\Theta_F)} \cos^m(\phi_{u,i}) \cos(\theta_{u,i}) & , \theta_{u,i} \leq \Theta_F \\ 0 & , \theta_{u,i} > \Theta_F \end{cases}, \tag{82}$$

where m is the Lambertian index which is equal to $-1/\log_2\cos(\theta_{1/2})$, $\theta_{1/2}$ is half-intensity radiation angle, A_p is the physical area of PD, and Θ_F is the half angle of the receiver field-of-view, which are not varying regarding to UE location. However, $d_{u,i}$, $\phi_{u,i}$, and $\theta_{u,i}$ that are the distance, angle of irradiation, and angle of incidence between the u^{th} UE and the i^{th} LED, respectively, take different values based on UE

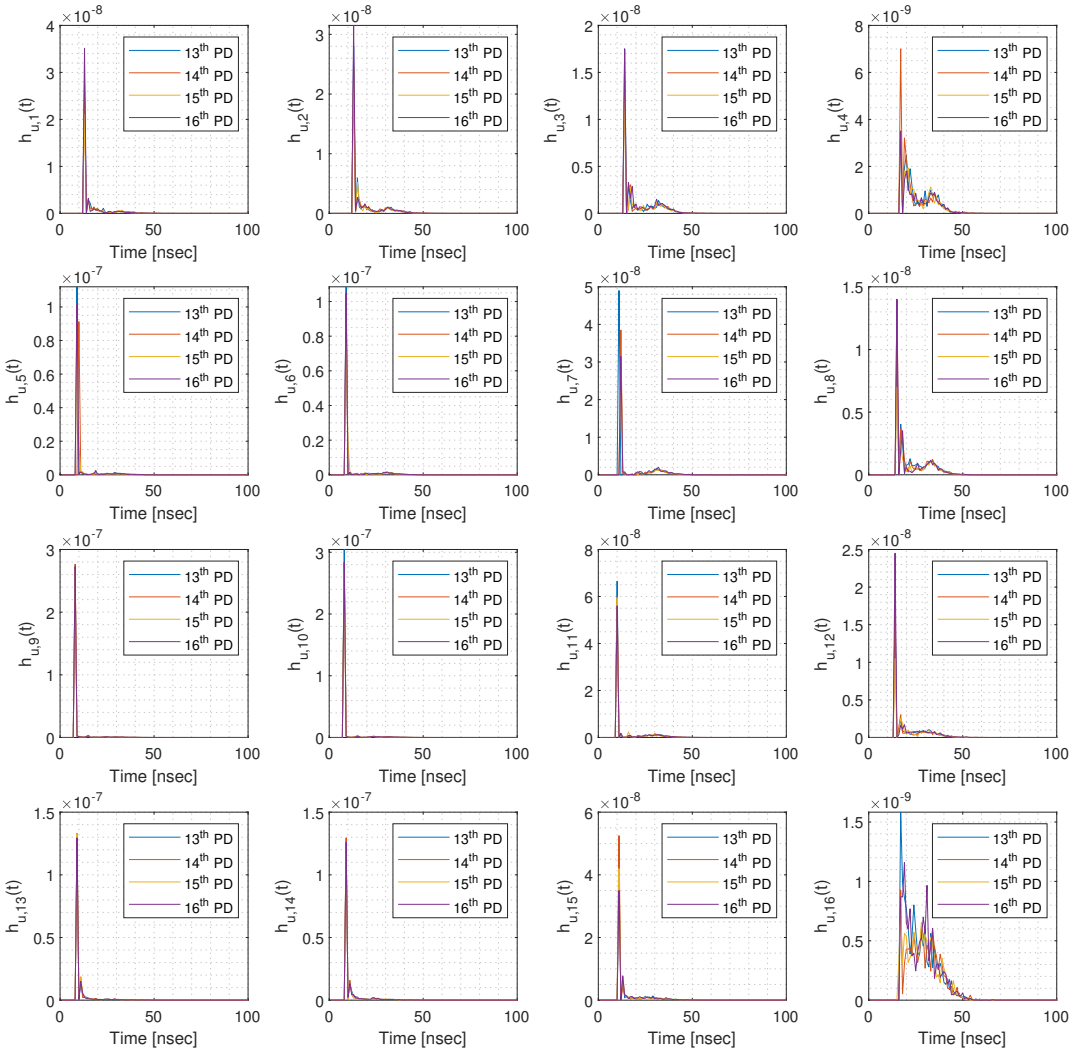

Figure 59: VLC channel responses for 4$^{\text{th}}$ USB hub

location. In the dissertation, all of the UEs are assumed to be faced upwards, then $\phi_{u,i}$ and $\theta_{u,i}$ become equal to each other (see Fig. 60).

A.3 LPF Effect of LED

The analytical expression of the natural LPF effect of the LED in frequency domain can be written as [93]

$$H_F(f) = \frac{1}{1 + j\frac{f}{f_{3-\text{dB}}}}, \tag{83}$$

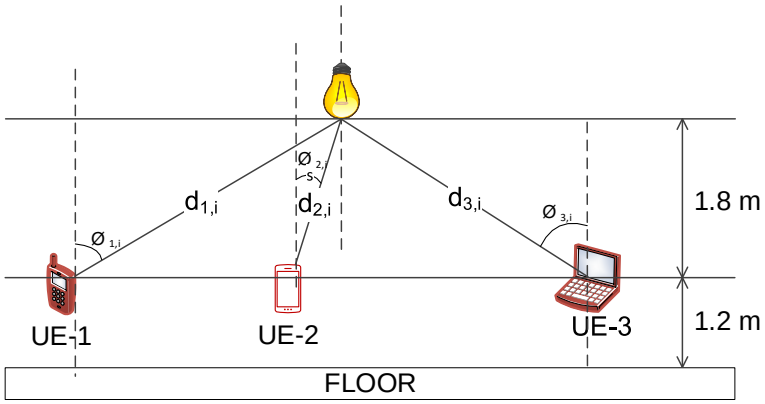

Figure 60: UEs locating under a VLC AP

where $f_{3-\mathrm{dB}}$ is 3-dB cut-off frequency of LED (please see Fig. 61 for $f_{3-\mathrm{dB}} = 10$ MHz). The effective channel response using the model obtained through the ray-tracing method is considered, analytical expression becomes

$$H_{u,i}^{\mathrm{VLC}}(f) = H_{u,i}^{\mathrm{RAY}}(f) H_F(f), \tag{84}$$

where $h_{u,i}^{\mathrm{RAY}}(f)$ is calculated as

$$H_{u,i}^{\mathrm{RAY}}(f) = \int_0^{\infty} h_{u,i}^{\mathrm{RAY}}(t) e^{-j2\pi ft} dt. \tag{85}$$

In similar way, the effective channel response using the LoS model defined in Section A.2 can be calculated as

$$H_{u,i}^{\mathrm{VLC}}(f) = h_{u,i}^{\mathrm{LOS}} H_F(f). \tag{86}$$

It should be noted that since there is not any multi-path component in the LoS model, channel gain is constant over all frequency range and frequency-selectively is related to LPF nature of LED.

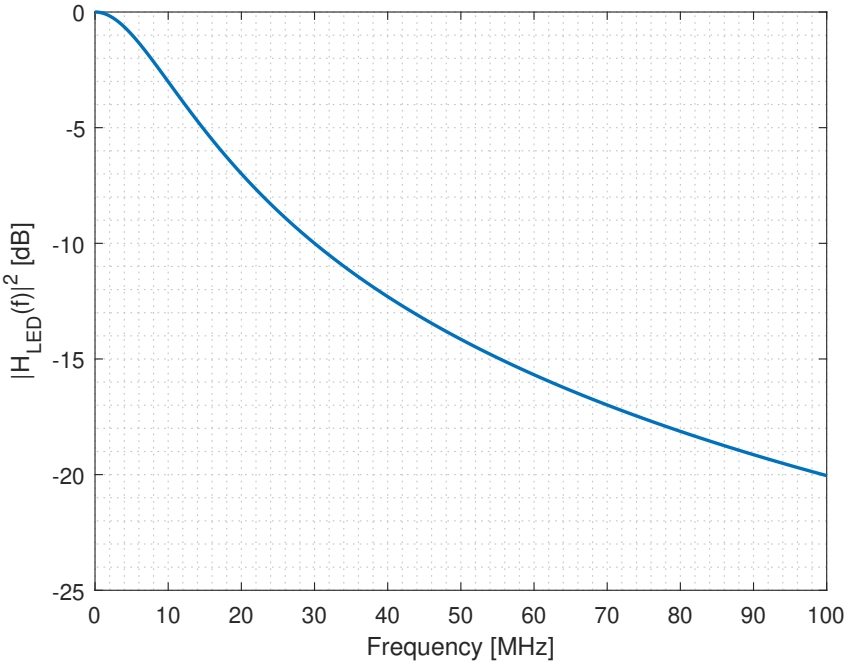

Figure 61: LPF effect of LEDs

A.4 MMW Channel Model

For the MMW channel model between the u^{th} UE and single MMW AP, the expression given in [71] is used, e.g.,

$$H_u^{\text{MMW}} = \sqrt{10^{\frac{-L_u^{\text{MMW}}}{10}}} \left(\sqrt{\frac{I}{I+1}} h_d + \sqrt{\frac{I}{I+1}} h_s \right), \tag{87}$$

where

$$L_u^{\text{MMW}} = L_{d_0} + 10v\log_{10} d_u + \gamma, \tag{88}$$

in which L_{d_0} is the reference path loss at a reference distance of d_0, d_u is the distance between the u^{th} UE and MMW AP, v is path loss exponent, γ is the shadowing component that is modeled as zero-mean Gaussian distributed random variable σ_γ^2 variance, I is the Rician factor, h_d is the LoS path fading channel coefficient, and h_s is the fading channel coefficient of the scattered path modelled as a complex Gaussian random variable with zero mean and unit variance.

APPENDIX B

PROPORTIONAL FAIR SCHEDULER

PF scheduler allocates the $\dot{k}^{\text{th}}$ RB to u^{th} UE if data rate balanced with fairness issue is the largest one, i.e.,

$$\dot{k} = \underset{k \in 1,2..N^{\text{RB}}}{\text{argmax}} \left\{ \frac{D_u^{\dot{k}}}{\bar{D}_u^{\dot{k}-1}} \right\}, \tag{89}$$

where N^{RB} is the total number of RB per transmission frame, $D_u^{\dot{k}}$ denotes the achievable data rate assuming the allocation of the $\dot{k}^{\text{th}}$ RB to the u^{th} UE, and $\bar{D}_u^{\dot{k}-1}$ is the calculated moving average data rate for the $\dot{k}$ RB allocation. The analytical expressions of $D_u^{\dot{k}}$ and $\bar{D}_u^{\dot{k}-1}$ can be written as

$$D_u^{\dot{k}} = \frac{1}{T^{\text{RB}}} \sum_{k,\tau \in \Gamma^{\dot{k}}} \Delta \times \log_2 \left(1 + \text{SINR}_u^{k,\tau}\right), \tag{90}$$

$$\bar{D}_u^{\dot{k}} = \frac{(\dot{k}-1)\bar{D}_u^{\dot{k}-1} + D_u^{\dot{k}}}{\dot{k}}, \tag{91}$$

where $\Gamma^{\dot{k}}$ denotes the indexes of subcarriers and sub-frames of $\dot{k}^{\text{th}}$ RB, Δ is the subcarrier spacing, and T^{RB} is RB duration in terms of sub-frame count.

Bibliography

[1] Cisco Visual Networking Index, "Cisco Visual Networking Index: Forecast and Trends, 2017–2022," 2018.

[2] J. G. Andrews, S. Buzzi, W. Choi, S. V. Hanly, A. Lozano, A. C. K. Soong, and J. C. Zhang, "What Will 5G Be?," *IEEE Journal on Selected Areas in Communications*, vol. 32, pp. 1065–1082, June 2014.

[3] A. Checko, H. L. Christiansen, Y. Yan, L. Scolari, G. Kardaras, M. S. Berger, and L. Dittmann, "Cloud RAN for Mobile Networks—A Technology Overview," *IEEE Communications Surveys Tutorials*, vol. 17, no. 1, pp. 405–426, 2015.

[4] A. Damnjanovic, J. Montojo, Y. Wei, T. Ji, T. Luo, M. Vajapeyam, T. Yoo, O. Song, and D. Malladi, "A survey on 3GPP heterogeneous networks," *IEEE Wireless Communications*, vol. 18, no. 3, pp. 10–21, 2011.

[5] H. Beyranvand, M. Lévesque, M. Maier, J. A. Salehi, C. Verikoukis, and D. Tipper, "Toward 5G: FiWi Enhanced LTE-A HetNets With Reliable Low-Latency Fiber Backhaul Sharing and WiFi Offloading," *IEEE/ACM Transactions on Networking*, vol. 25, no. 2, pp. 690–707, 2017.

[6] F. Mehmeti and T. Spyropoulos, "Performance Analysis of Mobile Data Offloading in Heterogeneous Networks," *IEEE Transactions on Mobile Computing*, vol. 16, no. 2, pp. 482–497, 2017.

[7] Nokia, "Services for Heterogeneous Networks (HetNets)." `https://onestore.nokia.com/asset/200234`, 2015. [Online; accessed 24-April-2020].

[8] P. I. Works, "Centralized SON An Effective Way of Automating End-to-End Network Management Towards 5G." `https://www.piworks.net/Upload/Document/Original/PIWorks_uSON_Centralized_SON.pdf`. [Online; accessed 24-April-2020].

[9] Huawei, "Small Cells Big Opportunities." `https://www.huawei.com/ilink/en/download/HW_330984`, 2015. [Online; accessed 24-April-2020].

[10] Ericsson, "Ericsson adds pico base station with integrated Wi-Fi access to its hetnet portfolio." `http://mb.cision.com/Main/15448/2245940/661983.pdf`, 2015. [Online; accessed 24-April-2020].

[11] S. Parkvall, E. Dahlman, A. Furuskar, and M. Frenne, "NR: The New 5G Radio Access Technology," *IEEE Communications Standards Magazine*, vol. 1, no. 4, pp. 24–30, 2017.

[12] "IEEE 802.15 WPAN Task Group 3c (TG3c) Millimeter Wave Alternative PHY." `http://www.ieee802.org/15/pub/TG3c.html`. [Online; accessed 24-April-2020].

[13] "P802.11bb - Standard for Information Technology–Telecommunications and Information Exchange Between Systems Local and Metropolitan Area Networks–Specific Requirements - Part 11: Wireless LAN Medium Access Control (MAC) and Physical Layer (PHY) Specifications Amendment: Light Communications." `https://standards.ieee.org/project/802_11bb.html`. [Online; accessed 24-April-2020].

[14] Nokia, "Massive MIMO." `https://onestore.nokia.com/asset/201128`, 2018. [Online; accessed 24-April-2020].

[15] T. L. Marzetta, "Noncooperative Cellular Wireless with Unlimited Numbers of Base Station Antennas," *IEEE Transactions on Wireless Communications*, vol. 9, pp. 3590–3600, November 2010.

[16] D. Tsonev, S. Videv, and H. Haas, "Light fidelity (Li-Fi): towards all-optical networking," in *Proc. SPIE*, vol. 9007, pp. 900702–900702, 2013.

[17] S. Arnon, *Visible light communication*. Cambridge University Press, 2015.

[18] N. Chi, *LED-Based Visible Light Communications*. Springer, 2018.

[19] S. Rajagopal, R. D. Roberts, and S. K. Lim, "IEEE 802.15.7 visible light communication: modulation schemes and dimming support," *IEEE Communications Magazine*, vol. 50, pp. 72–82, March 2012.

[20] "IEEE Standard for Local and Metropolitan Area Networks–Part 15.7: Short-Range Wireless Optical Communication Using Visible Light," *IEEE Std 802.15.7-2011*, pp. 1–309, 2011.

[21] J. Armstrong, "OFDM for Optical Communications," *Journal of Lightwave Technology*, vol. 27, pp. 189–204, Feb 2009.

[22] J. Armstrong and A. J. Lowery, "Power efficient optical OFDM," *Electronics Letters*, vol. 42, pp. 370–372, March 2006.

[23] D. Tsonev, S. Sinanovic, and H. Haas, "Novel Unipolar Orthogonal Frequency Division Multiplexing (U-OFDM) for Optical Wireless," in *2012 IEEE 75th Vehicular Technology Conference (VTC Spring)*, pp. 1–5, May 2012.

[24] N. Fernando, Y. Hong, and E. Viterbo, "Flip-OFDM for Unipolar Communication Systems," *IEEE Transactions on Communications*, vol. 60, pp. 3726–3733, December 2012.

[25] D. Tsonev, S. Videv, and H. Haas, "Unlocking Spectral Efficiency in Intensity Modulation and Direct Detection Systems," *IEEE Journal on Selected Areas in Communications*, vol. 33, pp. 1758–1770, Sept 2015.

[26] P. H. Pathak, X. Feng, P. Hu, and P. Mohapatra, "Visible Light Communication, Networking, and Sensing: A Survey, Potential and Challenges," *IEEE Communications Surveys Tutorials*, vol. 17, no. 4, pp. 2047–2077, 2015.

[27] "Ores LiFi. Fixed LED downlight LiFi Access Point." http://lumefficient.com/wp-content/uploads/2018/03/Ores-LiFi-Spec-Sheet.pdf. [Online; accessed 24-April-2020].

[28] PureLiFi, "LiFi-XC." https://purelifi.com/say-hello-to-the-lifi-xc/lifi-xc/. [Online; accessed 24-April-2020].

[29] "Light Communications for Wireless Local Area Networking." https://futurenetworks.ieee.org/tech-focus/may-2018/light-communications-for-wireless-local-area-networking. [Online; accessed 24-April-2020].

[30] V. Jungnickel, "High-bandwidth PHY." https://mentor.ieee.org/802.15/dcn/16/15-16-0356-00-007a-text-input-for-high-bandwidth-phy.docx, 2016. doc: IEEE 802.15-16/0356r0, [Online; accessed 24-April-2020].

[31] M. Uysal, O. Narmanlioglu, T. Baykas, and R. C. Kizilirmak, "Adaptive MIMO OFDM PHY proposal for IEEE 802.15.7r1." https://mentor.ieee.org/802.15/dcn/16/15-16-0008-02-007a-adaptive-mimo-ofdm-phy-proposal-for-ieee802\\15-7r1.pdf. [Online; accessed 24-April-2020].

[32] M. Agiwal, A. Roy, and N. Saxena, "Next Generation 5G Wireless Networks: A Comprehensive Survey," *IEEE Communications Surveys Tutorials*, vol. 18, no. 3, pp. 1617–1655, 2016.

[33] R. C. Kizilirmak, O. Narmanlioglu, and M. Uysal, "Centralized Light Access Network (C-LiAN): A Novel Paradigm for Next Generation Indoor VLC Networks," *IEEE Access*, vol. 5, pp. 19703–19710, 2017.

[34] T. Fath and H. Haas, "Performance Comparison of MIMO Techniques for Optical Wireless Communications in Indoor Environments," *IEEE Transactions on Communications*, vol. 61, pp. 733–742, February 2013.

[35] M. O. Damen, O. Narmanlioglu, and M. Uysal, "Comparative performance evaluation of MIMO visible light communication systems," in *2016 24th Signal Processing and Communication Application Conference (SIU)*, pp. 525–528, May 2016.

[36] O. Narmanlioglu, R. C. Kizilirmak, F. Miramirkhani, S. Safaraliev, S. M. Sait, and M. Uysal, "Effect of Wiring and Cabling Topologies on the Performance of Distributed MIMO OFDM VLC Systems," *IEEE Access*, vol. 7, pp. 52743–52754, 2019.

[37] A. Yesilkaya, E. Basar, F. Miramirkhani, E. Panayirci, M. Uysal, and H. Haas, "Optical MIMO-OFDM With Generalized LED Index Modulation," *IEEE Transactions on Communications*, vol. 65, pp. 3429–3441, Aug 2017.

[38] C. Chen, W. Zhong, and D. Wu, "Non-hermitian symmetry orthogonal frequency division multiplexing for multiple-input multiple-output visible light communications," *IEEE/OSA Journal of Optical Communications and Networking*, vol. 9, pp. 36–44, Jan 2017.

[39] C. He, T. Q. Wang, and J. Armstrong, "Performance of Optical Receivers Using Photodetectors With Different Fields of View in a MIMO ACO-OFDM System," *Journal of Lightwave Technology*, vol. 33, pp. 4957–4967, Dec 2015.

[40] Y. Hong and L. Chen, "Performance investigation of OCT precoding for MIMO-OFDM based indoor visible light communications," in *2016 18th International Conference on Transparent Optical Networks (ICTON)*, pp. 1–4, July 2016.

[41] C. Chen, W. Zhong, H. Yang, and P. Du, "On the Performance of MIMO-NOMA-Based Visible Light Communication Systems," *IEEE Photonics Technology Letters*, vol. 30, pp. 307–310, Feb 2018.

[42] Z. Feng, C. Guo, Z. Ghassemlooy, and Y. Yang, "The Spatial Dimming Scheme for the MU-MIMO-OFDM VLC System," *IEEE Photonics Journal*, vol. 10, pp. 1–13, Oct 2018.

[43] L. Wei, H. Zhang, and J. Song, "Experimental Demonstration of a Cubic-Receiver-Based MIMO Visible Light Communication System," *IEEE Photonics Journal*, vol. 9, pp. 1–7, Feb 2017.

[44] A. H. Azhar, T. Tran, and D. O'Brien, "Demonstration of high-speed data transmission using MIMO-OFDM visible light communications," in *2010 IEEE Globecom Workshops*, pp. 1052–1056, Dec 2010.

[45] A. H. Azhar, T. Tran, and D. O'Brien, "A Gigabit/s Indoor Wireless Transmission Using MIMO-OFDM Visible-Light Communications," *IEEE Photonics Technology Letters*, vol. 25, pp. 171–174, Jan 2013.

[46] L. Wu, Z. Zhang, J. Dang, and H. Liu, "Adaptive Modulation Schemes for Visible Light Communications," *Journal of Lightwave Technology*, vol. 33, pp. 117–125, Jan 2015.

[47] J. Vucic, C. Kottke, S. Nerreter, K. D. Langer, and J. W. Walewski, "513 Mbit/s Visible Light Communications Link Based on DMT-Modulation of a White LED," *Journal of Lightwave Technology*, vol. 28, pp. 3512–3518, Dec 2010.

[48] P. W. Berenguer, V. Jungnickel, and J. K. Fischer, "The benefit of frequency-selective rate adaptation for optical wireless communications," *10th International Symposium on Communication Systems, Networks and Digital Signal Processing (CSNDSP)*, pp. 1–6, July 2016.

[49] M. Wang, J. Wu, W. Yu, H. Wang, J. Li, J. Shi, and C. Luo, "Efficient coding modulation and seamless rate adaptation for visible light communications," *IEEE Wireless Communications*, vol. 22, pp. 86–93, April 2015.

[50] J. He, J. He, and J. Shi, "An Enhanced Adaptive Scheme With Pairwise Coding for OFDM-VLC System," *IEEE Photonics Technology Letters*, vol. 30, pp. 1254–1257, July 2018.

[51] Y. Hong, T. Wu, and L. K. Chen, "On the Performance of Adaptive MIMO-OFDM Indoor Visible Light Communications," *IEEE Photonics Technology Letters*, vol. 28, pp. 907–910, April 2016.

[52] K. H. Park, Y. C. Ko, and M. S. Alouini, "On the Power and Offset Allocation for Rate Adaptation of Spatial Multiplexing in Optical Wireless MIMO Channels," *IEEE Transactions on Communications*, vol. 61, pp. 1535–1543, April 2013.

[53] J. Y. Wang, J. X. Zhu, S. H. Lin, and J. B. Wang, "Adaptive Spatial Modulation Based Visible Light Communications: SER Analysis and Optimization," *IEEE Photonics Journal*, vol. 10, pp. 1–14, June 2018.

[54] P. F. Mmbaga, J. Thompson, and H. Haas, "Performance Analysis of Indoor Diffuse VLC MIMO Channels Using Angular Diversity Detectors," *Journal of Lightwave Technology*, vol. 34, pp. 1254–1266, Feb 2016.

[55] O. Narmanlioglu, R. C. Kizilirmak, T. Baykas, and M. Uysal, "Link Adaptation for MIMO OFDM Visible Light Communication Systems," *IEEE Access*, vol. 5, pp. 26006–26014, 2017.

[56] E. Telatar, "Capacity of multi-antenna Gaussian channels," *European transactions on telecommunications*, vol. 10, no. 6, pp. 585–595, 1999.

[57] E. Van den Bogaert, T. Bostoen, J. Van Elsen, R. Cendrillon, and M. Moonen, "DSM in practice: Iterative water-filling implemented on ADSL modems," in *2004 IEEE International Conference on Acoustics, Speech, and Signal Processing*, vol. 5, pp. V–337, IEEE, 2004.

[58] Y.-C. Liang, R. Zhang, and J. Cioffi, "Sub-channel grouping and statistical water-filling for MIMO-OFDM systems," in *The Thrity-Seventh Asilomar Conference on Signals, Systems & Computers, 2003*, vol. 1, pp. 997–1001, IEEE, 2003.

[59] M. Codreanu, D. Tujkovic, and M. Latva-aho, "Adaptive MIMO-OFDM systems with channel state information at TX side," in *IEEE International Conference on Communications, 2005. ICC 2005. 2005*, vol. 4, pp. 2645–2649 Vol. 4, 2005.

[60] B. S. Krongold, K. Ramchandran, and D. L. Jones, "Computationally efficient optimal power allocation algorithms for multicarrier communication systems," *IEEE Transactions on Communications*, vol. 48, pp. 23–27, Jan 2000.

[61] H. Zhang, J. Fu, and J. Song, "A Hughes-Hartogs Algorithm Based Bit Loading Algorithm for OFDM Systems," in *2010 IEEE International Conference on Communications*, pp. 1–5, May 2010.

[62] R. W. Heath and A. J. Paulraj, "Switching between diversity and multiplexing in MIMO systems," *IEEE Transactions on Communications*, vol. 53, no. 6, pp. 962–968, 2005.

[63] S. Catreux, V. Erceg, D. Gesbert, and R. W. Heath, "Adaptive modulation and MIMO coding for broadband wireless data networks," *IEEE Communications Magazine*, vol. 40, no. 6, pp. 108–115, 2002.

[64] G. Xu, Y. Li, J. Yuan, R. Monroe, S. Rajagopal, S. Ramakrishna, Y. H. Nam, J. Seol, J. Kim, M. M. U. Gul, A. Aziz, and J. Zhang, "Full Dimension MIMO (FD-MIMO): Demonstrating Commercial Feasibility," *IEEE Journal on Selected Areas in Communications*, vol. 35, pp. 1876–1886, Aug 2017.

[65] S. Jain, R. Mitra, and V. Bhatia, "Adaptive Precoding-Based Detection Algorithm for Massive MIMO Visible Light Communication," *IEEE Communications Letters*, vol. 22, pp. 1842–1845, Sep. 2018.

[66] K. Xu, H. Yu, and Y. Zhu, "Channel-Adapted Spatial Modulation for Massive MIMO Visible Light Communications," *IEEE Photonics Technology Letters*, vol. 28, pp. 2693–2696, Dec 2016.

[67] R. Mitra and V. Bhatia, "Precoding Technique for Ill-Conditioned Massive MIMO-VLC System," in *2018 IEEE 87th Vehicular Technology Conference (VTC Spring)*, pp. 1–5, June 2018.

[68] R. Mitra and V. Bhatia, "Minimum Error Entropy Criterion Based Channel Estimation for Massive-MIMO in VLC," *IEEE Transactions on Vehicular Technology*, vol. 68, no. 1, pp. 1014–1018, 2018.

[69] Z. Gao, Y. Wang, X. Liu, F. Zhou, and K. Wong, "FFDNet-Based Channel Estimation for Massive MIMO Visible Light Communication Systems," *IEEE Wireless Communications Letters*, vol. 9, no. 3, pp. 340–343, 2020.

[70] Y. Wang and H. Haas, "Dynamic Load Balancing With Handover in Hybrid Li-Fi and Wi-Fi Networks," *Journal of Lightwave Technology*, vol. 33, no. 22, pp. 4671–4682, 2015.

[71] Y. Wang and H. Haas, "Dynamic Load Balancing With Handover in Hybrid Li-Fi and Wi-Fi Networks," *Journal of Lightwave Technology*, vol. 33, pp. 4671–4682, Nov 2015.

[72] M. Kashef, M. Ismail, M. Abdallah, K. A. Qaraqe, and E. Serpedin, "Energy Efficient Resource Allocation for Mixed RF/VLC Heterogeneous Wireless Networks," *IEEE Journal on Selected Areas in Communications*, vol. 34, no. 4, pp. 883–893, 2016.

[73] X. Li, R. Zhang, and L. Hanzo, "Cooperative Load Balancing in Hybrid Visible Light Communications and WiFi," *IEEE Transactions on Communications*, vol. 63, pp. 1319–1329, April 2015.

[74] I. Stefan and H. Haas, "Hybrid Visible Light and Radio Frequency Communication Systems," in *2014 IEEE 80th Vehicular Technology Conference (VTC2014-Fall)*, pp. 1–5, 2014.

[75] L. Li, Y. Zhang, B. Fan, and H. Tian, "Mobility-Aware Load Balancing Scheme in Hybrid VLC-LTE Networks," *IEEE Communications Letters*, vol. 20, no. 11, pp. 2276–2279, 2016.

[76] M. Kashef, A. Torky, M. Abdallah, N. Al-Dhahir, and K. Qaraqe, "On the Achievable Rate of a Hybrid PLC/VLC/RF Communication System," in *2015 IEEE Global Communications Conference (GLOBECOM)*, pp. 1–6, 2015.

[77] X. Wu, M. Safari, and H. Haas, "Access Point Selection for Hybrid Li-Fi and Wi-Fi Networks," *IEEE Transactions on Communications*, vol. 65, no. 12, pp. 5375–5385, 2017.

[78] Y. Wang, X. Wu, and H. Haas, "Load Balancing Game With Shadowing Effect for Indoor Hybrid LiFi/RF Networks," *IEEE Transactions on Wireless Communications*, vol. 16, pp. 2366–2378, April 2017.

[79] M. Hammouda, S. Akın, A. M. Vegni, H. Haas, and J. Peissig, "Link Selection in Hybrid RF/VLC Systems Under Statistical Queueing Constraints," *IEEE Transactions on Wireless Communications*, vol. 17, no. 4, pp. 2738–2754, 2018.

[80] H. Tabassum and E. Hossain, "Coverage and Rate Analysis for Co-Existing RF/VLC Downlink Cellular Networks," *IEEE Transactions on Wireless Communications*, vol. 17, no. 4, pp. 2588–2601, 2018.

[81] D. A. Basnayaka and H. Haas, "Hybrid RF and VLC Systems: Improving User Data Rate Performance of VLC Systems," in *2015 IEEE 81st Vehicular Technology Conference (VTC Spring)*, pp. 1–5, 2015.

[82] M. Obeed, A. M. Salhab, S. A. Zummo, and M. Alouini, "Joint Load Balancing and Power Allocation for Hybrid VLC/RF Networks," in *GLOBECOM 2017 - 2017 IEEE Global Communications Conference*, pp. 1–6, 2017.

[83] M. Obeed, A. M. Salhab, S. A. Zummo, and M. Alouini, "Joint optimization of power allocation and load balancing for hybrid VLC/RF networks," *IEEE/OSA Journal of Optical Communications and Networking*, vol. 10, pp. 553–562, May 2018.

[84] D. A. Basnayaka and H. Haas, "Design and Analysis of a Hybrid Radio Frequency and Visible Light Communication System," *IEEE Transactions on Communications*, vol. 65, pp. 4334–4347, Oct 2017.

[85] "ETSI TS 136 331 V15.3.0. LTE; Evolved Universal Terrestrial Radio Access (E-UTRA); Radio Resource Control (RRC); Protocol specification (3GPP TS 36.331 version 15.3.0 Release 15) ." `https://www.etsi.org/deliver/etsi_ts/`

136300_136399/136331/15.03.00_60/ts_136331v150300p.pdf, 2018. [Online; accessed 24-April-2020].

[86] "ETSI TS 136 423 V12.3.0. LTE; Evolved Universal Terrestrial Radio Access (E-UTRA); X2 Application Protocol (X2AP) (3GPP TS 36.423 version 12.3.0 Release 12) ." https://www.etsi.org/deliver/etsi_ts/136400_136499/136423/12.03.00_60/ts_136423v120300p.pdf, 2014. [Online; accessed 24-April-2020].

[87] Y. Lin, L. Shao, Z. Zhu, Q. Wang, and R. K. Sabhikhi, "Wireless network cloud: Architecture and system requirements," *IBM Journal of Research and Development*, vol. 54, no. 1, pp. 4–1, 2010.

[88] TG7r1, "Technical considerations document." https://mentor.ieee.org/802.15/dcn/15/15-15-0492-03-007a-technical-considerations-document.docx, 2015. doc: IEEE 802.15-15/0492r3, [Online; accessed 24-April-2020].

[89] U. F. Siddiqi, O. Narmanlioglu, M. Uysal, and S. M. Sait, "Joint bit and power loading for adaptive MIMO OFDM VLC systems," *Transactions on Emerging Telecommunications Technologies*, 2020.

[90] K. Cho and D. Yoon, "On the general BER expression of one- and two-dimensional amplitude modulations," *IEEE Transactions on Communications*, vol. 50, pp. 1074–1080, July 2002.

[91] C. E. Shannon, "A mathematical theory of communication," *Bell system technical journal*, vol. 27, no. 3, pp. 379–423, 1948.

[92] International Standard, ISO 8995:2002 CIE S 008/E 2001, "Lighting of indoor work places." https://www.iso.org/standard/28857.html. [Online; accessed 24-April-2020].

[93] J. Grubor, S. Randel, K. Langer, and J. W. Walewski, "Broadband Information Broadcasting Using LED-Based Interior Lighting," *Journal of Lightwave Technology*, vol. 26, pp. 3883–3892, Dec 2008.

[94] E. G. Larsson, O. Edfors, F. Tufvesson, and T. L. Marzetta, "Massive MIMO for next generation wireless systems," *IEEE Communications Magazine*, vol. 52, pp. 186–195, February 2014.

[95] "ETSI TS 136 211 V15.3.0 LTE; Evolved Universal Terrestrial Radio Access (E-UTRA); Physical channels and modulation (3GPP TS 36.211 version 15.3.0 Release 15) ." https://www.etsi.org/deliver/etsi_ts/136200_136299/136211/15.03.00_60/ts_136211v150300p.pdf, 2018. [Online; accessed 24-April-2020].

[96] M. Uysal, F. Miramirkhani, T. Baykas, N. Serafimovski, and V. Jungnickel, "IEEE 802.11bb Reference Channel Models for Indoor Environments , doc:

IEEE 11-18-1236-01-00bb." https://mentor.ieee.org/802.11/dcn/18/11-18-1582-00-00bb-ieee-802-11bb-reference-channel-models-for\-indoor-environments.pdf. [Online; accessed 24-April-2020].

[97] F. Miramirkhani and M. Uysal, "Channel Modeling and Characterization for Visible Light Communications," *IEEE Photonics Journal*, vol. 7, pp. 1–16, Dec 2015.

[98] J. M. Kahn and J. R. Barry, "Wireless infrared communications," *Proceedings of the IEEE*, vol. 85, pp. 265–298, Feb 1997.

VITA

Omer Narmanlioglu received his B.Sc. and M.Sc. degrees from the Department of Electrical and Electronics Engineering at Bilkent University, Ankara, Turkey, in 2014, and Ozyegin University, Istanbul, Turkey, in 2016, respectively, and Ph.D. degree from Department of Electrical and Electronics Engineering at Ozyegin University in 2020. He is currently working with P.I. Works as RF (Radio-Frequency) & SON (Self-Organizing Networks) Consultant. His research interests are the physical and link layer aspects of communication systems, Self-Organizing Networks, and optimization and planning of Radio Access Networks. His major distinctions include Best Research Assistant Award, in Ozyegin University, in 2016, National Instruments Engineering Impact Award in Austin, Texas, USA, in 2017, and Best Paper Award in IEEE International Conference on the Network of the Future, London, United Kingdom, in 2017.